

A Thesis Submitted for the Degree of PhD at the University of Warwick

Permanent WRAP URL:

<http://wrap.warwick.ac.uk/80032>

Copyright and reuse:

This thesis is made available online and is protected by original copyright.

Please scroll down to view the document itself.

Please refer to the repository record for this item for information to help you to cite it.

Our policy information is available from the repository home page.

For more information, please contact the WRAP Team at: wrap@warwick.ac.uk

UNIVERSITY OF WARWICK

DOCTORAL THESIS

Temporal and spatial factors affecting synaptic transmission in cortex

Author:

Alex D. Bird

Supervisors:

Magnus J. E. Richardson

Mark J. Wall

*A thesis submitted in fulfilment of the requirements
for the degree of Doctor of Philosophy*

Theoretical Neuroscience Group

Warwick Systems Biology Doctoral Training Centre

Warwick Systems Biology Centre

School of Life Sciences

THE UNIVERSITY OF
WARWICK

February 2016

Declaration of Authorship

I, Alex Bird, declare that this thesis titled, ‘Temporal and spatial factors affecting synaptic transmission in cortex’ and the work presented in it are my own. I confirm that:

- This work was done wholly or mainly while in candidature for a research degree at this University.
- Where any part of this thesis has previously been submitted for a degree or any other qualification at this University or any other institution, this has been clearly stated.
- Where I have consulted the published work of others, this is always clearly attributed.
- Where I have quoted from the work of others, the source is always given. With the exception of such quotations, this thesis is entirely my own work.
- I have acknowledged all main sources of help.
- Where the thesis is based on work done by myself jointly with others, I have made clear exactly what was done by others and what I have contributed myself.

Signed:

Date:

Abstract


Synaptic transmission in cortex depends on both the history of synaptic activity and the location of individual anatomical contacts within the dendritic tree. This thesis analyses key aspects of the roles of both these factors and, in particular, extends many of the results for deterministic synaptic transmission to a more naturalistic stochastic framework.

Firstly, I consider how correlations in neurotransmitter vesicle occupancy arising from synchronous activity in a presynaptic population interact with the number of independent release sites, a parameter recently shown to be modified during long-term plasticity. I study a model of multiple-release-site short-term plasticity and derive exact results for the postsynaptic voltage variance. Using approximate results for the postsynaptic firing rate in the limits of low and high correlations, I demonstrate that short-term depression leads to a maximum response for an intermediate number of presynaptic release sites, and that this in turn leads to a tuning-curve response peaked at an optimal presynaptic synchrony set by the number of neurotransmitter release sites per presynaptic neuron. As the nervous system operates under constraints of efficient metabolism it is likely that this phenomenon provides an activity-dependent constraint on network architecture.

Secondly, I consider how synapses exhibiting short-term plasticity transmit spike trains when spike times are autocorrelated. I derive exact results for vesicle occupancy and postsynaptic voltage variance in the case that spiking is a renewal process, with uncorrelated interspike intervals (ISIs). The vesicle occupancy predictions are tested experimentally and shown to be in good agreement with the theory. I demonstrate that neurotransmitter is released at a higher rate when the presynaptic spike train is more regular, but that positively autocorrelated spike trains are better drivers of the postsynaptic voltage when the vesicle release probability is low. I provide accurate approximations to the postsynaptic firing rate, allowing future studies of neuronal circuits and networks with dynamic synapses to incorporate physiologically relevant spiking statistics.

Thirdly, I develop a Bayesian inference method for synaptic parameters. This expands on recent Bayesian approaches in that the likelihood function is exact for both the quantal and dynamic synaptic parameters. This means that it can be used to directly estimate parameters for common synaptic models with few release sites. I apply the method to simulated and real data; demonstrating a substantial improvement over analysis techniques that are based around the mean and variance.

Finally, I consider a spatially extended neuron model where the dendrites taper away from the soma. I derive an accurate asymptotic solution for the voltage profile in a dendritic cable of arbitrary radius profile and use this to determine the profile that optimally transfers voltages to the soma. I find a precise quadratic form that matches results from non-parametric numerical optimisation. The equation predicts diameter profiles from reconstructed cells, suggesting that dendritic diameters optimise passive transfer of synaptic currents.

 HANKS to Magnus Richardson and Mark Wall for continued guidance and support throughout the course of my PhD, they have made the time I have spent on this project both productive and enjoyable. They have been models of professionalism and shown how well experimental and theoretical collaboration in neuroscience can work. I would also like to thank Hermann Cuntz for the help with and time spent on our external collaboration.

I would like to thank the rest of the Theoretical Neuroscience Group for their help and companionship; in particular Ruth Harbord, Tim Kaufmann, and Michael Fisher for their expertise on the experimental side of the project. Thanks to my PhD committee members Yulia Timofeeva, Marco van den Top, and Colm Connaughton for their helpful advice over the years.

I would also like to thank the Warwick Systems Biology DTC for giving me the opportunity to undertake this project, and the studentship made available by the BBSRC. Travel grants from ACCN, OCNS, Guarantors of Brain, FIAS, and ISN* have helped me attend workshops and conferences and enriched my studies.

It has been a fantastic experience to spend time working at the Systems Biology Centre and I would like to thank the staff and students whom I have had the privilege of getting to know during my time at Warwick.

Finally thank you to my family for supporting me throughout my many, many years of study, and to Liz, for putting up with me over the last couple of months and bringing me cups of tea.

** Biotechnology and Biological Sciences Research Council, Advanced Course in Computational Neuroscience, Organisation of Computational Neuroscience Societies, Frankfurt Institute for Advanced Studies, and Integrated Systems Neuroscience.*



Temporal and spatial factors governing synaptic transmission in cortex

Theoretical Neuroscience Group
Systems Biology Doctoral Training Centre
Systems Biology Centre
School of Life Sciences

Doctor of Philosophy

Alex D. BIRD

Published Material

The following papers were published in the course of this study:

Bird A. D. and M. J. E. Richardson. Long-term plasticity determines the postsynaptic response to correlated afferents with multivesicular short-term synaptic depression. *Frontiers in Computational Neuroscience* vol. 8, art. 2. January 2014.

Contents

Declaration of Authorship	i
Abstract	ii
Acknowledgements	iii
Published material	iv
Contents	v
List of Figures	viii
List of Tables	x
Abbreviations	xi
Symbols	xii
1 Introduction	1
1.1 Introduction	1
1.1.1 Basic neuronal physiology	1
1.1.2 Brain architecture and cortical structure	4
1.2 Synaptic transmission	7
1.2.1 Structure of a chemical synapse	7
1.2.2 Function of a chemical synapse	10
1.3 Synaptic plasticity	11
1.3.1 Short-term synaptic plasticity	11
1.3.2 Long-term synaptic plasticity	14
1.3.3 Spike-train statistics	14
1.3.4 Neuromodulators and retrograde transmission	16
1.3.5 Paired whole-cell patch-clamp recording	16
1.4 Neurons	17
1.4.1 Thick-tufted Layer V pyramidal cell	17
1.4.2 Other neurons	19
1.5 Optimality in dendritic structure	21
1.5.1 Spatially extended neuron models	22

1.5.2	Synaptic equalisation and ‘dendritic democracy’	23
1.6	Thesis Structure	23
2	Long-term plasticity determines the postsynaptic response to correlated afferents with multivesicular short-term synaptic depression	25
2.1	Overview	25
2.1.1	Author contributions	26
2.2	Intoduction	27
2.3	Methods	28
2.4	Results	29
2.4.1	Vesicle occupancy crosscorrelations	30
2.4.2	Neurotransmitter release crosscorrelations	30
2.4.3	Membrane voltage mean and variance	31
2.4.4	Release site number and postsynaptic rate	32
2.4.5	Long-term plasticity and response to synchrony	33
2.4.6	Optimal response and synchrony jitter	33
2.4.7	Optimal-response curves are a robust feature of synaptic homeostasis	34
2.5	Discussion	34
2.6	References	35
2.7	Appendix	37
2.7.1	Derivation of the voltage variance	37
2.8	Additional Discussion	38
2.8.1	Synaptic kernels	38
2.8.2	Location of the maximum in the postsynaptic voltage variance . .	38
2.8.3	Validity of the low n approximation	40
2.8.4	The limit $R_r \rightarrow \infty$	40
2.8.5	Setting tuning curves with release probability p	40
3	Synaptic transmission of spike trains with arbitrary interspike interval statistics	42
3.1	Overview	42
3.1.1	Author contributions	43
3.2	Introduction	44
3.3	Methods and Models	45
3.4	Results	48
3.4.1	Prespike and overall occupancy means for a renewal process	49
3.4.2	Gamma ISIs	50
3.4.3	Experimental validation of predicted $\langle x \rangle_\infty$ values	51
3.4.4	Fluctuation-driven ISIs	51
3.4.5	Autocorrelations in vesicle release	53
3.4.6	The postsynaptic response	56
3.4.7	Effect of multiple release sites	57
3.4.8	Postsynaptic firing rates estimated by the matched-variance method	59
3.5	Discussion	60
3.5.1	Extensions	62
4	Bayesian inference for the quantal parameters of dynamic synapses	64
4.1	Overview	64

4.1.1	Author contributions	64
4.2	Introduction	66
4.3	Methods	68
4.4	Results	74
4.4.1	Computing exact likelihoods	74
4.4.2	Example likelihood calculation	78
4.4.3	Identifiability of number of release site number n and release probability p_0	80
4.4.4	Depression at juvenile synapses for noisy connections	80
4.4.5	Adenosine at juvenile synapses	82
4.5	Discussion	82
4.5.1	Extensions	84
5	Optimal current transfer in dendrites	85
5.1	Overview	85
5.1.1	Author contributions	85
5.2	Optimal current transfer in dendrites	86
5.3	Supplementary material: Overview	93
5.4	Derivation of the cable equation for an arbitrary dendritic radius profile	93
5.5	First-order multiple scales approximation	95
5.5.1	Homogenous solution	95
5.5.2	Current injection	96
5.5.3	Proximal voltage propagation	97
5.6	Validity of approximation in real dendrites	98
5.7	Extending the approximation	98
5.7.1	Higher-order terms	98
5.7.2	Transient solution	99
5.7.3	Complex dendritic structures	100
5.8	Optimality of current transfer	101
5.8.1	Algorithm for optimising an arbitrary dendritic tree	103
5.9	Morphological data and numerical methods	103
5.9.1	Dendritic morphologies and passive parameters	103
5.9.2	Numerical methods	104
6	Discussion	105
6.1	Introduction	105
6.2	Extensions	107
6.3	Concluding Remarks	108
	Bibliography	109

List of Figures

1.1	Cortical neurons, chemical synapses, and distributed inputs	2
1.2	Basic neuronal physiology	5
1.3	Brain architecture and cortical structure	7
1.4	Structure of a chemical synapse	10
1.5	Short-term synaptic plasticity	11
1.6	Correlations between neurons and within spike trains	15
1.7	Thick-tufted Layer V pyramidal cell	18
1.8	Other neuronal morphologies	21
2.1	Stochastic quantal model	28
2.2	Release-site occupancy is correlated, neurotransmitter release events are anticorrelated	31
2.3	Exact voltage variance for a postsynaptic neuron receiving multiple depressing synaptic contacts from a presynaptic population	32
2.4	Membrane voltage distributions become markedly non-Gaussian as correlations increase	32
2.5	The postsynaptic firing rate exhibits a maximum as a function of the number of pre-to-post release sites n	33
2.6	Long-term plasticity that alters release-site number n sets the sensitivity to presynaptic synchrony	34
2.7	Impact of synchrony jitter on the optimal response curves	34
2.8	Curves with a maximal postsynaptic rate at intermediate n are a robust feature	35
3.1	Gamma interspike intervals demonstrate the effects of regularity on theoretical vesicle occupancy	50
3.2	Changes in mean EPSP amplitude for experimental paired-cell recordings	52
3.3	Theoretical vesicle occupancy for noise-driven LIF neurons	54
3.4	Theoretical release autocorrelations and voltage variances	55
3.5	The theoretical effect of multiple release sites per presynaptic neuron	60
3.6	Simulated postsynaptic firing rates are well-approximated by the matched-variance method	61
4.1	An illustration of the procedure for calculating exact likelihoods	76
4.2	Identifiability of parameters in a quantal model with no uncertainty in ‘mini’ quantal size (simulated data)	77
4.3	Joint distribution of release-site number n and release probability p_0 (Simulated data)	78
4.4	DEP model applied to a noisy juvenile synapse (experimental data)	81

4.5	Change in synaptic dynamics after application of adenosine (experimental data)	83
5.1	Cable theory with arbitrary diameters: Accuracy of the asymptotic approximation	87
5.2	Diameter profiles to optimise current transfer	88
5.3	Real dendrites are constrained by current transfer optimality	91
5.4	Regions of reconstructed dendrites where the asymptotic approximation holds strongly	97
5.5	Second-order approximation provides better results when ϵ is larger . . .	99
5.6	Asymptotic solution allows recovery of classical cable properties	104

List of Tables

2.1	Typical parameters used for figures	30
3.1	Typical parameter values used for figures	48
4.1	Table of synaptic models used and their inferred parameters	70
4.2	Table of inferred, fixed, and dynamic, synaptic parameters used in the model and their ranges	73

Abbreviations

AHP	Afterhyperpolarisation
AMPA	α -amino-3-hydroxy-5-methyl-4-isoxazoleproponic acid
AMPAR	α -amino-3-hydroxy-5-methyl-4-isoxazoleproponic acid receptor
Ca^{2+}	Calcium anion
Cl^-	Chloride cation
EPSP	Excitatory postsynaptic potential
GABA	γ -aminobutyric acid
HS	Horizontal system (of the blowfly lobula plate)
K^+	Potassium anion
ISI	Interspike interval
LIF	Leaky integrate-and-fire (neuron model)
mGluR	Metabotropic glutamate receptor
Na^+	Sodium anion
NMDA	N-methyl-D-aspartate
NMDAR	N-methyl-D-aspartate receptor
VS	Vertical system (of the blowfly lobula plate)

Symbols

a	amplitude of voltage increase induced by a single neurotransmitter vesicle	mV
a_e	mean amplitude of shot noise	mV
E_0	resting membrane voltage	mV
g_l	membrane conductance per unit area	$\Omega^{-1}\text{m}^{-2}$
I_h	hyperpolarisation-activated depolarising current	A
M	total number of presynaptic vesicle release sites (nN)	
n	number of vesicle release sites at a single synapse	
N	number of neurons that synapse onto a single postsynaptic cell	
p	neurotransmitter release probability	
r_a	axial resistance of a neurite	Ωm
R_a	rate of presynaptic spiking	Hz
R_e	rate of excitatory shot noise drive	Hz
R_r	rate of vesicle replacement ($\frac{1}{\tau_D}$)	Hz
v	membrane voltage above rest ($V - E_0$)	mV
V	membrane voltage	mV
V_{re}	membrane reset voltage after a spike	mV
V_{th}	membrane threshold voltage for spike initiation	mV
x	occupancy of a vesicle release site	
y	total occupancy of all release sites at a synapse	
α	shape parameter of a gamma distribution	
ζ	neurotransmitter release train from presynaptic population	Hz
μ_f	mean interspike interval	s
σ_v	strength of gaussian noise	mV
τ	membrane time constant (see τ_L)	s

τ_D	depression time constant ($\frac{1}{R_r}$)	s
τ_l	membrane time constant (see τ)	s
χ	neurotransmitter release train from single site	Hz

Note: *Additional symbols and units are used in the discussion of various forms of plasticity in Chapter 4 and are tabulated there (Table 4.2).*

For K

Chapter 1

Introduction

1.1 Introduction



THE neocortex is the largest part of the human brain and is involved in higher functions such as sensory perception, generation of motor commands, spatial reasoning, conscious thought, and language. The complexity that enables it to perform these roles arises largely from the diversity of the hundreds of trillions of connections between a hundred billion excitatory neurons (Fig. 1.1). These connections, or synapses, adapt to activity on timescales ranging from milliseconds to days. In addition, they are located on a spatially extended dendritic tree and are often hundreds of microns from the postsynaptic cell body, introducing potential for synaptic signals to decay before they reach the body of the cell.

This thesis examines how the properties of chemical synapses govern transmission of signals across the cortex. The study follows two complementary routes, analysing both the temporal dynamics and spatial distribution of synaptic connections. The key factors considered are short-term synaptic plasticity, activity-dependent changes in synaptic efficacy, and current transfer, the location-dependent flow of synaptic currents to the body of the cell.

1.1.1 Basic neuronal physiology

Neurons store and process information by holding a voltage across their cell membranes. This is achieved through maintaining a high concentration of Na^+ sodium and Ca^{2+} calcium ions outside the cell, balanced to some extent by a higher concentration of K^+ potassium inside (Fig. 1.2a). Cl^- chloride ions are also important and are more concentrated outside the cell. Structurally, the membrane consists of a lipid bilayer, which is

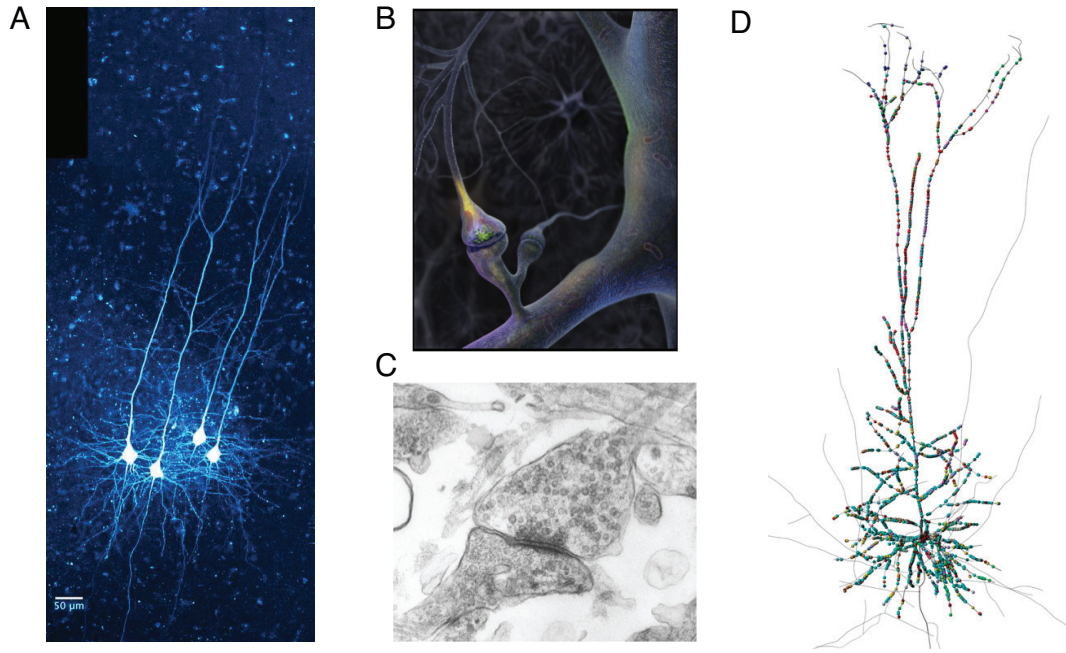


Figure 1.1: Cortical neurons, chemical synapses, and distributed inputs. **(A)** Four layer-V pyramidal neurons filled with fluorescent dye. This class of neuron is a major subject of this thesis. **(B)** A schematic of a chemical synapse. Presynaptic action potentials arrive in the bouton (top), released neurotransmitter diffuses across the synaptic cleft and binds to receptors on the postsynaptic density of a dendritic spine (bottom), causing a local change in conductance which allows a synaptic current to flow. **(C)** An electron microscope image of a synapse. Neurotransmitter vesicles are visible in the presynaptic terminal (right). **(D)** Predicted synaptic inputs onto a reconstruction of a layer-V pyramidal neuron. Panels from: **A** R Harbord, University of Warwick, **B** G Johnson, *Science*, **C** NeuralNoises, and **D** (Hill et al. 2012).

relatively impermeable to charged particles, containing embedded proteins which allow ions to pass through either passively under a voltage, actively against a voltage or passively only once a certain voltage has been exceeded. The lipid bilayer of the membrane therefore stores charge, acting as a capacitor, with ion channels acting as resistors in parallel for different ionic species (Fig. 1.2a).

The $\text{Na}^+ - \text{K}^+$ pump actively transports Na^+ out of the cell, against the electrochemical gradient, and K^+ into the cell; constructing the ionic imbalance that causes the transmembrane voltage. A higher concentration of K^+ channels means that the effective permeability of the membrane is higher for K^+ ions than for Na^+ , allowing them to diffuse across under the electrochemical gradient. Perturbations to the resting potential across a membrane decay with a timescale τ_l . A typical resting value for the membrane potential of a cortical Layer V cell is -70mV and τ_l is around 10ms . If the voltage is above rest the cell is said to be depolarised and if the voltage is below it is hyperpolarised.

Neurons are excitable. A sufficient deviation in the membrane voltage ($\approx 10\text{mV}$ in

Layer V pyramidal cells) causes voltage-gated Na^+ channels to open and a fast influx of positive ions increases the membrane voltage by around 100mV, before slower-opening voltage-gated K^+ channels return the cell to rest (Fig. 1.2b). This is referred to as an action potential, or spike, and the cell is said to have spiked, or fired (Hodgkin et al. 1952). The whole process takes less than a few milliseconds. The action potential is the most important feature of a neuron and allows individual cells to integrate inputs before giving rise to an ‘all-or-nothing’ event which is transmitted to other cells. The decay of voltage fluctuations from the resting potential mean that inputs must be temporally close to be successfully combined into a deviation sufficient to cause a spike. Neurons are assumed to transmit signals through either the overall rate at which they spike, or with the precise timing of their action potentials (de Charms and Merzenich 1996; Averbeck et al. 2006); a succession of action potentials is referred to as a spike train. The times between spikes in a train are called interspike intervals (ISIs). The importance of spiking sometimes allows neurons to be abstracted as a decaying membrane voltage equipped with a mechanism to record a spike and reset the voltage when a threshold is reached. This is the influential leaky integrate-and-fire (LIF) model (Lapicque 1907; Brunel and van Rossum 2007) that is used throughout the first two chapters of the thesis.

Neurons are typically spatially extended, making connections far from the cell body, or soma. The processes branching from the cell body are collectively referred to as neurites and are grouped into two broad classes: dendrites and axons. Dendrites typically receive connections from other cells and axons typically make them (Fig. 1.2c). These are broad categories and the existence has been noted, alongside the ‘classical’ axo-dendritic and axo-somatic contacts, of dendro-dendritic (Rall et al. 1966), axo-axonal (Atwood and Morin 1970) and dendro-axonal (Gobell 1976) connections. Connections are referred to as synapses (Sherrington 1906).

Action potentials are initiated in the soma or segments of axon immediately adjacent to it and propagate largely by active means. Axons in the peripheral nervous system can extend up to 1m (from the base of the spinal column to the foot), but in the brain are mostly a few hundred microns in length. Longer sections are often myelinated: wrapped in an additional lipid sheath to insulate the neurite, reducing energy loss and delay when transmitting spikes. Dendrites are also often capable of initiating active processes when the local voltage reaches a certain threshold (Llinás 1988). These features help to propagate distant synaptic signals to the soma and allow regions of the dendrite to separately process synaptic inputs, making a single neuron capable of performing substantial computations (London and Häusser 2005). Regions of neurite far from the soma are referred to as distal and those close to the soma are referred to as proximal.

Synapses are typically grouped into excitatory, which increase the likelihood of the post-synaptic cell generating an action potential, and inhibitory which reduce this likelihood. Excitatory synapses achieve this through opening ion channels that allow depolarising current to flow into the cell, whereas inhibitory synapses either hyperpolarise the cell or increase the permeability of the membrane, allowing excitatory currents to decay faster and reducing the ‘window’ within which excitatory events can be integrated. The second type of inhibition is referred to as ‘shunting’. This description is again simplified slightly as an effect known as post-inhibitory rebound (Sherrington 1913; Granit 1956) can cause cells to fire after receiving a barrage of inhibition due to delayed compensation by depolarising currents.

1.1.2 Brain architecture and cortical structure

Different regions of the brain have different roles and so contain very different classes of neurons. This thesis is mostly concerned with the neocortex, but many of the results also apply to other brain regions. An overview of brain architecture helps to relate the local functionality discussed here with the broader computational role of the brain.

The central nervous system generally receives sensory signals as inputs and generates motor signals as outputs. The basic functionality necessary to maintain life is found in the brain stem, which regulates cardiac rhythms and breathing. The brain stem forms part of the hindbrain alongside the cerebellum, or ‘little brain’, which is associated with balance and motor coordination (Fig. 1.3a). A unique feature of the cerebellum is that the output to other brain regions is made up entirely of inhibitory synapses. The midbrain acts as a relay for sensory information arriving from the peripheral nervous system via the pons in the brainstem and is also associated with emotion and control of hormones. Two midbrain regions of note here are the hippocampus, which is associated with navigation and memory formation, and the thalamus, which synapses onto the cerebral cortex.

The outer layer of the cerebral cortex is the evolutionarily youngest part of the cortex, and is referred to as the neocortex. It is this region that is associated with higher cognitive functions such as processing sensory information, generating motor commands, storing of memories, and reasoning. Different spatial regions have different functions, for example processing visual input or generating motor output, and slightly different structures, but the neocortex has remarkably well-conserved features across its considerable area (Silberberg et al. 2002). The mammalian neocortex, henceforth shortened to cortex, contains six layers (Fig. 1.3b), distinguishable both visually and by types of cell

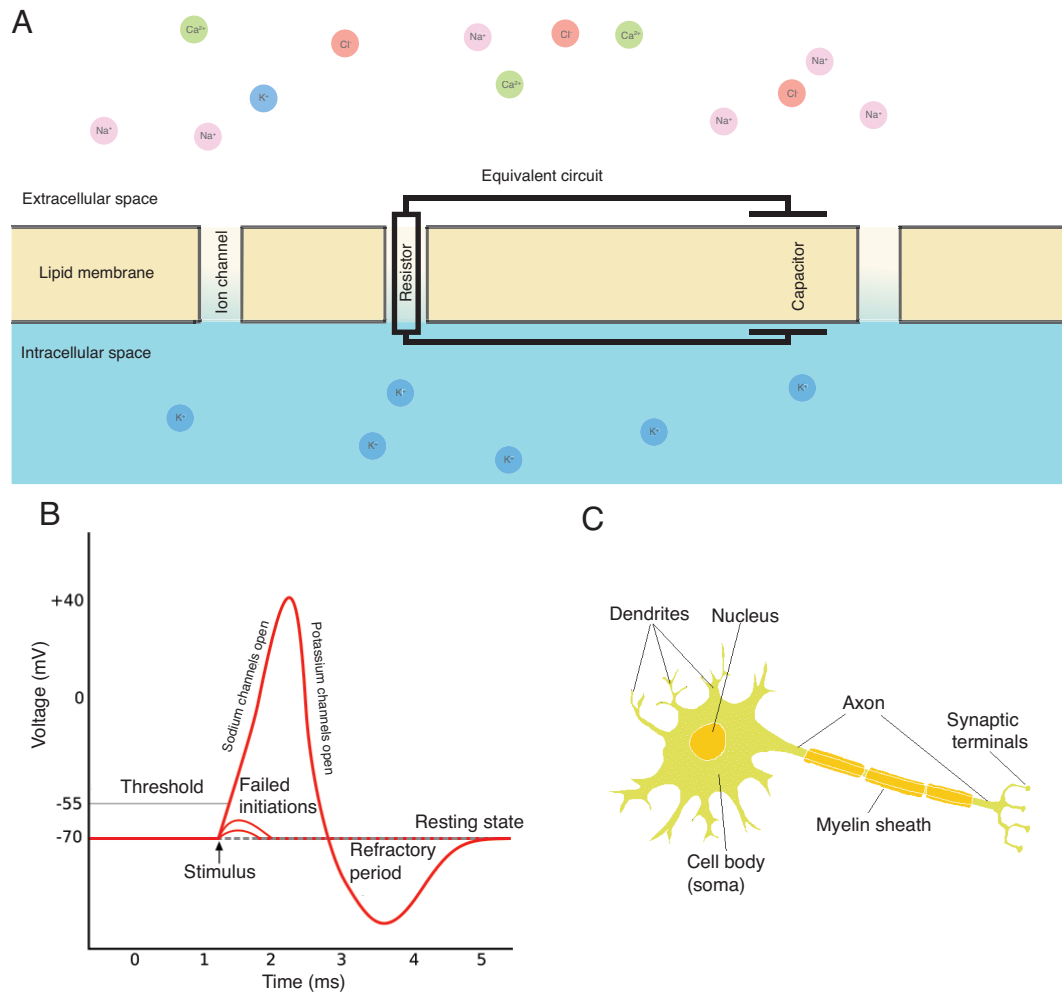


Figure 1.2: Basic neuronal physiology. **(A)** Schematic of neuronal membrane and equivalent circuit. K^+ is more concentrated within the cell and Na^+ is more concentrated outside, creating a potential difference across the membrane. The lipid bilayer acts as a capacitor, storing charge, and the ion-specific transmembrane channels act as resistors. **(B)** Schematic of an action potential. Stimulus below the threshold fails to initiate an ‘all-or-nothing’ action potential. Once the threshold is crossed, Na^+ channels open, allowing a fast influx of current. This is counteracted by the slower opening of K^+ channels that allow current to leave the cell. After an action potential, the neuron is temporarily unable to initiate another due to the effect of the K^+ and undergoes a refractory afterhyperpolarisation (AHP). Panel adapted from www.innovateus.net. **(C)** Spatially extended neuron, showing axon, dendrite, and soma. Panel adapted from C Boeree, Shippensburg University

found there (Fig. 1.3c). The basic structure and function of these layers are discussed below:

Layer I. The uppermost layer, Layer I, contains very few cell bodies. Dendrites from neurons with soma in deeper cortical regions branch extensively in this region, where they receive excitatory and inhibitory synapses. Often the excitatory synapses are from cells with soma in a different layer to that of the postsynaptic cell, allowing interlaminar communication, or are from different cortical regions or the thalamus (Rubio-Garrido et al. 2009). These synapses can be considered long-range.

Layer II/III. Layers II and III are often considered together as they differ strongly only in the cortical areas processing visual input. Excitatory neurons in this layer receive excitatory synapses from Layer IV and synapse both intralaminarly and onto cells with bodies in Layer V (Feldmeyer et al. 2002).

Layer IV. Layer IV is the major target of long-range connections from both different cortical areas and the thalamus. It is notably absent in the region of cortex associated with generating motor commands. The neurons here make excitatory interlaminar connections to Layer II/III.

Layer V. Layer V is the cortical layer most considered in this thesis. Layer V provides the major outputs to other areas of cortex and brain. The cell class most discussed here, the thick-tufted Layer-V neuron, is found mostly in the lower portion of this layer, where they receive long-range excitatory input from the thalamus, via Layers IV and II/III, and inhibitory input from interneurons with soma in Layer V. They also form well-structured local networks with other Layer V pyramidal cells (Song et al. 2005; Perin et al. 2011), with synapses located mostly within Layer V (Markram et al. 1997).

Layer VI. The deepest cortical layer is commonly referred to as the polymorphic layer as the cells found here are more heterogeneous than in other layers (Fig. 1.3c). The functions of these cells are less easily categorised than those in other layers, but an important output is to the thalamus, providing cortico-thalamic feedback to the strong thalamo-cortical inputs (Crandall et al. 2015).

Alongside this vertical layered structure, the cortex is organised horizontally around columns that span all six layers (Mountcastle et al. 1957). Connections are more probable between neurons sharing a column and inputs to and outputs from a column tend to be shared. The region of cortex that processes sensory inputs that are not visual or auditory is called the somatosensory cortex. In a part of this region in the rodent brain, cortical columns correspond precisely with individual whiskers: a single whisker induces activity in a single column (Woosley and van der Loos 1970).

The final subdivision of the cortex is the microcircuit. Neocortical microcircuits are defined by stereotyped intracolumnar, interlaminar connectivity (Douglas et al. 1989). They are conserved across brain regions and species and are well-studied as a potential canonical and fundamental unit of computation (Lübke and Feldmeyer 2007).

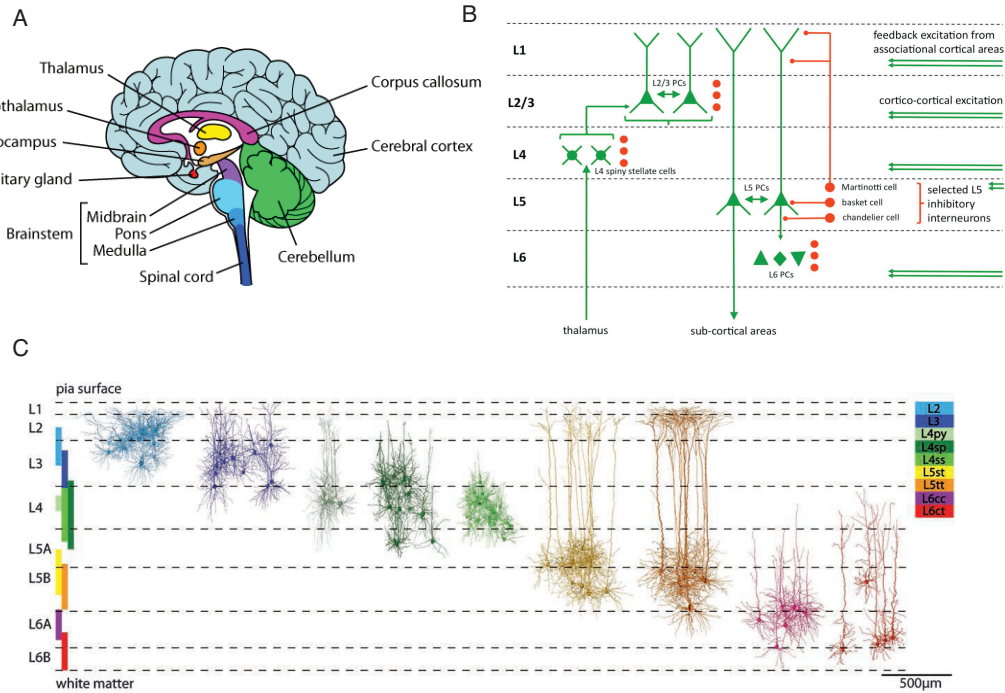


Figure 1.3: Brain architecture and cortical structure. **(A)** Schematic of the human brain, with areas discussed in the text labelled. Panel from D McDaniel, Arizona State University. **(B)** Schematic of the neocortex, showing key excitatory and inhibitory connections between and within cortical layers. Panel from M Richardson, University of Warwick. **(C)** Diversity of excitatory cell classes by layer. Thick-tufted Layer V pyramidal cells are third from the right. Panel from (Oberlaender et al. 2012).

1.2 Synaptic transmission

Neurons are generally insulated from one another (Waldeyer 1891; Cajal 1899); changes in voltage cannot propagate between cells without synaptic intermediaries. The more evolutionarily and structurally primitive method of sharing voltage between cells is an electrical synapse or gap junction: a partially uninsulated section of membrane between two neurons. This allows a flow of current between the two cells and provides a fast and simple method of transmitting information. In the mammalian cortex, however, the vast majority of synapses are chemical and rely on an intermediary neurotransmitter to communicate. The structure and functional roles of this form of synaptic transmission are discussed below, followed by an introduction to rate- and timing-based neuronal codes.

1.2.1 Structure of a chemical synapse

A synapse is defined as the connection between a presynaptic neuron and a postsynaptic neuron (Sherrington 1906). This connection generally consists of a number of anatomical contacts that together allow signal transmission. Some synapses are mixed, with contacts

that function via neurotransmitter and others via direct electrical coupling (Hamzei-Sichani et al. 2012), but most consist entirely of neurotransmitter-mediated contacts. A chemical synaptic contact is made up of a presynaptic terminal, a synaptic cleft, and a postsynaptic density (Fig. 1.4).

Within the presynaptic terminal, the neurotransmitter is contained within a lipid bilayer membrane, forming a structure known as a vesicle around 40nm in diameter (Südhof 2004). The presynaptic terminal has a number of active, or release, sites on the membrane where neurotransmitter vesicles can dock (Schikorski and Stevens 2001). When the presynaptic cell spikes, voltage-gated calcium channels in the presynaptic terminal open and allow an influx of Ca^{2+} . The Ca^{2+} has the potential to trigger a release of neurotransmitter from vesicles docked at release sites (Fatt and Katz 1954; Katona and Freund 1969; Neher and Sakaba 2008; Nakamura et al. 2015). The probability that a single docked vesicle will release neurotransmitter on arrival of an action potential is typically quite low, often less than half. Synapses are thus ‘reliably unreliable’ (Goda and Südhof 1997; Ribault et al. 2011).

The synaptic cleft is on the order of 20nm wide and neurotransmitter molecules pass across it by diffusion. On reaching the postsynaptic density, the neurotransmitter molecules bind to transmitter-gated ion channels, causing them to open and thus alter the conductance of the postsynaptic cell. Transmitter molecules do not remain in the cleft for long, they are either broken down by enzymes, taken up by non-neuronal glial cells, or recycled into vesicles in the presynaptic cell for re-use. Vesicles filled with recycled or newly synthesised neurotransmitter are trafficked to empty release sites. Recent experimental techniques allowing manipulation of individual vesicles have greatly enhanced understanding of the details of this process (Trigo et al. 2012; Park et al. 2012).

At the postsynaptic cell, open transmitter-gated ion channels can have a variety of effects. Excitatory neurotransmitters typically open sodium and potassium channels causing an influx of Na^+ anions that depolarise the postsynaptic cell causing an excitatory postsynaptic potential (EPSP). The fast opening and slow closing of transmitter-gated ion channels means that the EPSP takes the form of a difference of exponentials (Eccles et al. 1941; Richardson and Silberberg 2008). Inhibitory neurotransmitters typically target K^+ or Cl^- channels, allowing K^+ to diffuse down its concentration gradient out of the cell or Cl^- to flow down its concentration gradient into the cell; both have a hyperpolarising effect. As neurotransmitters increase the conductance of the membrane, they allow excitatory currents to decay more quickly by reducing the effective membrane time constant τ_l . This reduces the time window over which temporally separated excitatory inputs can be integrated and leads to a form of inhibition referred to as silent, or

‘shunting’, inhibition (Eccles 1964). An important feature of excitatory synapses is that due to the equilibrium potential of Na^+ being much higher than the resting potential of the cell, the voltages induced by excitatory neurotransmitters from different vesicles can be well-approximated by a linear sum (Burke 1967; Bekkers 2003). This approximation is used throughout the thesis.

The fact that neurotransmitter is released from vesicles means that EPSPs are ‘built up’ statistically of small all-or-none units which are identical in size with the spontaneous ‘miniature’ postsynaptic potentials (del Castillo and Katz 1954). Synaptic transmission is therefore quantal (Boyd and Martin 1956; Liley 1956), and the EPSP induced by a single quanta of neurotransmitter is referred to as a ‘mini’ EPSP, following del Castillo and Katz.

Neurotransmitters were first identified by Otto Loewi in 1921. In cortex, the most prevalent excitatory and inhibitory neurotransmitters are glutamate and γ -aminobutyric acid (GABA) respectively. Synapses that use glutamate are referred to as glutamatergic and those that use GABA are referred to as GABAergic. Glutamate receptors for transmitter-gated ion channels in the postsynaptic density include the α -amino-3-hydroxy-5-methyl-4-isoxazolepropionic acid receptor (AMPA) and N-methyl-D-aspartate receptor (NMDAR). Both are implicated in long term changes to the strength of synapses, discussed below. In addition to the fast action of ion-channel-linked (ionotropic) receptors, other, metabotropic, neurotransmitter receptors indirectly influence neuronal function through second-messenger signalling: triggering the release of ‘second’ messenger molecules from intracellular stores. An important class is the metabotropic glutamate receptors (mGluRs), which have slower and longer-lasting actions than those triggered by AMPARs and NMDARs (Nakanishi 1994). mGluRs have a variety of effects, causing excitation or inhibition or modulating the efficacy of synapses onwards from the postsynaptic cell (Pin and Duvoisin 1995). Neurotransmitters are generally abundant and easy to synthesise: glutamate, for example, is an amino acid and GABA is directly synthesised from it. This helps to mitigate the high metabolic costs of synaptic transmission (Harris et al. 2012).

It is important to note that the number of anatomical contacts forming a synapse is in general not equal to the number of active sites from which neurotransmitter can be released. This ‘single-vesicle’ hypothesis was widely held (Kuno 1971; Korn et al. 1981; Redman 1990), particularly in cortex (Silver 2003), but more recent work has found that the distribution of cortical postsynaptic responses observed (Song et al. 2005; Lefort et al. 2009) is best explained by a number of release sites that can be substantially higher than the number of anatomical contacts (Loebel et al. 2009; Regehr 2012).

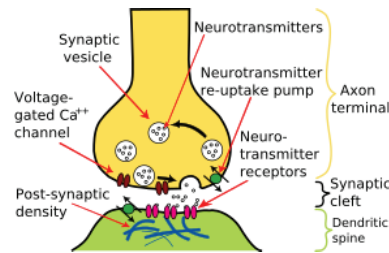


Figure 1.4: Structure of a chemical synapse. The presynaptic terminal (top) contains a number of active sites to which vesicles containing neurotransmitter can dock. On arrival of an action potential, neurotransmitter is probabilistically released and diffuses to receptors in the postsynaptic density (bottom). The site from which neurotransmitter has been released is inactive until a full vesicle is trafficked to the site. Panel from *Wikipedia*.

1.2.2 Function of a chemical synapse

Chemical synapses have a number of functional advantages over electrical synapses, despite growing evidence of interactions between the two modes of synaptic transmission (Pereda 2014) and the fact that electrical synapses have their own complexity (Landisman and Connors 2005). Chemical synapses transmit neuronal codes based either on a firing-rate or precise spike-timing (de Charms and Merzenich 1996) and are able to reverse the sign of transmission through use of inhibitory neurotransmitters; they also have an important gating role in only feeding a signal forward after the presynaptic cell has integrated its own synaptic inputs.

Chemical synapses are plastic: their strength alters through time. These changes occur on both short and long timescales and are a major subject of Chapters 2, 3, and 4. Synaptic plasticity is discussed in depth below.

Finally, chemical synapses are stochastic: an action potential is unlikely to induce release of neurotransmitter from all docked vesicles and will sometimes induce release from none (Kuno and Weakly 1972; Goda and Südhof 1997; White et al. 2000; Faisal et al. 2008; Ribault et al. 2011). This feature of synaptic function is surprising and has been well studied. From an information-theoretic point of view, synaptic unreliability enhances the information content of some codes (Zador 1998) and reduces the metabolic requirements of many others (Levy and Baxter 2002; Goldman 2004). The substantial ‘noise’ introduced by variability in synaptic transmission will also have a potentially critical effect on the firing-rate dynamics of a large-scale neuronal network (Salinas and Sejnowski 2000; Kuhn 2004; de la Rocha and Parga 2005). At an individual synapse, transmission will show a great deal of trial-to-trial variability and the models in Chapters 2, 3, and 4 specifically account for this.

For the rest of this thesis, the term ‘synapse’ without qualification will refer to a chemical synapse.

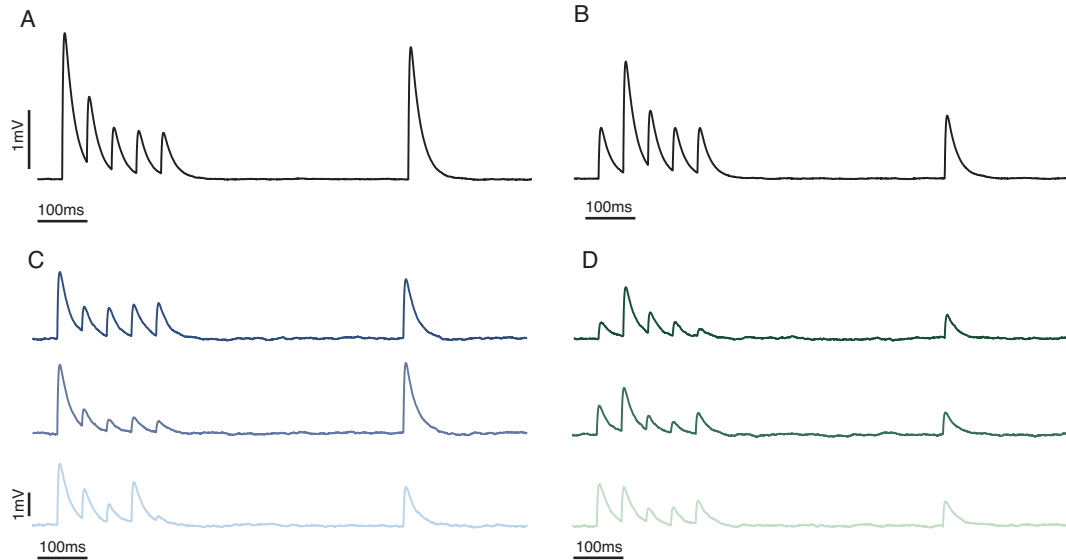


Figure 1.5: Short-term synaptic plasticity. Simulated EPSPs showing effects of vesicle depletion depression (left) and facilitation (right). **(A)**, **(B)** The average responses over 50 trials, showing the typical effects of depression and facilitation. **(C)**, **(D)** Individual postsynaptic responses, displaying considerable trial-to-trial variability.

1.3 Synaptic plasticity

Chapters 2, 3, and 4 of this thesis study the effects of short-term synaptic plasticity. The current section first introduces the basic ideas behind this phenomenon, before examining longer-term changes in synaptic strength which are an important part of the work introduced in Chapter 2. The next subsection discusses patterns of spiking activity seen *in vivo*, which are considered alongside short-term plasticity in Chapters 2 and 3. The penultimate subsection introduces the idea of neuromodulators, which alter neuronal and synaptic function over wider areas, one of which is studied in Chapter 4. The final subsection here briefly describes paired whole-cell patch-clamping, the experimental technique used to gather data about synaptic function.

1.3.1 Short-term synaptic plasticity

Changes in synaptic efficacy due to the immediate history of a synapse are referred to as short-term synaptic plasticity (Zucker and Regehr 2002). The most commonly seen and studied forms are vesicle depletion depression and facilitation (Fig. 1.5). Vesicle depletion depression occurs after an action potential has induced release from docked vesicles at presynaptic active zones, leaving those zones without the ability to release neurotransmitter until a new vesicle has been trafficked to the site, a process that typically takes a few hundred milliseconds (Eccles et al. 1941; Liley 1956; Vere-Jones 1966; Südhof 2004; Neher and Sakaba 2008). Facilitation arises when Ca^{2+} builds up in the presynaptic

terminal during persistent activity (Dudel and Kuffler 1961; Katona and Freund 1969). This residual calcium increases the probability that neurotransmitter will be released by subsequent action potentials and can increase the size of the second EPSP in a closely-spaced pair to five times the size of the first (Zucker and Regehr 2002). Together the two processes gives the synapse a ‘memory’ that lasts around ten to a hundred times longer than voltage fluctuations in the postsynaptic membrane (Mongillo et al. 2008), and have a variety of postulated computational roles (Abbott and Regehr 2004), including: gain control (Abbott 1997; Rothman et al. 2009), increasing information transmission (Zador 1998; Kilpatrick 2013; Scott et al. 2012), sensory adaptation (Furukawa et al. 1982; Hallermann and Silver 2013), and filtering inputs (Fortune and Rose 2001; Lindner et al. 2009; Rosenbaum et al. 2012; Nagel et al. 2015). The results presented in Chapters 2, 3, and 4 do not rely on a specific interpretation of the function of vesicle depletion depression, focussing mainly on the implications for firing rates in the postsynaptic cell and recovering information about synaptic parameters from experiments.

Different regions of cortex and different developmental states imply different ratios of depression and facilitation. Depression is more prevalent in cortical areas associated with sensory input (Thomson 1997) and in thalamocortical synapses (Boudreau and Ferster 2005), whereas facilitation becomes more prevalent in non-sensory cortical areas (Mongillo et al. 2008). Age is also an important factor, with a shift from predominately depressing to facilitating synapses throughout development in rodent models (Reyes and Sakmann 1999), although some regions of mature human cortex have been observed to exclusively depress (Testa-Silva et al. 2014). The parameter that most determines the ratio between depression and facilitation is the probability that an individual docked vesicle will release neurotransmitter on arrival of an isolated spike, p . A low p is likely to lead to facilitation dominating as a relatively low proportion of vesicles are released after the first spike and increases in release probability will have more of an impact. There is also a dependence on the spike-train that is being transmitted and some neurons are believed to route spike-trains with different statistics to different targets through different synaptic responses, with very high frequency spike trains causing depression and lower frequency trains inducing facilitation (Middleton et al. 2011; Nagel et al. 2015; Crandall et al. 2015).

The most influential models of short-term depression and facilitation are those of Abbott (1997) and Tsodyks and Markram (1997). These phenomenological models have enabled understanding of the dynamics of large networks of cells, revealing emergent behaviours that do not arise in models of static synapses (Tsodyks et al. 1998; Cortes et al. 2013). These models consider synaptic ‘resources’, which are deterministically depleted by a presynaptic action potential and recover at a fixed rate in the absence of stimulus. They are therefore a very good fit to the average behaviour of a synapse, but neglect the

stochasticity in both probabilistic vesicle release and variable vesicle recovery times, as well as the quantal nature of transmission (Fig. 1.5c and d). Models taking full account of this stochasticity have been applied where effects of trial-to-trial variability are particularly important (Fuhrmann et al. 2002; de la Rocha and Parga 2005; Rosenbaum et al. 2012); Chapters 2, 3, and 4 of this thesis apply a stochastic quantal model.

Whilst vesicle depletion depression and facilitation are the most commonly observed forms of short-term plasticity, the diversity and complexity of synapses (O’Rourke et al. 2012) mean that many other forms have also been described. Facilitation due to residual calcium decays on timescales with orders of hundreds of milliseconds, but less substantial increases in postsynaptic responses have been observed with timescales that are much longer. Augmentation has timescales of seconds to tens of seconds and post-tetanic potentiation has timescales of minutes; both can be explained by long-lived changes to the efficacy of the ion pumps at presynaptic terminals during stimulus, which alter the amount of Ca^{2+} that can enter during a subsequent spike (Regehr 1997; Zhong et al. 2001), and by effects on enzyme concentration (Fioravante and Regehr 2011). These processes occur on slightly longer timescales than those modelled in this thesis.

A more relevant alternative form of plasticity is release-independent depression (RID) (Dobrunz et al. 1997; Thomson and Bannister 1999), where the reduction in size of a second EPSP is uncorrelated with the size of the first. The mechanism for this is not entirely clear, but is believed to be a stimulus-dependent reduction in the rate at which Ca^{2+} can enter the terminal (Catterall and Few 2008; Regehr 2012) and is best modelled by a decrease in the release probability for successive spikes (Fuhrmann 2004). RID initially decays on timescales around 500ms, but is highly-correlated with frequency-dependent recovery (FDR), a reduction in the decay timescale during sustained activity. Both mechanisms are incorporated in the models fitted to synaptic datasets in Chapter 4.

Another feature that can reduce the impact of depression is a stimulation-dependent increase in the rate at which fresh vesicles are trafficked to empty release sites. The mechanism behind this is unclear but is believed to relate to the build-up of calcium in the presynaptic terminal (Wang and Kaczmarek 1998). The recovery of vesicles under intense stimulus follows a double exponential, suggesting two distinct processes, with a slow timescale that is invariant to stimulus and a fast timescale that is stimulus-dependent (Hosoi et al. 2007). This is believed to be an important factor in maintaining synaptic transmission at high-frequencies (Fioravante and Regehr 2011; Hallermann and Silver 2013).

Synaptic depression is sometimes also attributed to saturation and desensitisation of the receptors in the postsynaptic density (Kiskin et al. 1986; Otis et al. 1996) alongside

vesicle depletion. The two effects are indistinguishable under the phenomenological models of Abbott (1997) and Tsodyks and Markram (1997), but would have an impact on the interpretation of quantal models of release. Experiments to distinguish between these pre- and postsynaptic modes of depression have shown that neuronal mechanisms can specifically counteract receptor desensitisation (DiGregorio et al. 2007; Heine et al. 2008), that desensitisation is relatively unimportant for presynaptic firing rates on the order of 10Hz, and that vesicle depletion accounts for the majority of observed depression (Wong et al. 2003; Foster and Regehr 2004).

1.3.2 Long-term synaptic plasticity

Long-term changes in synaptic strength are the physiological correlate of memory formation (Hebb 1949). The factors that induce this are varied and beyond the scope of this thesis (Abbott and Nelson 2000; Markram et al. 2011), but the mechanism behind changing weights at excitatory glutamatergic synapses is important for Chapter 2. The glutamate receptors AMPAR and NMDAR can, under certain conditions, activate initially blocked channels in the postsynaptic density, increasing synaptic strength quickly, and induce changes in genetic transcription that strengthen the synapse over longer timescales (Kandel 2001; Bayazitov et al. 2007). These post-synaptic changes can be matched presynaptically by an increase in the number of vesicle release sites so that the average ‘mini’ EPSP amplitude is unchanged, but the total synaptic strength increases over a timescale of hours (Loebel et al. 2013).

Long-term depression has a similar mechanism, where the ‘mini’ amplitude is unchanged but the total strength decreases due to matched reductions in presynaptic release sites and postsynaptic receptors. As the long-term plasticity that gives rise to memories can provide positive-feedback, where synapses between co-active neurons strengthen repeatedly (Hebb 1949), a form of homeostatic plasticity is observed to balance ‘runaway’ connection strengths by weakening others (Turrigiano and Nelson 2004). This homeostatic plasticity is another consideration in Chapter 2.

1.3.3 Spike-train statistics

When dealing with stochastic quantal models of synaptic function it is often mathematically convenient to make the assumption that presynaptic spike times are uncorrelated (Fig. 1.6a) (Fuhrmann et al. 2002; Rosenbaum et al. 2012). This is not necessarily the case and analysis of *in vivo* spiking reveals correlations both between neurons (Aertsen et al. 1989; Schneidman et al. 2006) and autocorrelations within a single spike train (Fellous et al. 2003; Reyes 1999; Buzsaki and Draguhn 2004; Shinomoto et al. 2009).

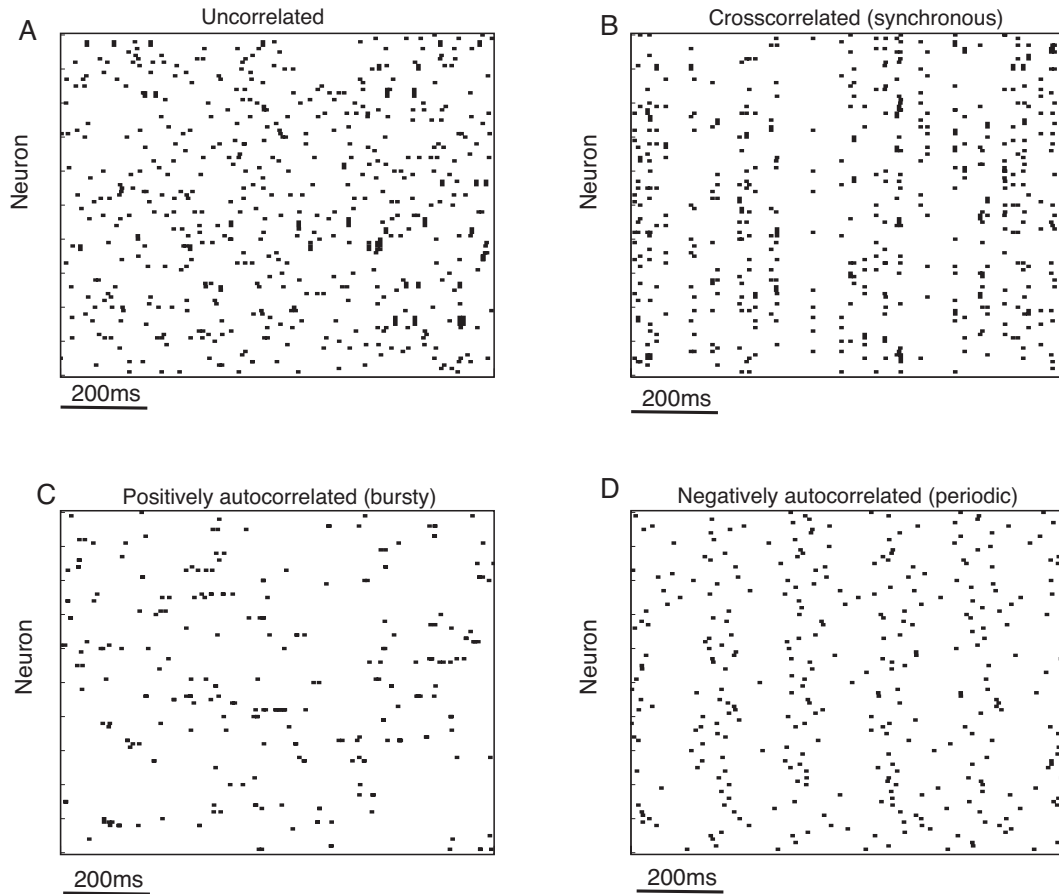


Figure 1.6: Correlations between neurons and within spike trains. Raster plots displaying the spike times of one hundred neurons under different types of correlation. **(A)** Independent neurons with Poisson spike trains. **(B)** Crosscorrelated (synchronous) neurons with individually Poisson spike trains. **(C)** Independent neurons, each firing as a positively autocorrelated spike (bursty) train. **(D)** Independent neurons, each with a negatively autocorrelated (periodic) spike train.

The results in Chapter 2 involve correlated spiking between presynaptic neurons, and those in Chapter 3 consider spike trains that are autocorrelated.

Correlations between spike trains (Fig. 1.6b) have relevance for encoding sensory information (von der Malsburg 1981; de Charms and Merzenich 1996; Averbeck et al. 2006), motor control (Baker et al. 2001; Capaday et al. 2013) and decision making (Cohen and Newsome 2008; Cain and Shea-Brown 2013). Recent work suggests that modulation of correlations can be more significant for neuronal coding than alterations in the presynaptic firing rate (Seriès et al. 2004; Mitchell et al. 2009; Cohen and Kohn 2011). Correlations within spike trains (Fig. 1.6 c and d) are an important part of neuronal codes (Ramcharan et al. 2000; Sherman 2001) and have substantial effects on how well spike trains propagate (Cateau and Reyes 2006; Lindner 2006; Reich and Rosenbaum 2013; Pipa et al. 2013; Dummer et al. 2014). Further effects are discussed in detail in Chapters 2 and 3.

1.3.4 Neuromodulators and retrograde transmission

In addition to the very local effects of neurotransmitters, neuronal and synaptic properties are also affected on a larger scale by neuromodulators (see Marder 2012, for a review). These are typically released during activity and can have profound effects on the effective connectivity and function of neuronal networks. Recent work by Kerr et al. (2013) has implicated the neuromodulator adenosine (Boison 2006) in the developmental shift in glutamatergic synaptic properties from depressing to facilitating (Reyes and Sakmann 1999; Chen and Buonomano 2012); the analysis introduced in Chapter 4 is applied to the effects of adenosine on synaptic function.

Synapses are also modulated locally by retrograde signalling; where the postsynaptic cell releases a transmitter that alters synaptic efficacy. This allows the postsynaptic cell to control afferent signals from selected presynaptic neurons. Endocannabinoids are retrograde transmitters that temporally reduce the amount of conventional neurotransmitter released by the presynaptic cell (Katz 2012) and so can alter the dominant short-term plasticity displayed presynaptically from depression to facilitation (Brenowitz and Regehr 2005).

1.3.5 Paired whole-cell patch-clamp recording

Data on synaptic properties is gathered through paired-cell patch clamping. This procedure is described exactly in the Methods sections of Chapters 3 and 4, but a brief overview here may clarify some points about synaptic datasets. Glass electrodes are placed against the membrane of two cells and suction is applied until the membranes break and the electrodes can record from the interior of the cells; the process is known as whole-cell patch clamping (Neher 1991; Sakmann 1991). Current is injected into one cell to induce it to fire and the voltage of the other cell is monitored to detect an EPSP. In particular, this method does not distinguish between synaptic currents induced at individual anatomical contacts.

Paired whole-cell recording has advantages over experimental protocols using extracellular stimulating electrodes and intracellular recording electrodes as it is possible to precisely stimulate a single presynaptic cell whilst recording its voltage. Precise stimulation means that EPSPs are certain to come from a single synapse and presynaptic voltage recording allows failed action potential initiation to be distinguished from failed neurotransmitter release. Experiments are done *in vitro* on slices of tissue typically taken from young animals.

Tissue slices are ‘quiet’, they have very little background spiking activity compared to a living brain. This must be considered when extrapolating from *in vitro* slice data to *in vivo* living systems; in particular it means that stimulated activity in slice causes additional initial depression and facilitation compared to the same activity *in vivo*. In practice theoretical studies account for this easily by considering steady-state behaviour or explicit transitions in the activity levels (Tsodyks and Markram 1997). Inference of dynamic synaptic properties is also more straightforward in a quiet slice due to the larger initial changes in EPSP amplitude on stimulation onset (Eccles et al. 1941; Bekkers 1994).

1.4 Neurons

So far this chapter has discussed the broad structure and basic behaviour of neurons without much emphasis on the specifics of different cell classes. An understanding of the functionality discussed in this thesis does require consideration of the properties of the different cell classes discussed. The broadest categorisation of cells comes from the effect of the synapses they form: excitatory neurons form excitatory synapses and inhibitory neurons form inhibitory synapses. Beyond this, the brain region in which the cells are found and their location within this region, alongside morphological, genetic, and electrophysiological properties are used to define neuron classes (Wang et al. 2001; Oberlaender et al. 2012).

The major class of neuron discussed in this paper, and that for which experimental evidence is gathered in Chapters 3 and 4, is the thick-tufted pyramidal cell from Layer V of the cerebral cortex. The first subsection below describes the properties of this cell class in some detail and the second outlines unique properties of other cell classes discussed in Chapter 5.

1.4.1 Thick-tufted Layer V pyramidal cell

Layer V pyramidal cells are a major output cell of the cortex and are heavily implicated in complex computation (Markram et al. 1997; London and Häusser 2005; Spruston 2008; Ramaswamy and Markram 2015). These cells have soma lying in Layer V of the cerebral cortex, typically in the lower half, often referred to as Layer Vb (Fig. 1.7). They have a large dendrite that heads vertically up through the cortical layers to Layer I, where it branches extensively. This main dendrite is referred to as the apical dendrite, and the branches are referred to as tuft dendrites. The apical and tuft dendrites are over $1000\mu\text{m}$ long. There are also around 4 or 5 basal dendrites, which leave the soma within the

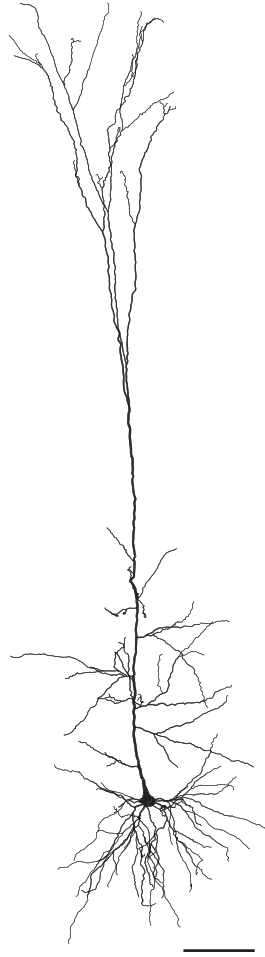


Figure 1.7: Thick-tufted Layer V pyramidal cell. Scale bar $100\mu\text{m}$. Morphology taken from (Hay et al. 2011), with all dendritic radii increased by $0.5\mu\text{m}$ for ease of visualisation.

plane of Layer V and are shorter, typically spanning around $300\mu\text{m}$. The soma is around $25\mu\text{m}$ in diameter (all measurements from Markram et al., 1997). A single axon leaves the soma and branches extensively, occasionally reaching up to higher layers within a cortical column, targeting basal dendrites of other pyramidal cells, and projecting down out of the cortex as a major output pathway. The characteristic pyramidal shape is found throughout the nervous systems of mammals, birds, fish, and reptiles suggesting a highly conserved computational role (Spruston 2008).

Layer V pyramidal cells receive synapses across their dendritic trees, with fairly stereotyped presynaptic locations. Excitatory synapses on the tuft dendrites tend to be long-range, from different cortical areas or the thalamus (Rubio-Garrido et al. 2009; Meyer et al. 2010). The basal dendrites are targets of short-range glutamergic synaptic connections from other Layer V cells within a cortical column and can be considered short-range (Markram et al. 1997; Hay et al. 2011). There is evidence that anatomical contacts on basal dendrites further from the postsynaptic soma are stronger to equalise their voltage effects at the soma (Markram et al. 1997). Each cell receives on the order of

5000 synapses onto its basal dendrites (O’Kusky and Colonnier 1982; Spruston 2008). Pyramidal cells also receive a complex pattern of inhibition from a variety of inhibitory cells within the cortical microcircuit that are not discussed in detail here, but have rich and varied effects on the excitability of the pyramidal cell (London and Häusser 2005; Silberberg and Markram 2007; Fino and Yuste 2011; Hill et al. 2012; Gidon and Segev 2012).

Layer V pyramidal cells have active dendrites. The most striking aspect of this is a concentration of voltage-gated calcium channels near the top of the apical dendrites, which instigate calcium spikes that propagate to the soma when the voltage in the calcium channel region exceeds a threshold (Williams and Stuart 2002; London and Häusser 2005; Hay et al. 2011). This helps transmit long-range signals to the soma. A hyperpolarisation-activated depolarising current denoted I_h is also present, with the I_h cation channels decreasing in density towards the soma. The relatively slow timescale of these channels means that EPSPs recorded at the soma are succeeded by a ‘sag-rebound’ in voltage (Berger et al. 2001; Silberberg and Markram 2007). A third active process is the NMDA spike, which has only been observed in the thinner basal and tuft dendrites and requires direct glutamatergic synaptic input (Schiller et al. 2000; Antic et al. 2010). Action potentials initiated in the soma can backpropagate into the dendrites (Stuart and Sakmann 1994), a function that appears to play a crucial role in long-term synaptic plasticity (Spruston 2008). Together with ion channels in the soma, these active processes play a part in spike-frequency adaptation (Fuhrmann et al. 2002). Adaptation is a modulation of a cell’s response to persistent stimulation (Wang 1998; Benda et al 2005; Peron and Gabbiani 2009). A key feature of adaptation currents is in the creation of correlations between interspike intervals (Schwalger et al. 2010; Schwalger and Lindner 2013), generating non-renewal spike trains which are discussed in Chapter 3.

1.4.2 Other neurons

Whilst the mathematical results in Chapters 2, 3, and 4 are general and can be applied to any synaptic contacts, both the experimental verification and main interpretations are centred around Layer V pyramidal cells. In Chapter 5, a morphological constraint is derived and experimental validation requires an analysis of the geometries of a number of other cell classes. Their structure and proposed functions are outlined below.

Purkinje cell. Purkinje cells (1.8a) are the major output neuron of the cerebellum. Like the cortex the cerebellum has a layered structure, but with an even greater degree of homogeneity. Purkinje cell bodies lie within the Purkinje cell layer and the extensively

branched dendrites receive excitatory synaptic inputs from two main sources. Climbing fibres from the medulla in the brainstem make strong excitatory synapses on proximal regions of dendrite. Each Purkinje cell receives climbing fibre input from a single presynaptic cell, and the activation of this synapse induces a complex spike, where a large initial action potential is succeeded by a burst of action potentials with lower amplitudes. Purkinje cells can also fire simple spikes, which are individual action potentials. Parallel fibres from cerebellar granule cells make a very large number, in the region of 200,000, of weak glutamatergic synapses to the distal regions of the dendrite, and can induce simple spikes. The dendrites of Purkinje cells allow for many active processes (Roth and Häusser 2001).

The site of action potential initiation is relatively far down the axon compared to the majority of neurons (Stuart and Häusser 1994). The output of Purkinje cells is inhibitory, and axon collaterals branch off from the main tract to specifically target proximal regions of neighbouring Purkinje cells with GABAergic synapses. Purkinje cells have a notably different genetic profile to many other neurons (Kirsch et al. 2012).

Dentate gyrus granule cell. The dentate gyrus lies within the hippocampus. Granule cells (1.8b) have small bodies ($\sim 10\mu\text{m}$ in diameter) and their conical arrangement of dendrites receives input from Layer II of the cortical region associated with memory formation and navigation (Schmidt-Hieber et al. 2007). Their activity is relatively sparse and strongly associated with spatial exploration. They are one of the few neuronal classes known to undergo adult neurogenesis (Cameron and McKay 2001).

Blowfly lobula plate HS and VS neurons. The structure of invertebrate brains is very different to that of mammals, but the constraints in Chapter 5 are also shown to apply to neurons from the fly central nervous system. The lobula plate of the blowfly *calliphora vicina* lies within the region of the brain that receives visual inputs and consists of around a dozen giant neurons; three of which, the HS cells (1.8c), process horizontal motion, and nine to eleven of which, the VS cells (1.8d), process vertical motion (Hausen et al. 1980; Scott et al. 2002). These cells are large and have a membrane conductance a factor of ten higher than many mammalian neurons. The layout of these cells is highly-stereotyped and the dendritic morphology is not experience-dependent, suggesting that the cells are genetically relatively hard-coded (Karmeier et al. 2001). The lobula plate has an important computational role, receiving inputs from a large number of presynaptic cells that retain a direct spatial mapping from the retina and producing the outputs necessary to control flight (Borst et al. 2010).

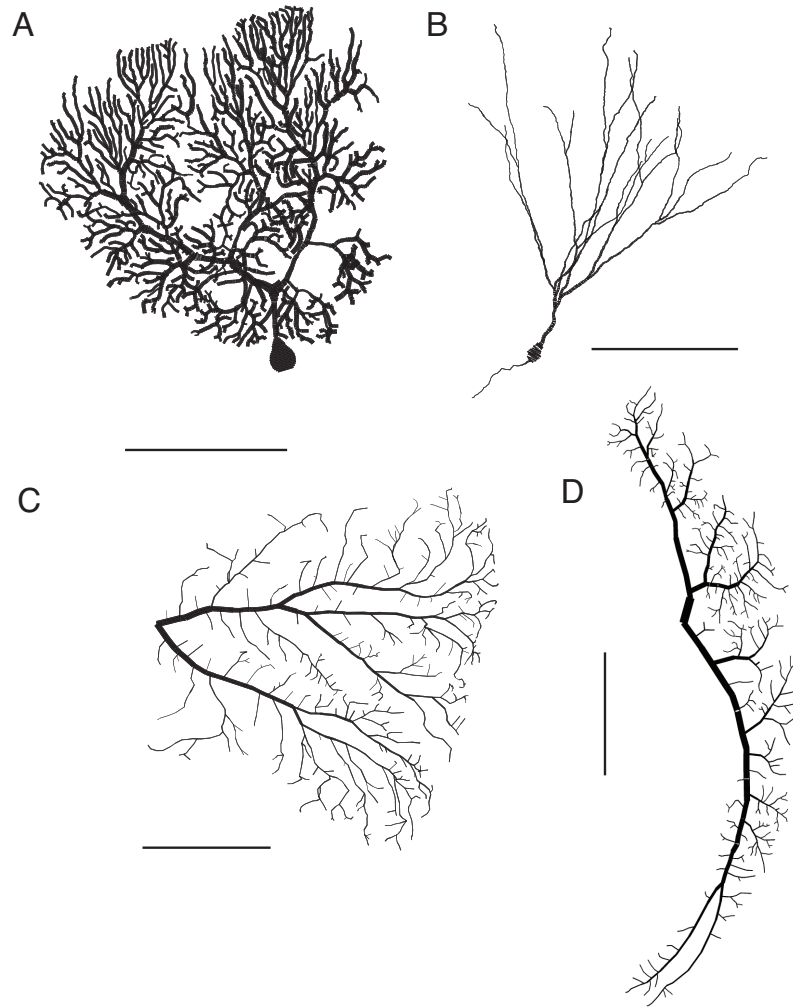


Figure 1.8: Other neuronal morphologies. **(A)** Purkinje cell (Roth and Häusser 2001). **(B)** Dentate gyrus granule cell (Schmidt-Hieber et al. 2007). **(C)**, **(D)** Blowfly lobula plate HS **(C)** and VS **(D)** neurons (Cuntz et al. 2010). All scale bars $100\mu m$ and all radii increased by $0.5\mu m$ for ease of visualisation.

1.5 Optimality in dendritic structure

The results presented in Chapter 5 involve studying a spatially extended neuron model, in contrast to the point neurons in Chapters 2, 3, and 4 that allow analytical results even when the input is stochastic and temporally complex (Brunel and Hakim 1999; Gerstner 2000; Fourcaud-Trocmé et al 2003). Spatially extended models attempt to account for the full morphological properties of real cells and are an important consideration in understanding synaptic function. The results in Chapter 5 consider dendritic optimality: how well dendrites are adapted for the task of propagating synaptic currents passively to the soma. To put this in context, I will introduce the ideas behind a spatially extended neuron model, and discuss the idea that synapses at different locations have equal effects,

an idea known as ‘dendritic democracy’ (Jaffe and Carnevale 1999; Magee and Cook 2000; Häusser 2001).

1.5.1 Spatially extended neuron models

The results of Wilfrid Rall in describing the properties of voltage in dendritic trees (Rall 1959; Rall 1969; Rall and Rinzel 1973) were critical in illustrating the function of extended dendrites. Previous work had neglected the importance of dendritic trees, overestimating the attenuation of voltage with distance (Eccles 1957). Rall was able to demonstrate that physiological values of dendritic radius and passive electrical properties meant that dendritic trees would have a substantial effect on somatic voltage (Rall 1959); thereby introducing neuronal cable theory, the study of voltage and current in leaky neurites. The governing cable equation is derived in the supplementary material to Chapter 5 for a cable with arbitrary radius profile; the classical form is for constant radius. The lengthscale of a cable depends on its radius and passive properties and is referred to as electrotonic length. A further innovation of Rall was to allow a branching dendritic tree to be modelled as a single cylinder under certain conditions. These conditions are rarely met in real neurons (Whitehead and Rosenberg 1993) (but see Desmond and Levy, 1984), but the ‘equivalent cable’ allowed an intuitive mathematical understanding of complex dendritic structures (Segev et al. 1995).

Further analytical approaches to the problem of resolving voltages in branched dendrites applied various transforms to allow efficient computation (Butz and Cowan 1974; Koch and Poggio 1985; Abbott et al. 1991; Zador et al. 1995), but arguably lacked the intuitive value of an equivalent cable interpretation (Whitehead and Rosenberg 1993). The equivalent cable idea was therefore extended to relax many of the original constraints (Schierwagen 1989; Poznanski 1991; Jaffe and Carnevale 1999; Lindsay et al. 2003), and solutions were found for many types of non-cylindrical or passively non-uniform dendritic cable (Goldstein and Rall 1974; Holmes and Rall 1992; London et al. 1999). These solutions did, however, lack complete generality, leaving room for the asymptotic solution to arbitrary taper introduced in Chapter 5.

The active processes in many dendrites, combined with the branching complexity, has led to widespread adoption of numerical methods for resolving voltages in realistic morphologies (Hines and Carnevale 1997), but analytical studies of passive properties do still have the potential to generate important new insights into dendritic function (Timofeeva et al. 2008; Gidon and Segev 2012).

1.5.2 Synaptic equalisation and ‘dendritic democracy’

The main result of Chapter 5 is a derivation of the optimal dendritic radius profile to transmit synaptic currents to the soma. This profile is optimal from the perspective of energy conservation (Cuntz et al. 2007), but due to the distance-dependent attenuation in a passive tree, is also the profile that best equalises somatic EPSPs from different anatomical synaptic contacts. The concept that synaptic weights from different anatomical contacts and the passive properties of certain neurons are adapted to equalise somatic currents in this way is referred to as ‘dendritic democracy’ (Jaffe and Carnevale 1999; Magee and Cook 2000; Häusser 2001; Timofeeva et al. 2008). Dendritic architecture and the strengths of synaptic contacts in some neurons (particularly hippocampal pyramidal neurons) appear to scale in a way that allows contacts at different distances to have an approximately equal impact at the soma (Rumsey and Abbott 2006).

1.6 Thesis Structure

The Chapters of this thesis are either published (Chapter 2), submitted (Chapter 5), or in preparation (Chapters 3 and 4). Each chapter is therefore written as a self-contained manuscript, with the addition of an initial overview that outlines my contribution as first author on each.

Chapter 2 examines the relationship between correlations in a presynaptic population and the individual weights of synapses, which are determined by long-term plasticity. In the paper I derive exact analytical forms for a number of key quantities, confirming previous numerical (de la Rocha and Parga 2005) and approximate (Rosenbaum et al. 2012) results, and use these to estimate the postsynaptic firing rate, demonstrating an optimal balance between presynaptic correlation and synaptic strength.

Chapter 3 considers how well spike trains with arbitrary statistics propagate across depressing synapses. I derive exact analytical results for key quantities when the spike train is a renewal process, with uncorrelated ISIs but (generally) correlated spike times. I demonstrate that synapses release neurotransmitter at a higher rate when the spike train is more regular, confirming previous numerical results (Reich and Rosenbaum 2013), but that when release probability p is low, positively autocorrelated spike trains are better drivers of the postsynaptic cell. The first of these results is confirmed experimentally by a collaborator. I finally demonstrate that it is possible to accurately estimate the postsynaptic firing rate for renewal spike trains with depressing synapses, allowing future incorporation of dynamic synapses in analytic studies of neuronal networks where spiking has temporal structure.

Chapter 4 introduces a novel method of Bayesian inference for synaptic datasets. This extends recent two applications of Bayesian inference in this context (Bhumbra and Beato 2013; Costa et al. 2013) by modelling both correlated quantal aspects and short-term plasticity of a synapse. The accuracy of the method is demonstrated on synthetic data, where the full posterior distribution allows identification of regions of parameter space where estimation is particularly difficult. The procedure is applied to data gathered by a collaborator in control and under high extracellular adenosine concentration, confirming previous studies on the effect of adenosine on synaptic dynamics (Kerr et al. 2013).

Chapter 5 considers spatially extended neuron models. I derive an asymptotic approximation to the voltage in a dendritic cable with arbitrary radius profile and demonstrate its accuracy. The first-order approximation is used to derive an analytical form for the radius profile that maximises the proximal effects of synaptic currents and this is shown to match the effects of non-parametric numerical optimisation (Cuntz et al. 2007), as well as predict the radii of a variety of cell classes. This chapter is structured slightly differently, with an overview, the main manuscript without sub-headings, and extensive supplementary information detailing the derivations behind the key results.

Chapter 6 is the Discussion, summarising the thesis and highlighting the original contributions and context of my work.

Chapter 2

Long-term plasticity determines the postsynaptic response to correlated afferents with multivesicular short-term synaptic depression

2.1 Overview

THIS chapter is motivated by the recent finding that a major mechanism of long-term plasticity is a change in the number of vesicle release sites n , matched by corresponding adjustments in the postsynaptic density such that the ‘mini’ amplitude a is unaltered (Loebel et al. 2013). The correlations in neurotransmitter release between active sites on a single presynaptic neuron will therefore change in a manner modulated by the more transient correlations between release from different neurons arising from synchrony in the network (Averbeck et al. 2006). I investigate the interaction between these two forms of correlation (between release sites and between neurons) with a stochastic quantal model of synaptic function (Fuhrmann et al. 2002); exact results are derived for the auto- and crosscorrelations in vesicle release. This allows the subthreshold mean and variance of the postsynaptic voltage to be exactly determined, confirming previous numerical (de la Rocha and Parga 2005) and approximate (Rosenbaum et al. 2012) results. The postsynaptic firing rate is estimated in situations of low and high release correlation, revealing a non-monotonic relationship with an intermediate maximum response. This suggests that there is an

optimal balance between levels of synchrony and individual synaptic weights across a neuronal network. The optimal balance is shown to be robust to variation in the temporal coherence between neuronal correlations and appears to arise under general forms of long-term homeostatic plasticity.

The main paper is followed by a brief discussion of interesting issues raised since publication.

2.1.1 Author contributions

Conceived the study: MJER and ADB. Derived and solved equations: ADB and MJER. Wrote code for simulations: ADB. Prepared figures: ADB. Wrote the paper: ADB and MJER.

The first draft was written entirely by ADB. The abstract was then substantially rewritten by MJER. All equations used in the final results were initially derived by ADB. Equations 3-6, which shorten and simplify the different calculations for auto- and cross-correlations were introduced by MJER.



Long-term plasticity determines the postsynaptic response to correlated afferents with multivesicular short-term synaptic depression

Alex D. Bird^{1,2,3*} and Magnus J. E. Richardson¹

¹ Warwick Systems Biology Centre, University of Warwick, Coventry, UK

² Warwick Systems Biology Doctoral Training Centre, University of Warwick, Coventry, UK

³ School of Life Sciences, University of Warwick, Coventry, UK

Edited by:

Tatjana Tchumatchenko, Max Planck Institute for Brain Research, Germany

Reviewed by:

Jean-Pascal Pfister, Cambridge University, UK (in collaboration with Simone Surace)

Michael Graupner, New York University, USA

*Correspondence:

Alex D. Bird, Warwick Systems Biology Centre, Senate House, University of Warwick, CV4 7AL, Coventry, UK
e-mail: a.d.bird@warwick.ac.uk

Synchrony in a presynaptic population leads to correlations in vesicle occupancy at the active sites for neurotransmitter release. The number of independent release sites per presynaptic neuron, a synaptic parameter recently shown to be modified during long-term plasticity, will modulate these correlations and therefore have a significant effect on the firing rate of the postsynaptic neuron. To understand how correlations from synaptic dynamics and from presynaptic synchrony shape the postsynaptic response, we study a model of multiple release site short-term plasticity and derive exact results for the crosscorrelation function of vesicle occupancy and neurotransmitter release, as well as the postsynaptic voltage variance. Using approximate forms for the postsynaptic firing rate in the limits of low and high correlations, we demonstrate that short-term depression leads to a maximum response for an intermediate number of presynaptic release sites, and that this leads to a tuning-curve response peaked at an optimal presynaptic synchrony set by the number of neurotransmitter release sites per presynaptic neuron. These effects arise because, above a certain level of correlation, activity in the presynaptic population is overly strong resulting in wastage of the pool of releasable neurotransmitter. As the nervous system operates under constraints of efficient metabolism it is likely that this phenomenon provides an activity-dependent constraint on network architecture.

Keywords: long-term plasticity, short-term plasticity, synaptic depression, correlations and synchrony, voltage fluctuations

1. INTRODUCTION

Synapses play a key role in transmitting and processing information throughout the nervous system and long-term shifts in synaptic efficacy are believed to underpin learning and memory (Hebb, 2002; Markram et al., 2011). Synapses function through release of neurotransmitters that then bind to receptors on the postsynaptic cell and transiently alter the membrane conductance. Neurotransmitters in the presynaptic terminal are stored and transported in vesicles (Fox, 1988; Hu et al., 2008). A number of vesicles are positioned at active sites where they have a certain probability of being released when the presynaptic cell spikes. Empty release sites are restocked after a variable period, with an overall rate of a few Hz (Südhof, 2004). Both the number of contacts per presynaptic cell and the activity in the presynaptic network can generate correlations in the release of neurotransmitter at synapses onto a single neuron; we demonstrate that postsynaptic activity is governed by a balance between these two sources of correlation.

The usage of vesicles due to presynaptic firing and stochastic replenishment means that the number of vesicles available for release is a highly dynamic quantity that is dependent on the history of afferent activity. In the immature cortex, the relatively high release probability and limited availability of vesicles causes a progressive reduction in synaptic efficacy during a period

of sustained neuronal activity (Reyes and Sakmann, 1999; Chen and Buonomano, 2012). This short-term reduction in synaptic strength is known as vesicle depletion depression: an unstocked active site cannot induce a postsynaptic response to any incident action potential (Abbot, 1997; Tsodyks and Markram, 1997; Zucker and Regehr, 2002). The phenomenon is believed to play a role in gain control (Abbot, 1997; Abbott and Regehr, 2004; Rothman et al., 2009), information transmission (Zador, 1998; Kilpatrick, 2012; Scott et al., 2012), and adaptation to sensory stimuli (Furukawa et al., 1982; Hallermann and Silver, 2012). The synaptic plasticity models introduced by Abbot (1997) and Tsodyks et al. (1998) capture short-term depression accurately; they match empirical data and allow a richness of network behavior (Tsodyks et al., 1998) to emerge beyond that predicted by static synapses. Such models consider the mean efficacy of the synapse, averaged across several presentations of the same presynaptic stimulus; the predicted postsynaptic response therefore varies continuously. Several recent studies have considered a quantal model of synaptic function incorporating short-term depression, with probabilistic vesicle release and replacement to reflect trial-to-trial variability (Fuhrmann et al., 2002; de la Rocha and Parga, 2005; Rosenbaum et al., 2012). The impact of stochastic vesicle dynamics is particularly marked when mean synaptic drive is insufficient to bring the postsynaptic neuron to threshold

and spiking activity is governed by fluctuations in the system (Gerstein and Mandelbrot, 1964; Kuhn, 2004). To induce post-synaptic firing in such a system it is necessary for the variable synaptic drive to exhibit coincidences; this occurs most regularly when that drive is correlated.

Correlations in neurotransmitter release between different sites can arise from two sources: from multiple contacts onto a postsynaptic neuron from the same presynaptic cell and from synchronous activity across the presynaptic population. The number of sites between a pair of neurons is fixed over short timescales, unlike the number of vesicles ready to release from the sites, but can vary widely over longer periods (Loebel et al., 2013) following potentiation or depression. Connections between neurons potentiate and depress in the long term chiefly through changes in this synaptic parameter—the number of independent release sites can be seen as a fundamental unit of memory. Synchronous firing in the presynaptic population emerges from the connectivity of neuronal networks (Aertsen et al., 1989) and has relevance for encoding sensory information (von der Malsburg, 1981; deCharms and Merzenich, 1996; Averbeck et al., 2006), motor control (Baker et al., 2001; Capaday, 2013) and decision making (Cohen and Newsome, 2008; Cain and Shea-Brown, 2013). Recent work suggests that modulation of correlations can be more significant for neuronal coding than alterations in the presynaptic firing rate (Seriès et al., 2004; Mitchell et al., 2009; Cohen and Kohn, 2011). Population synchronization is a transient phenomenon relative to the structural changes underlying long-term plasticity.

A detailed stochastic model of neurotransmitter dynamics at the presynaptic terminal is required to analyze the effects of presynaptic synchrony, particularly when long-term plasticity varies the structure of synapses through altering the number of release sites. It can be noted that multiple contacts between cells and transient correlations within a presynaptic population are likely to introduce considerable redundancy in the usage of vesicles: correlated events may lead to EPSPs many times larger than that required to reach threshold. However, evidence points to the nervous system operating under constraints of efficient metabolism (Levy and Baxter, 2002; Taschenberger et al., 2002; Savtchenko et al., 2012) suggesting such wastage would not commonly arise *in vivo*. It is therefore of interest to examine the effect on the postsynaptic cell of the interaction of partially synchronized afferent drive with multiple contacts per presynaptic cell. To this end, we analyze a model of a postsynaptic cell receiving input from a population of release sites distributed between different numbers of presynaptic neurons and with different levels of synchrony.

Following the basic model definitions, we first derive exact forms for the crosscorrelations of vesicle occupancies and release at multiple contacts from the same and different presynaptic cells. These correlations were previously derived by Rosenbaum et al. (2012) using a diffusion and additive-noise approximation, and our results show that this earlier method gave exact results for these quantities. We then go on to calculate the exact voltage mean and variance and, through comparison with the typical EPSP amplitude, argue that synaptic noise can become significantly non-Gaussian. We then derive two approximate limiting forms for the firing rate for low and high correlations and demonstrate that the postsynaptic response is optimal at intermediate levels of

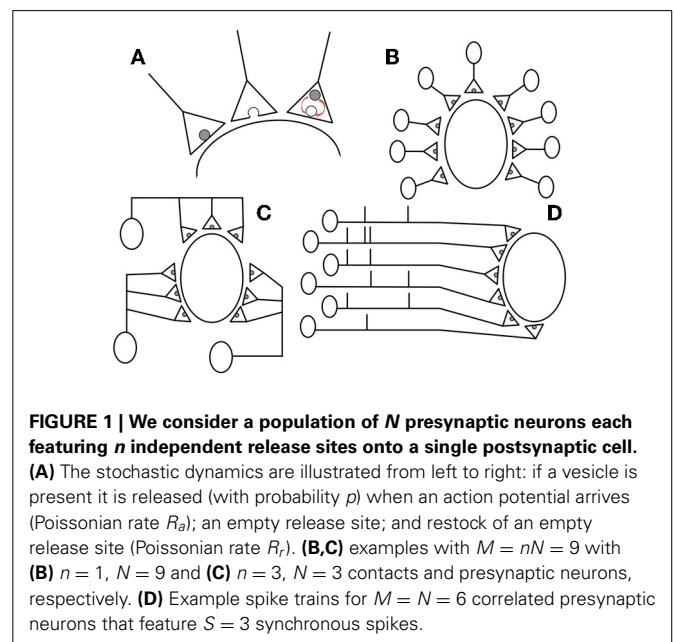
afferent correlations. We finally show that this effect is robust for neurons in which there is some level of synaptic homeostasis or soft limit on the total number of release sites.

2. METHODS

We consider a population of N presynaptic neurons synapsing onto a single postsynaptic neuron. A presynaptic neuron makes synapses with n vesicle occupancy sites from each of which neurotransmitter may be independently released with a probability p on the arrival of a presynaptic action potential, occurring at a constant Poissonian rate R_a . In between presynaptic action potentials, empty release sites are restocked independently at a constant Poissonian rate R_r . Initially, we consider that the total number of release sites onto the postsynaptic cell is fixed at $M = nN$ (example configurations are provided in **Figures 1A–C**). The number of independent release sites n was recently shown (Loebel et al., 2013) to be the synaptic parameter most closely correlated with the structural changes arising from long-term plasticity and so we will consider the effects of varying n (while initially keeping M constant) on the postsynaptic response. The binary variable x will be used to signify vesicle release-site occupancy: $x = 1$ if present or $x = 0$ if absent. The evolution of vesicle occupancy is given by the stochastic differential equation

$$\frac{dx}{dt} = (1 - x) \sum_m \delta(t - t_m) - \sum_k q_k(x) \delta(t - t_k) \quad (1)$$

where m counts the restock events occurring at a rate R_r and k counts the presynaptic action potentials occurring at a rate R_a . The binary random variable $q_k(x)$ signifies whether a release was successful at the k th action potential: if $x = 1$ then $q_k(x) = 1$ with probability p to model a successful release of neurotransmitter, and is 0 otherwise to model a failed release from a stocked site; if $x = 0$ then no release is possible and $q_k(x) = 0$. The δ s are



Dirac delta functions and whenever a delta function multiplies a dynamic variable it is assumed that the value of the variable used is that immediately before the delta event occurs. In other words, the equations are non-anticipating and should be interpreted in an Itô sense (Gardiner, 2010).

2.1. CORRELATIONS FROM STRUCTURE

When a presynaptic neuron spikes, available vesicles at each of the n sites release their contents independently with probability p , and so the total number of release events is binomially distributed. Note that because these sites receive the same incoming action potentials correlations will arise despite the independent conditional release and restock events at each site. Globally, we first hold the total number of release sites, given by $M = nN$, constant so that the postsynaptic neuron receives a fixed overall excitatory drive. In this study we set $M = 5000$, which is of-the-order-of estimates by O’Kusky and Colonnier (1982), Megias et al. (2001), and Spruston (2008). This has the effect of maintaining the overall level of excitatory drive to the postsynaptic cell and in biological terms can be seen as a constraint of metabolic efficiency across the presynaptic population: as some contacts potentiate, others die out. The effects of relaxing this condition are discussed later. Recent analysis of long-term plasticity data has shown that changes in EPSP amplitude are captured by models in which the number of independent release sites n increases or decreases. Depending on the protocol, n can potentiate or depress by a factor of 5 or more (Loebel et al., 2013); a typical range for n is 5–50. However, contacts with a binomial n as low as 1 or as high as 100 sites have also been observed. Though the upper bound is unbiological, for completeness we vary n between 1 and 5000 in simulations.

2.2. CORRELATIONS FROM PRESYNAPTIC SYNCHRONY

The population of neurons driving a common target often displays substantial synchrony in spiking activity (Salinas and Sejnowski, 2000; Averbeck et al., 2006; Cohen and Kohn, 2011) (see Figure 1D). Here we model correlations in the presynaptic population by using a variation of the Multiple Interaction Process (MIP) introduced in Kuhn et al. (2003). We implement the process by considering a master spike train with a constant Poissonian rate NR_a/S . For each spike in the master train we pick S of the presynaptic neurons at random and assign a synchronous spike in their trains. If $S = 1$ this would imply no correlations in the presynaptic population and $S = N$ would be a fully synchronous presynaptic population. Note that the spiking of each presynaptic neuron is Poissonian at rate R_a as required and also that, given that one presynaptic neuron spikes, the probability that a particular other presynaptic neuron has a spike at the same time is $c = (S - 1)/(N - 1)$. In reality, shared spikes will not be entirely synchronous and so in later simulations (specifically, those leading to Figures 6, 7) we add independent, normally distributed jitter to the spike times with mean 0 and standard deviation τ_j following de la Rocha and Parga (2005) and Cohen and Kohn (2011). Note that in Figures 5, 6A,B, 7 the curves are truncated for increasing n because, for fixed S and fixed $M = nN$, it is invalid to have S greater than N . This is also the case for Figures 6B,C with increasing S .

2.3. POSTSYNAPTIC VOLTAGE

We treat the postsynaptic neuron as a leaky integrate-and-fire model with each neurotransmitter release event causing the voltage to jump by an amount a . The membrane voltage V has a resting value E and a spike threshold V_{th} . After a spike, V is reset to E and held there for a time τ_r to model the refractory period. If N presynaptic neurons each have n neurotransmitter release sites then the postsynaptic voltage is governed by

$$\tau \frac{dV}{dt} = E - V + a\tau \sum_{i=1}^N \sum_{j=1}^n \sum_k Q_k^{ij}(x_{ij}) \delta(t - t_k^i) \quad (2)$$

where τ is the membrane time constant, x_{ij} is the occupancy variable for the i th presynaptic neuron’s release site number j and k labels the order of incoming action potentials to release site with occupancy x_{ij} . Note that the spike times t_k^i are identical for all release sites with the same presynaptic neuron i and that some of the spike times will be common to release sites with distinct presynaptic neurons, depending on the level of synchrony given by the correlated MIP process parameterized by S . The values of other parameters used in simulations (unless otherwise stated) are given in (Table 1).

3. RESULTS

We first derive exact forms for the crosscorrelations of vesicle-occupancy and of neurotransmitter-release time series. The latter can then be used to calculate the exact membrane voltage variance. Two approximations of the postsynaptic firing rate then lead us to the main result of the paper: that long-term synaptic plasticity—through its alternation of the synaptic parameter n —sets the optimal postsynaptic response to a presynaptic population with correlated firing. Throughout this section the notation $\langle \phi \rangle$ denotes the steady-state expectation of the fluctuating quantity ϕ .

For the calculation of the crosscorrelations of objects separated by a time T , it is useful to consider how the steady-state expectation of the product of the occupancy x with some quantity ψ evaluated at an earlier time evolves with the separation time:

$$\frac{d}{dT} \langle x(T)\psi(0) \rangle = \langle (1 - x(T))\psi(0) \rangle R_r - \langle x(T)\psi(0) \rangle pR_a \quad (3)$$

where the first term on the right-hand side is the rate that an empty site is filled and the second term is the rate that a full site releases its contents. This equation can be rearranged into the form

$$\tau_x \frac{d}{dT} \langle x(T)\psi(0) \rangle = \langle x \rangle \langle \psi \rangle - \langle x(T)\psi(0) \rangle \quad (4)$$

where the time constant τ_x and steady-state occupancy $\langle x \rangle$ are

$$\tau_x = \frac{1}{R_r + pR_a} \text{ and } \langle x \rangle = \frac{R_r}{R_r + pR_a}. \quad (5)$$

That the second quantity must be the steady-state occupancy $\langle x \rangle$ can be inferred by noting that in the limit $T \rightarrow \infty$ the expectation

Table 1 | Typical parameters used for the figures.

Parameter	Interpretation	Value
V	Postsynaptic membrane voltage	Varies
S	Number of presynaptic cells that fire together	Varies
n	Number of release sites per presynaptic neuron	Varies
N	Number of presynaptic neurons	Varies
M	Total number of vesicle release sites (nN)	5000
R_r	Rate at which empty vesicles are replaced at release sites	2 Hz
R_a	Rate of presynaptic spiking	2 Hz
p	Probability of spike arrival inducing neurotransmitter release at a site with a vesicle present	0.66
τ_j	Jitter standard deviation timescale	2 ms
E	Resting membrane voltage	-70 mV
V_{th}	Threshold at which action potentials are initiated	-55 mV
τ_r	Refractory period of a neuron after a spike	2 ms
τ	Membrane time constant	10 ms
a	EPSP amplitude induced by neurotransmitter released from a single vesicle	0.2 mV

$\langle x(T)\psi(0) \rangle$ in Equation (3) loses its T dependence and factorises into the product $\langle x \rangle \langle \psi \rangle$. Note that the exponential solution to the differential Equation (4) implies that all crosscorrelations that include the occupancy x take a simple exponential form

$$\text{Crosscorr}(x, \psi) = (\langle x\psi \rangle - \langle x \rangle \langle \psi \rangle) e^{-t/\tau_x} \quad (6)$$

where $\langle x\psi \rangle$ is the expectation evaluated in the limit $T \rightarrow 0$.

3.1. VESICLE OCCUPANCY CROSSCORRELATIONS

The autocorrelation of release-site occupancy can be calculated by making use of the fact that for the binary variable x we have $x^2 = x$ and so $\langle x^2 \rangle = \langle x \rangle$. Putting $\psi = x$ in equation (6) gives

$$\text{Autocorr}(x) = \langle x \rangle (1 - \langle x \rangle) e^{-|T|/\tau_x} = \frac{pR_a R_r}{(R_r + pR_a)^2} e^{-|T|/\tau_x} \quad (7)$$

where the extension of the exponential to negative times comes from a symmetry argument. For the crosscorrelation between different release sites, with occupancy variables x and x' , we need to distinguish between cases where the release sites either share the same presynaptic neuron or have different presynaptic neurons when deriving $\langle xx' \rangle$. However, the derivation can be written in

the same form by introducing a quantity γ that is the proportion of shared spikes: $\gamma = 1$ for release sites with the same presynaptic neuron or $\gamma = c = (S - 1)/(N - 1)$ for different presynaptic neurons. A steady-state equation for the zero-time expectation $\langle xx' \rangle$ can be found by considering the state where both sites are occupied and balancing the total rates into and out of this state

$$\langle x(1 - x') \rangle R_r + \langle (1 - x)x' \rangle R_r = \langle xx' \rangle (2R_a p - \gamma R_a p^2). \quad (8)$$

The terms on the left-hand side represent the total rate into the double occupancy state, whereas the terms on the right-hand side multiplying the expectation are the combined rates of individual vesicle release minus the coincidence term to prevent overcounting of events. We now combine terms to obtain the required expectation

$$\langle xx' \rangle_\gamma = \frac{2R_r \langle x \rangle}{2R_r + R_a p (2 - \gamma p)} \quad (9)$$

where the γ subscript will be used later to distinguish the different cases. It can be inserted into Equation (6) with $\psi = x'$ to give

$$\text{Crosscorr}(x, x') = \frac{\gamma p^2 R_a R_r^2 e^{-|T|/\tau_x}}{(2R_r + pR_a(2 - \gamma p))(R_r + pR_a)^2}. \quad (10)$$

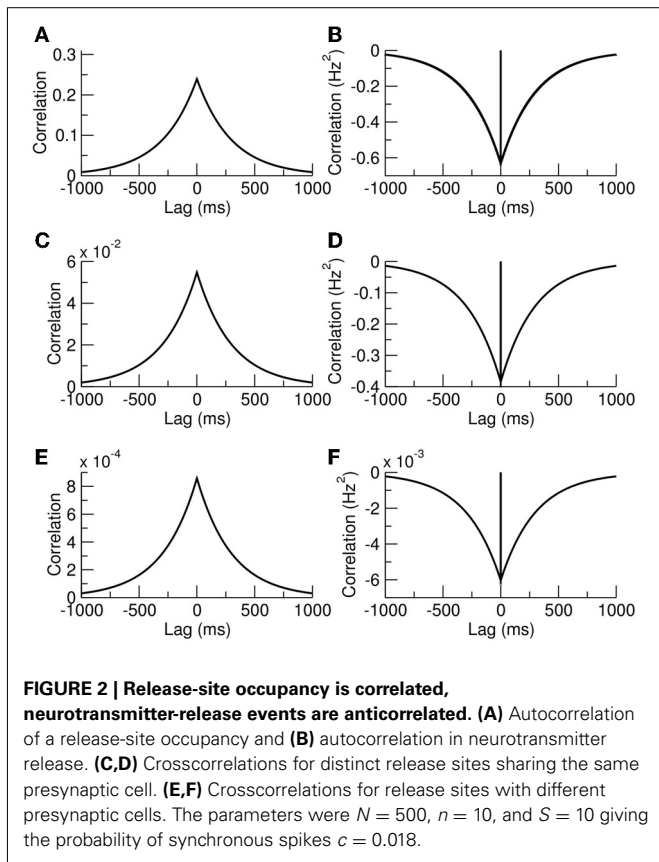
Example plots of Equation (7), and Equation (10) for cases with $\gamma = 1$ and $\gamma = c$ are given in **Figures 2A,C,E**. It is interesting to note that our exact results are identical to those previously calculated in Rosenbaum et al. (2012) using a combined diffusion and additive-noise approximation, validating their method up to second-order statistics.

3.2. NEUROTRANSMITTER RELEASE CROSSCORRELATIONS

Though synchrony in the presynaptic population leads to positive correlations for release-site occupancy, we now show that the delayed restock following release leads to negative cross-correlations in the release events themselves. Let $\chi(t)$ and $\chi'(t)$ be trains of delta pulses representing neurotransmitter release from sites with occupancies defined by $x(t)$ and $x'(t)$, respectively, so that:

$$\chi(t) = \sum_k q_k(x) \delta(t - t_k) \quad (11)$$

where k counts incoming action potentials at the contact with site occupancy x . In the steady state we have $\langle \chi \rangle = pR_a \langle x \rangle$ because the rate of release is equal to the release rate pR_a given vesicle occupancy multiplied by the occupancy probability $\langle x \rangle$. The auto and crosscorrelations can be straightforwardly calculated using the general result of Equation (6) by setting $\psi = \chi'$ and noting that $\langle \chi(T)\chi'(0) \rangle = pR_a \langle x(T)\chi'(0) \rangle$. However, some care needs to be taken when considering the case $T = 0$. The result of Equation (6) is valid in the limit $T \rightarrow 0$; but there is an additional delta function in the crosscorrelation when $T = 0$ with an amplitude equal to the rate of simultaneous events in χ and χ' that arises from the delta functions in Equation (11). The autocorrelation



function for χ therefore takes the form

$$\text{Autocorr}(\chi) = pR_a \langle x \rangle \delta(T) - (pR_a \langle x \rangle)^2 e^{-|T|/\tau_x} \quad (12)$$

where the rate of simultaneous events for the autocorrelation is just the mean release rate $pR_a \langle x \rangle$ and prefactor of the exponential is only $-\langle x \rangle^2$ because in the limit $T \rightarrow 0$ the expectation of $\langle \chi(T)\chi(0) \rangle$ is zero as there is no time for a restock. A similar consideration gives the result for the crosscorrelation

$$\begin{aligned} \text{Crosscorr}(\chi, \chi') &= \gamma p^2 R_a \langle xx' \rangle_\gamma \delta(T) \\ &+ R_a^2 p^2 ((1 - \gamma p) \langle xx' \rangle_\gamma - \langle x \rangle^2) e^{-|T|/\tau_x} \end{aligned} \quad (13)$$

where we are treating cases for which the release is from distinct contacts sharing the same presynaptic neuron $\gamma = 1$ or from distinct presynaptic neurons where $\gamma = c$. In Equation (13) the prefactor of the delta function arises from the rate of simultaneous releases, which is equal to the arrival of simultaneous spikes γR_a multiplied by the probability that each contact releases a vesicle $p^2 \langle xx' \rangle_\gamma$. The prefactor of the exponential shares the same squared component $-\langle x \rangle^2 = -(pR_a \langle x \rangle)^2$ as the autocorrelation, but also has a non-zero contribution from $\langle \chi(T)\chi'(0) \rangle$ in the limit $T \rightarrow 0$. This quantity is equal to the probability that both sites are occupied $\langle xx' \rangle_\gamma$ multiplied by the probability of a release from site x' but no release from site x from a simultaneous presynaptic event, which is $R_a p(1 - \gamma p)$ multiplied by a

subsequent release from site x just afterwards due to a second presynaptic spike, pR_a . This exact result is again identical to that derived previously using a diffusion and additive-noise approximation (Rosenbaum et al., 2012). Example autocorrelation and crosscorrelation functions are plotted in **Figures 2B,D,F**.

3.3. MEMBRANE VOLTAGE MEAN AND VARIANCE

The tonic component of the presynaptic drive can be characterized by the mean voltage, which is straightforward to calculate in the absence of a threshold. The dynamics of this quantity can be found by taking the expectation of Equation (2) to yield the steady-state result

$$\langle V \rangle = E + aM\tau pR_a \langle x \rangle = E + \frac{aM\tau pR_a R_r}{R_r + pR_a}. \quad (14)$$

Note that the mean voltage is independent of the synchrony S and is also independent of release-site number n when $M = nN$ is held fixed.

The effect of correlated synaptic fluctuations on the postsynaptic neuron can also be characterized by deriving the steady-state variance of the postsynaptic voltage (again in the absence of a threshold-reset mechanism). This quantity is derived in the Appendix using the auto and crosscorrelations of χ (Equations 12, 13) and takes the form

$$\begin{aligned} \text{Var}(V) &= \frac{a^2 \tau N n p R_a}{2} (\langle x \rangle + (n-1)p \langle xx' \rangle_1 + (N-1)ncp \langle xx' \rangle_c) \\ &+ \frac{Nn(a\tau p R_a)^2}{1 + \tau R_r + p\tau R_a} ((n-1)(1-p) \langle xx' \rangle_1 \\ &+ (N-1)n(1-cp) \langle xx' \rangle_c - Nn \langle x \rangle^2). \end{aligned} \quad (15)$$

The first term arises from the δ -functions in Equations (12, 13) and the second term comes from the negative correlations in vesicle release due to short-term depression (the terms featuring exponentials in the same equations). For a related model (de la Rocha and Parga, 2005) it was demonstrated that on increasing the presynaptic rate a maximum can be seen in the conductance fluctuations. The exact result of Equation (15) allows for this effect of fluctuations in depressing synapses on the voltage itself to be analyzed. Example variances as a function of presynaptic rate are shown in **Figure 3** and, as expected from the previous analysis of conductance fluctuations (de la Rocha and Parga, 2005), the variance also shows a maximum at intermediate presynaptic rates.

Though the voltage variance measures one aspect of presynaptic fluctuations, it misses its increasing shot-noise nature as the correlations increase. Shot noise causes a non-Gaussian component in the tails of the membrane voltage distribution that, because they extend to the region of action-potential initiation, can significantly affect the post-synaptic firing rate (Richardson and Swarbrick, 2010). The mean EPSP amplitude can be used to see this effect: it is proportional to the mean of the vesicles released by a spike given the occupancy levels already computed, and so

$$\langle \text{EPSP} \rangle = apnS \langle x \rangle = \frac{apSnR_r}{R_r + pR_a}. \quad (16)$$

As correlations from increasing n or S become stronger, the mean EPSP amplitude increases. However, as noted above, the mean voltage (Equation 14) does not change under increasing n or S . Taken together, the implications are that in the limit of high correlations the synaptic drive becomes temporally sparse with large amplitude EPSPs generated from correlated events. This effect can be seen in simulations of the model with different parameter regimes (Figure 4). For parameters $N = 125$, $n = 1$, and $S = 1$ (no presynaptic synchrony) the presynaptic

spikes (Figure 4A) and neurotransmitter release (Figure 4D) are uncorrelated, and in the full system with $M = 5000$ the EPSPs are relatively small (Figures 4G,H) and the resulting voltage distribution is close to Gaussian (Figure 4I). Increasing n (Figure 4B) or S (Figure 4C) to 25 leads to correlations in neurotransmitter release (Figures 4E,F), larger EPSPs (Figures 4J,K,M,N) and a more variable and skewed membrane voltage (Figures 4L,O). Note the right-hand tails from the skewed membrane voltages under conditions of presynaptic correlation that extend toward voltages where action potentials would be initiated.

3.4. RELEASE SITE NUMBER AND POSTSYNAPTIC RATE

As the analyses of the previous section and examples in Figure 4 demonstrate, for the case of few release sites and low synchrony the voltage distribution is close to Gaussian. However, for the case of many release sites the synchronous release events generate large EPSPs that are reminiscent of shot noise. With this in mind, approximations for the firing of the postsynaptic cell may be found for the cases of low n , when the voltage distribution is roughly Gaussian, and high n for which the EPSP amplitudes are of-the-order-of or larger than threshold.

3.4.1. Few release sites

For the low n approximation we rely on a recent observation (Alijani and Richardson, 2011) that the firing rate of integrate-and-fire neurons is relatively insensitive to temporal correlations as long as the subthreshold voltage mean and variance are matched. To this end we approximate the firing rate of the neuron by a white-noise equivalent that has a voltage mean μ equal to that

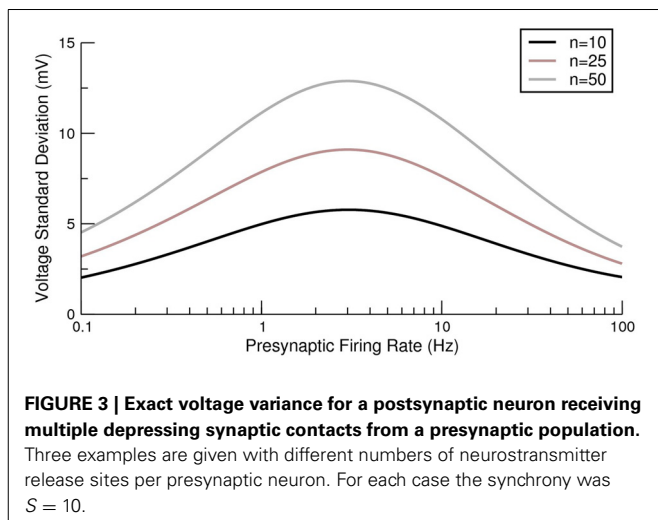


FIGURE 3 | Exact voltage variance for a postsynaptic neuron receiving multiple depressing synaptic contacts from a presynaptic population. Three examples are given with different numbers of neurotransmitter release sites per presynaptic neuron. For each case the synchrony was $S = 10$.

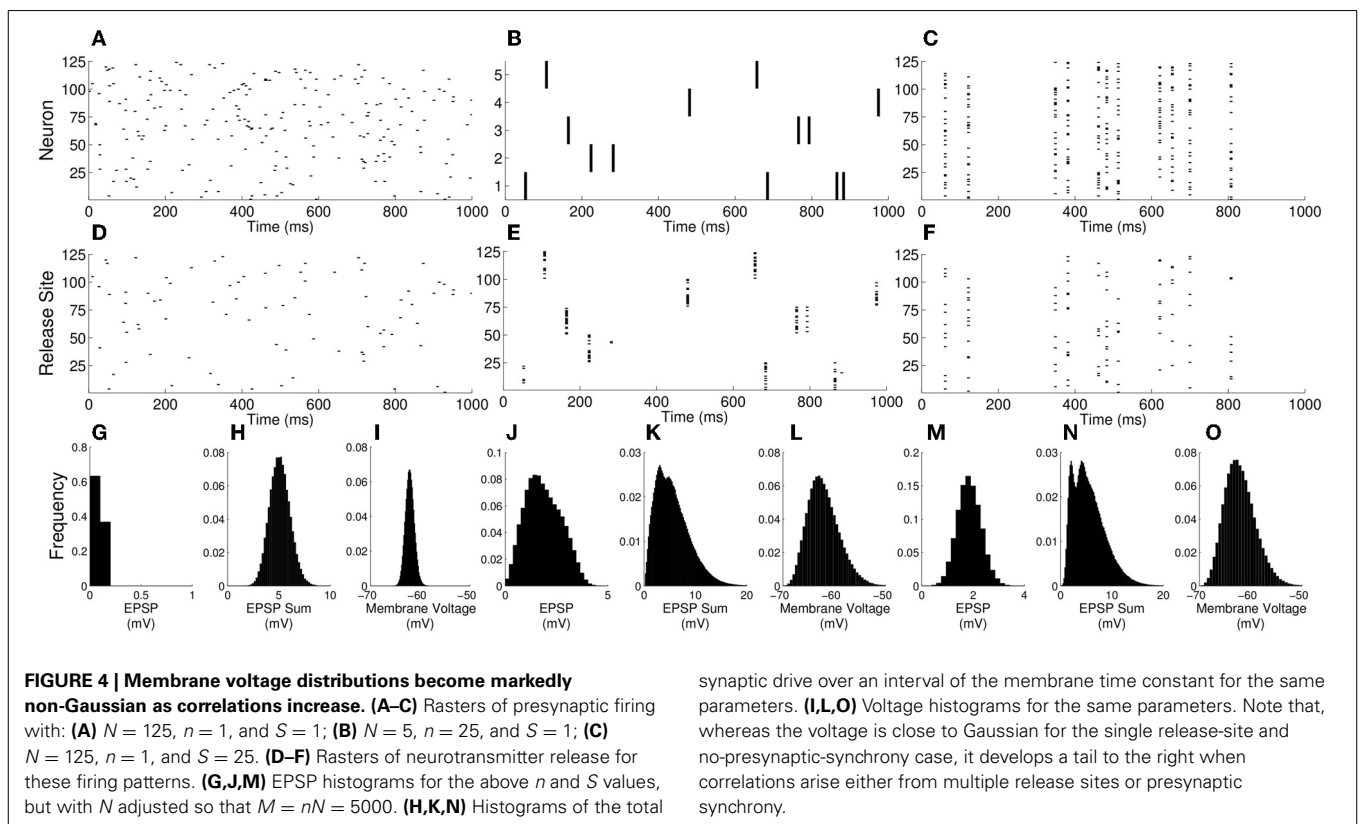


FIGURE 4 | Membrane voltage distributions become markedly non-Gaussian as correlations increase. (A–C) Rasters of presynaptic firing with: **(A)** $N = 125$, $n = 1$, and $S = 1$; **(B)** $N = 5$, $n = 25$, and $S = 1$; **(C)** $N = 125$, $n = 1$, and $S = 25$. **(D–F)** Rasters of neurotransmitter release for these firing patterns. **(G,J,M)** EPSP histograms for the above n and S values, but with N adjusted so that $M = nN = 5000$. **(H,K,N)** Histograms of the total

synaptic drive over an interval of the membrane time constant for the same parameters. **(I,L,O)** Voltage histograms for the same parameters. Note that, whereas the voltage is close to Gaussian for the single release-site and no-presynaptic-synchrony case, it develops a tail to the right when correlations arise either from multiple release sites or presynaptic synchrony.

of Equation (14) and variance σ^2 equal to that of Equation (15). The firing rate of a leaky-integrate-and-fire neuron with these parameters is given (Brunel and Hakim, 1999) by the reciprocal of

$$\tau \int_0^\infty \frac{dz}{z} e^{-z^2/2} (e^{zz_{th}} - e^{zz_{re}}) \quad (17)$$

where $z_{th} = (V_{th} - E - \mu)/\sigma$ and in this case $z_{re} = -\mu/\sigma$.

3.4.2. Many release sites

For sufficiently large n the mean EPSPs are greater than that required to bring the neuron to threshold $apnS \langle x \rangle \gg V_{th} - E$, and so each synchronous presynaptic event is likely to cause the postsynaptic cell to spike. The postsynaptic cell receives input at a total rate of NR_a/S and so we can approximate the rate in the large n case by

$$r \sim \frac{NR_a}{S} = \frac{MR_a}{nS}. \quad (18)$$

Therefore, increasing the presynaptic synchrony S will reduce the postsynaptic response when n is large.

3.4.3. Optimal release-site number

Under conditions of a fixed number of release sites onto the postsynaptic cell $M = nN$, increasing n has no effect on the voltage mean (Equation 14), but increases the voltage variance (Equation 15). Therefore, as n increases from an initially small value, the approximation given by Equation (17) predicts that the postsynaptic cell will fire at an increasing rate. However, from Equation (18), which is valid for high n , we see that the postsynaptic firing rate decreases as n increases. Hence, there must be an intermediate n for which the response of the postsynaptic cell is optimized. This effect can be clearly seen in the examples given in Figure 5 in which the postsynaptic rate is plotted as a function of n for fixed M . The intersections of the two approximations for

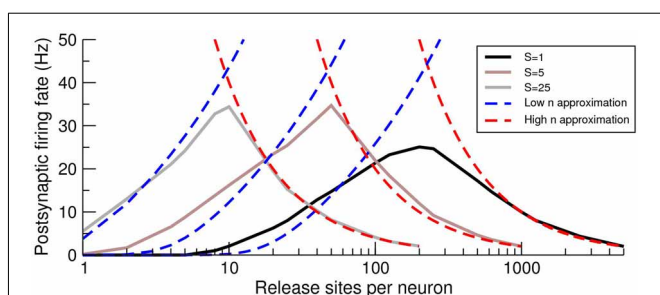


FIGURE 5 | The postsynaptic firing rate exhibits a maximum as a function of the number of pre-to-post release sites n . Firing-rate simulations (solid lines), low n approximation (Equation 17; blue dashed lines) and high n approximation (Equation 18; red-dashed lines) for various levels of presynaptic synchrony S as a function of the number of release sites n per presynaptic cell. The maximal postsynaptic response is close to the intersection of the approximate forms and the optimum n decreases with increasing synchrony S . Note that the curves are limited on their right because of the restriction $S \leq N$ (the maximal allowable synchrony is equal to the number of presynaptic neurons) so that the maximum n is $n = M/S$. This upper bound on n holds for similar curves in later figures.

each curve provide an estimate for the optimal n , which decreases as the presynaptic synchrony increases. It should be noted that this effect, which has a maximum as a function of release-site number at constant presynaptic rate, is a distinct phenomenon to the tuning curve as a function of presynaptic rate analyzed in de la Rocha and Parga (2005).

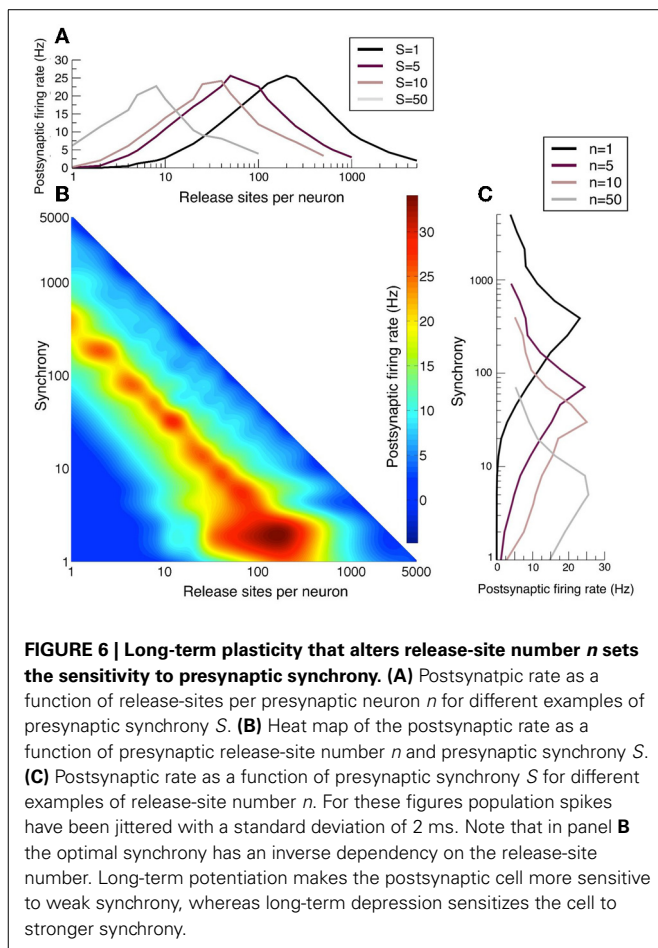
3.5. LONG-TERM PLASTICITY AND RESPONSE TO SYNCHRONY

The post-synaptic firing rate is sensitive to correlations arising from multiple release sites, as discussed above, as well as to presynaptic synchrony (de la Rocha and Parga, 2005). In particular, the firing rate has a maximal response at an optimal n that is a function of the presynaptic synchrony as can be seen in Figure 6. When neurotransmitter release is too strongly correlated in the presynaptic population, the postsynaptic response weakens because the quantity of neurotransmitter released is in excess of that necessary to take the postsynaptic cell to threshold and therefore this limited resource is wasted. The reduction in response to over-strong correlations gives rise to the optimal responses in the space of n and S seen in Figures 6A–C. Note that the band of optimal postsynaptic response is linear with negative gradient in the n , S log–log plot and so the optimal synchrony in the presynaptic population has an inverse relation to the number of release sites n each presynaptic cell makes onto the postsynaptic target.

Analyses of long-term plasticity data (over a 12 h period) by Loebel et al. (2013) demonstrated that connections between thick-tufted layer-5 pyramidal cells in the rat somatosensory cortex alter their efficacy by changing the binomial parameter n , in preference to probability of release or quantal amplitude. Among the experiments analyzed certain connections potentiated four-fold, from an effective binomial n of ~ 25 to ~ 100 . Assuming that the mean excitatory drive remains constant, this potentiation would lead to the postsynaptic cell becoming maximally responsive to signals encoded by weaker presynaptic synchrony (see Figure 6C). It would also cease to amplify strongly correlated stimuli as effectively. Other connections showed four-fold reductions in n from ~ 40 to ~ 10 under protocols that cause long-term depression. In this case the postsynaptic cell would now act as a better amplifier of stimuli encoded with larger correlations.

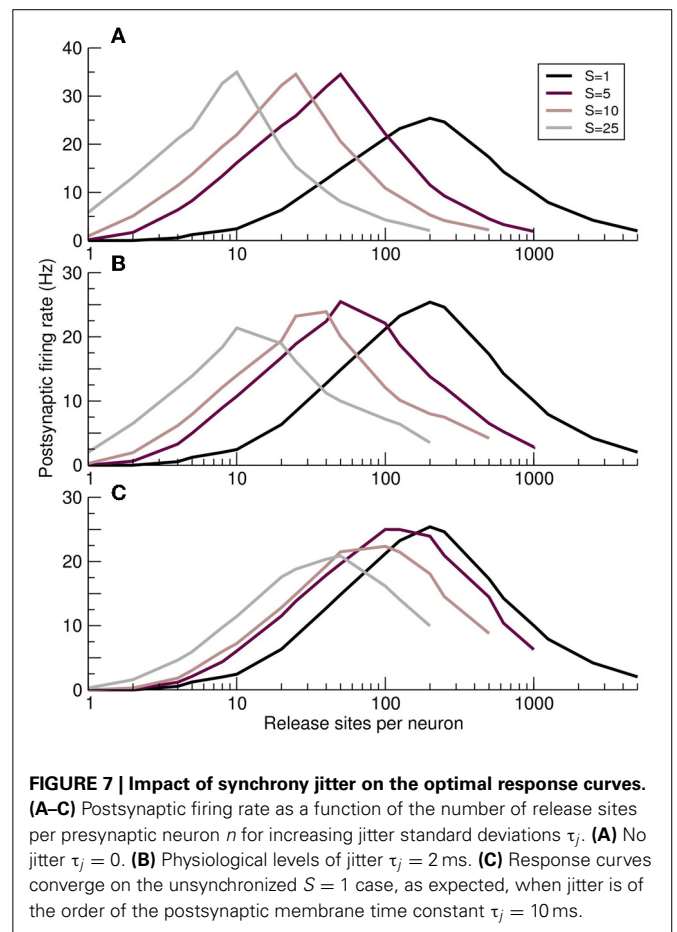
3.6. OPTIMAL RESPONSE AND SYNCHRONY JITTER

The effects of fluctuations in a synchronous presynaptic population can be modeled by adding a Gaussian-distributed jitter, of timescale τ_j , to the timing of each action potential. When the individual components of the synchronous MIP event are too dispersed temporally, i.e., when the jitter is greater than the membrane time constant $\tau_j > \tau$, the MIP event will fail to integrate in the postsynaptic cell. Under these circumstances the effect of correlations is diminished, as illustrated in Figure 7. When jitter is absent (Figure 7A), different values of presynaptic synchrony S produce distinct and clearly defined optimal response curves. With a physiological jitter timescale of $\tau_j = 2$ ms (Figure 7B) the curves for different synchronies shift upwards in n and the peak postsynaptic firing rate falls, particularly for larger synchrony. When $\tau_j = \tau$ (Figure 7C) only relatively strong synchrony values are significantly different from the independent case ($S = 1$).



3.7. OPTIMAL-RESPONSE CURVES ARE A ROBUST FEATURE OF SYNAPTIC HOMEOSTASIS

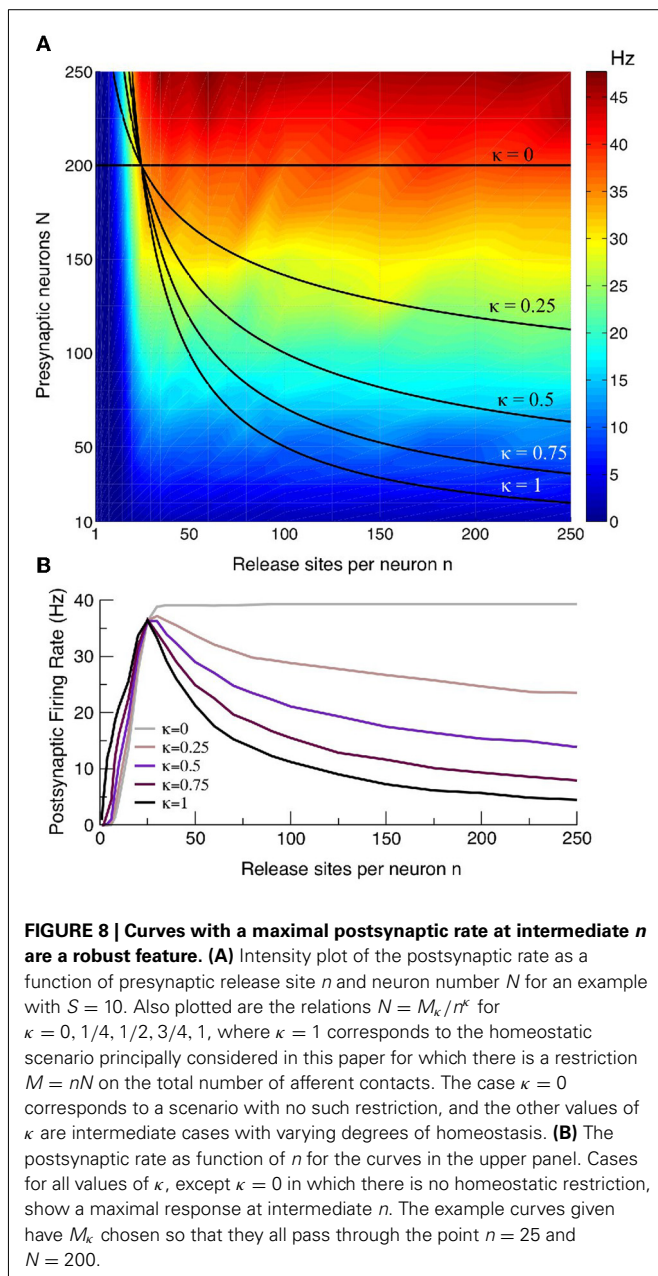
Throughout much of the above analysis we held the total number of release sites $M = nN$ constant and demonstrated an optimal response curve in which the postsynaptic rate peaks at an intermediate n , which is dependent on the presynaptic synchrony S . The rationale for this choice is that, under conditions of homeostasis, synaptic potentiation (increasing n) amongst a subpopulation of presynaptic neurons will occur at the expense of pruning neurons that do not contribute to postsynaptic firing. This will lead to the postsynaptic neuron receiving afferent drive from fewer presynaptic neurons, though each of these will make more contacts (and vice-versa for long-term depression). The theoretical results and simulations are not predicated on the assumption of constant M and so it is interesting to investigate whether the optimal-response effect persists if this restriction is relaxed. Using the example $S = 10$ we plotted the postsynaptic rate as a function of the presynaptic neuron N and release site number n (see Figure 8A). As expected the postsynaptic rate increases with an increasing number of presynaptic neurons N or release sites n . Plotted on the same figure is the curve $N = M/n$ with $M = 5000$ that, because of its reciprocal relation will have low rates at either asymptotes, and an intermediate maximum (see Figure 8B). Also plotted is the curve $N = M_0$ where M_0 is a constant. This corresponds to a scenario in which the entire presynaptic population



has either potentiated or depressed their contacts, thereby changing the number of release sites n a presynaptic neuron makes without altering the total number of presynaptic neurons N . For this case, which is arguably an extremum from the point-of-view of homeostasis, the intermediate maximum is lost: the postsynaptic rate increases monotonically and loses its n dependence when n is sufficiently large, as expected from the first form of Equation (18). However, for intermediate cases of homeostasis of the form $N = M_\kappa/n^\kappa$ with $\kappa = 3/4, 1/2, 1/4$ a maximal postsynaptic rate again occurs at some intermediate n (see Figure 8B). Given the dependence of the postsynaptic rate on n and N in Figure 8A it can be seen geometrically that any curve in which there is a reciprocal relation between N and n will likely feature a maximum at intermediate n and so the optimal-response curves are a robust feature of a postsynaptic neuron in which there is some degree of homeostatic restriction on the total number of afferent contacts.

4. DISCUSSION

We considered the effects of afferent correlations arising from multiple neurotransmitter release sites and a partially synchronized presynaptic population. We derived exact forms for the crosscorrelations of vesicle release site occupancy and vesicle release, and demonstrated that these are identical to those recently obtained from a diffusion and additive-noise approximation (Rosenbaum et al., 2012), validating that approach up



to second-order statistics and explaining their perfect agreement between theoretical and simulational results. We further calculated the exact variance of the membrane voltage, in absence of spike threshold. This quantity extends previous calculations (de la Rocha and Parga, 2005) of synaptic conductance fluctuations and allows for an estimation of the postsynaptic rate in the low-correlation Gaussian regime. For the high-correlation regime, due to multiple release sites n or strong synchrony S , we argued that the EPSPs become increasingly large, the nature of the synaptic fluctuations increasingly shot-noise like, and so the postsynaptic rate tends to the rate of synchronous presynaptic events. Combining these two results for the low and high correlation regimes, we demonstrated that the postsynaptic response is maximal for an intermediate number of release sites or synchrony. The system

therefore exhibits a tuning-curve response to synchrony that can be modulated by long-term plasticity, which alters the number of release sites n .

Neurons respond maximally to specific stimuli when processing sensory input. A coordination of long-term plasticity, afferent synchrony and short-term depression therefore provides a potential tuning mechanism for cells to achieve this sensitivity. Efficient responsiveness would then depend on historical changes in synaptic connectivity (Taschenberger et al., 2002; Loebel et al., 2013) and the transient correlations evoked by a particular stimulus (Averbeck et al., 2006; Cohen and Kohn, 2011). More generally, neuronal networks balance fidelity of signal transmission with the metabolic costs associated with neurotransmitter recycling (Levy and Baxter, 2002; Savtchenko et al., 2012). Although a release of neurotransmitter beyond that necessary to induce a postsynaptic spike may have medium-term conductance implications or counteract strongly fluctuating inhibition, an efficient network would not be expected to exceed the degree of pairwise connectivity that maximizes response to common spike frequencies and correlations. On the other hand, signals encoded by small numbers of cells would require highly potentiated connections to transmit information with any degree of consistency. This implies that across a neuronal network the degree of clustering would be optimally balanced with individual synaptic weights.

To investigate maximal firing rate response to a defined excitatory drive, we have neglected the effects of synaptic inhibition. As *in vivo* network behaviors arise from a balance of excitation and inhibition, a development of the ideas presented here along the above lines would need to incorporate inhibitory effects on the total synaptic conductance. By altering the timescales on which excitatory inputs are integrated, inhibitory drive could allow a more finely-tuned response to afferent sub-populations with varying degrees of temporal dispersion. Another extension of this work would be to incorporate different forms of short-term synaptic plasticity into the model. This would be particularly appropriate when studying connections between specific cell-types where there is experimental evidence for other forms of synaptic dynamics. It is also likely that effects moderating synaptic depression, such as the increasing facilitation in the maturing neocortex (Reyes and Sakmann, 1999) would lead to qualitatively different behavior as cortical networks develop.

FUNDING

This research was supported by a Warwick Systems Biology Doctoral Training Centre fellowship to Alex D. Bird funded by the UK EPSRC and BBSRC funding agencies.

REFERENCES

- Abbott, L. F. (1997). Synaptic depression and cortical gain control. *Science* 275, 221–224. doi: 10.1126/science.275.5297.221
- Abbott, L. F., and Regehr, W. G. (2004). Synaptic computation. *Nature* 431, 796–803. doi: 10.1038/nature03010
- Aertsen, A. M., Gerstein, G. L., Habib, M. K., and Palm, G. (1989). Dynamics of neuronal firing correlation: modulation of “effective connectivity”. *J. Neurophysiol.* 61, 900–917.
- Alijani, A. K., and Richardson, M. J. E., (2011). Rate response of neurons subject to fast or frozen noise: from stochastic and homogeneous to deterministic and heterogeneous populations. *Phys. Rev. E* 84, 011919. doi: 10.1103/PhysRevE.84.011919

- Averbeck, B. B., Latham, P. E., and Pouget, A. (2006). Neural correlations, population coding and computation. *Nat. Rev. Neurosci.* 7, 358–366. doi: 10.1038/nrn1888
- Baker, S. N., Spinks, R., Jackson, A., and Lemon, R. N. (2001). Synchronization in monkey motor cortex during a precision grip task. I. Task-dependent modulation in single-unit synchrony. *J. Neurophysiol.* 85, 869–885.
- Brunel, N., and Hakim, V. (1999). Fast global oscillations in networks of integrate-and-fire neurons with low firing rates. *Neural Comput.* 11, 1621–1671. doi: 10.1162/089976699300016179
- Cain, N., and Shea-Brown, E. (2013). Impact of correlated neural activity on decision-making performance. *Neural Comput.* 25, 289–327. doi: 10.1162/NECO_a_00398
- Capaday, C., Ethier, C., Van Vreeswijk, C., and Darling, W. G. (2013). On the functional organization and operational principles of the motor cortex. *Front. Neural Circ.* 7:66. doi: 10.3389/fncir.2013.00066
- Chen, W. X., and Buonomano, D. V. (2012). Developmental shift of short-term synaptic plasticity in cortical organotypic slices. *Neuroscience* 213, 38–46. doi: 10.1016/j.neuroscience.2012.04.018
- Cohen, M. R., and Kohn, A. (2011). Measuring and interpreting neuronal correlations. *Nat. Neurosci.* 14, 811–819. doi: 10.1038/nn.2842
- Cohen, M. R., and Newsome, W. T. (2008). Context-dependent changes in functional circuitry in visual area MT. *Neuron* 60, 162–173. doi: 10.1016/j.neuron.2008.08.007
- de la Rocha, J., and Parga, N. (2005). Short-term synaptic depression causes a non-monotonic response to correlated stimuli. *J. Neurosci.* 25, 8416–8431. doi: 10.1523/JNEUROSCI.0631-05.2005
- deCharms, R. C., and Merzenich, M. M. (1996). Primary cortical representation of sounds by the coordination of action-potential timing. *Nature* 381, 610–613. doi: 10.1038/381610a0
- Fox, G. Q. (1988). A morphometric analysis of synaptic vesicle distributions. *Brain Res.* 475, 103–117. doi: 10.1016/0006-8993(88)90203-X
- Fuhrmann, G., Segev, I., Markram, H., and Tsodyks, M. (2002). Coding of temporal information by activity-dependent synapses. *J. Neurophysiol.* 87, 140–148. doi: 10.1152/jn.00258.2001
- Furukawa, T., Kuno, M., and Matsuura, S. (1982). Quantal analysis of a decremental response at hair cell-afferent fibre synapses in the goldfish sacculus. *J. Physiol.* 322, 181–195.
- Gardiner, C. (2010). *Stochastic Methods: A Handbook for the Natural and Social Sciences*. Berlin: Springer.
- Gerstein, G. L., and Mandelbrot, B. (1964). Random walk models for the spike activity of a single neuron. *Biophys. J.* 4, 41–68. doi: 10.1016/S0006-3495(64)86768-0
- Hallermann, S., and Silver, R. A. (2012). Sustaining rapid vesicular release at active zones: potential roles for vesicle tethering. *Trends Neurosci.* 36, 1–10. doi: 10.1016/j.tins.2012.10.001
- Hebb, D. O. (2002). *The Organization of Behavior: A Neuropsychological Theory*. Mahwah, NJ: L. Erlbaum Associates.
- Hu, Y., Qu, L., and Schikorski, T. (2008). Mean synaptic vesicle size varies among individual excitatory hippocampal synapses. *Synapse* 62, 953–957. doi: 10.1002/syn.20567
- Kilpatrick, Z. P. (2012). Short term synaptic depression improves information transfer in perceptual multistability. *Front. Comput. Neurosci.* 7:85. doi: 10.3389/fncom.2013.00085
- Kuhn, A. (2004). Neuronal integration of synaptic input in the fluctuation-driven regime. *J. Neurosci.* 24, 2345–2356. doi: 10.1523/JNEUROSCI.3349-03.2004
- Kuhn, A., Aertsen, A., and Rotter, S. (2003). Higher-order statistics of input ensembles and the response of simple model neurons. *Neural Comput.* 15, 67–101. doi: 10.1162/089976603321043702
- Levy, W. B., and Baxter, R. A. (2002). Energy-efficient neuronal computation via quantal synaptic failures. *J. Neurosci.* 22, 4746–4755.
- Loebel, A., Le Be, J. V., Richardson, M. J. E., Markram, H., and Herz, A. V. M. (2013). Matched pre- and post-synaptic changes underlie synaptic plasticity over long time scales. *J. Neurosci.* 33, 6257–6266. doi: 10.1523/JNEUROSCI.3740-12.2013
- Markram, H., Gerstner, W., and Sjöström, P. J. (2011). A history of spike-timing-dependent plasticity. *Front. Synaptic Neurosci.* 3:4. doi: 10.3389/fnsyn.2011.00004
- Megias, M., Emri, Z., Freund, T. F., and Gulyás, A. I. (2001). Total number and distribution of inhibitory and excitatory synapses on hippocampal CA1 pyramidal cells. *Neuroscience* 102, 527–540. doi: 10.1016/S0306-4522(00)00496-6
- Mitchell, J. F., Sundberg, K. A., and Reynolds, J. H. (2009). Spatial attention decorrelates intrinsic activity fluctuations in Macaque area V4. *Neuron* 63, 879–888. doi: 10.1016/j.neuron.2009.09.013
- O’Kusky, J., and Colonnier, M. (1982). A laminar analysis of the number of neurons, glia, and synapses in the adult cortex (area 17) of adult macaque monkeys. *J. Comp. Neurol.* 210, 278–290. doi: 10.1002/cne.902100308
- Reyes, A., and Sakmann, B. (1999). Developmental switch in the short-term modification of unitary EPSPs evoked in layer 2/3 and layer 5 pyramidal neurons of rat neocortex. *J. Neurosci.* 19, 3827–3835.
- Richardson, M. J. E., and Swarbrick, R. (2010). Firing-rate response of a neuron receiving excitatory and inhibitory synaptic shot noise. *Phys. Rev. Letts.* 105:178102. doi: 10.1103/PhysRevLett.105.178102
- Rosenbaum, R., Rubin, J., and Doiron, B. (2012). Short term synaptic depression imposes a frequency dependent filter on synaptic information transfer. *PLoS Comput. Biol.* 8:e1002557. doi: 10.1371/journal.pcbi.1002557
- Rothman, J. S., Cathala, L., Steuber, V., and Silver, R. A. (2009). Synaptic depression enables neuronal gain control. *Nature* 457, 1015–1018. doi: 10.1038/nature07604
- Salinas, E., and Sejnowski, T. J. (2000). Impact of correlated synaptic input on output firing rate and variability in simple neuronal models. *J. Neurosci.* 20, 6193–6209.
- Savtchenko, L. P., Sylantyev, S., and Rusakov, D. A. (2012). Central synapses release a resource-efficient amount of glutamate. *Nat. Neurosci.* 16, 10–12. doi: 10.1038/nn.3285
- Scott, P., Cowan, A. L., and Stricker, C. (2012). Quantifying impacts of short-term plasticity on neuronal information transfer. *Phys. Rev. E* 85, 041921. doi: 10.1103/PhysRevE.85.041921
- Seriès, P., Latham, P. E., and Pouget, A. (2004). Tuning curve sharpening for orientation selectivity: coding efficiency and the impact of correlations. *Nat. Neurosci.* 7, 1129–1135. doi: 10.1038/nn1321
- Spruston, N. (2008). Pyramidal neurons: dendritic structure and synaptic integration. *Nat. Rev. Neurosci.* 9, 206–221. doi: 10.1038/nrn2286
- Südhof, T. C. (2004). The synaptic vesicle cycle. *Annu. Rev. Neurosci.* 27, 509–547. doi: 10.1146/annurev.neuro.26.041002.131412
- Taschenberger, H., Leão, R. M., Rowland, K. C., Spirou, G. A., and von Gersdorff, H. (2002). Optimizing synaptic architecture and efficiency for high-frequency transmission. *Neuron* 36, 1127–1143. doi: 10.1016/S0896-6273(02)01137-6
- Tsodyks, M., Pawelzik, K., and Markram, H. (1998). Neural networks with dynamic synapses. *Neural Comput.* 10, 821–835. doi: 10.1162/089976698300017502
- Tsodyks, M. V., and Markram, H. (1997). The neural code between neocortical pyramidal neurons depends on neurotransmitter release probability. *Proc. Natl. Acad. Sci. U.S.A.* 94, 719–723. doi: 10.1073/pnas.94.2.719
- von der Malsburg, C. (1981). “Internal Report 81-2, Neurobiology, Max-Planck Institute for Biophysical Chemistry,” in *The Correlation Theory of Brain Function*, (Göttingen).
- Zador, A. A. (1998). Impact of synaptic unreliability on the information transmitted by spiking neurons. *J. Neurophysiol.* 79, 1219–1229.
- Zucker, R. S., and Regehr, W. G. (2002). Short-term synaptic plasticity. *Annu. Rev. Physiol.* 64, 355–405. doi: 10.1146/annurev.physiol.64.092501.114547

Conflict of Interest Statement: The authors declare that the research was conducted in the absence of any commercial or financial relationships that could be construed as a potential conflict of interest.

Received: 06 August 2013; accepted: 07 January 2014; published online: 30 January 2014.

Citation: Bird AD and Richardson MJE (2014) Long-term plasticity determines the postsynaptic response to correlated afferents with multivesicular short-term synaptic depression. *Front. Comput. Neurosci.* 8:2. doi: 10.3389/fncom.2014.00002
This article was submitted to the journal *Frontiers in Computational Neuroscience*.
Copyright © 2014 Bird and Richardson. This is an open-access article distributed under the terms of the Creative Commons Attribution License (CC BY). The use, distribution or reproduction in other forums is permitted, provided the original author(s) or licensor are credited and that the original publication in this journal is cited, in accordance with accepted academic practice. No use, distribution or reproduction is permitted which does not comply with these terms.

APPENDIX

DERIVATION OF THE VOLTAGE VARIANCE

The voltage equation can be written in the form

$$\tau \frac{dV}{dt} = E - V + a\tau\zeta \quad (19)$$

where ζ is the summation of the release trains across the N presynaptic neurons and each of their n contacts

$$\zeta = \sum_{i=1}^N \sum_{j=1}^n \chi_{ij} \quad (20)$$

where χ_{ij} takes the form of Equation (11) for the i th presynaptic neuron's j th contact. The autocorrelation of ζ is therefore comprised of Nn autocorrelations of χ in the form of Equation (12), $Nn(n-1)$ crosscorrelations of χ for distinct release trains sharing the same presynaptic neuron given by Equation (13) with $\gamma = 1$ and $N(N-1)n^2$ crosscorrelations of χ for release trains with different presynaptic neurons given by Equation (13) with $\gamma = c$.

Taking expectations of both side of Equation (19) in the steady state gives

$$\langle V \rangle = E + a\tau \langle \zeta \rangle = E + aM\tau R_{ap} \langle x \rangle. \quad (21)$$

We can now solve Equation (19) to give

$$V - \langle V \rangle = a \int_{-\infty}^t dt' e^{-(t-t')/\tau} (\zeta(t') - \langle \zeta \rangle) \quad (22)$$

so that the voltage variance can be written as an integral over the autocorrelation of ζ , $\text{Autocorr}(\zeta) = \langle (\zeta(t') - \langle \zeta \rangle) (\zeta(t'') - \langle \zeta \rangle) \rangle$

$$(V - \langle V \rangle)^2 = a^2 \int_{-\infty}^t dt' \int_{-\infty}^t dt'' e^{-(t-t')/\tau} e^{-(t-t'')/\tau} \text{Autocorr}(\zeta). \quad (23)$$

As discussed above, the autocorrelation of ζ is the sum of the various crosscorrelations of χ so that it must take the form

$$\text{Autocorr}(\zeta) = \alpha \delta(t' - t'') + \beta e^{-|t' - t''|/\tau_x} \quad (24)$$

where α and β are obtained from the prefactors of the terms in Equations (12, 13) multiplied by their respective contributions. Inserting Equation (24) into (23) and performing the integration gives

$$\text{Var}(V) = a^2 \left(\frac{\alpha\tau}{2} + \frac{\beta\tau^2\tau_x}{\tau + \tau_x} \right). \quad (25)$$

On substituting the appropriate forms for α and β the result given in Equation (15) is obtained.

2.8 Additional Discussion

Since publication, a number of points about this paper have been raised that bear discussion here.

2.8.1 Synaptic kernels

This chapter treats neurotransmitter release and the subsequent EPSP as point events: χ and ζ are trains of delta functions. In reality, EPSPs take a form closer to a difference of exponentials as neurotransmitter-gated channels open and close (Eccles et al. 1941; Richardson and Silberberg 2008). It would be possible to include a synaptic kernel accounting for a more physiologically accurate EPSP form. The effect of this is relatively minor, the width of an excitatory synaptic kernel is a few milliseconds making it much shorter than the other important timescales, and the key effects are preserved. On minor effect is to make the postsynaptic response slightly less dependent on perfect synchrony in vesicle release: the changing jitter in Figure 7 would have less of an impact.

2.8.2 Location of the maximum in the postsynaptic voltage variance

Eq. 15 gives the postsynaptic voltage variance as a function of the synaptic parameters, and Figure 3 shows that it is non-monotonic as a function of the presynaptic firing rate R_a . It is therefore of interest to find analytically where this maximum occurs. This maximum occurs when $\frac{\partial(\text{Var}(V))}{\partial R_a} = 0$. To solve this equation, it is useful to compute the following derivatives

$$\begin{aligned}\frac{\partial \langle x \rangle}{\partial R_a} &= \frac{-pR_r}{(R_r + pR_a)^2} \\ \frac{\partial \langle xx' \rangle_\gamma}{\partial R_a} &= \frac{-2pR_r^2(2p(2 - \gamma p)R_a + R_r(4 - \gamma p))}{(R_r + pR_a)^2(2R_r + pR_a(2 - \gamma p))^2} \\ \frac{\partial}{\partial R_a} \left(\frac{R_a^2}{1 + \tau R_r + p\tau R_a} \right) &= \frac{R_a(p\tau R_a + 2(1 + \tau R_r))}{(1 + \tau R_r + p\tau R_a)^2}\end{aligned}\tag{2.1}$$

Obtaining a general closed form solution is unfortunately impossible as it is equivalent to solving an eighth-order polynomial in R_a .

However, in the case where release is reliable ($p = 1$) and there is only a single presynaptic neuron ($N = 1$), the variance equation reduces to a more tractable form but still provides some insight. In this case, the variance $\text{Var}(V)$ is given by

$$\text{Var}(V) = \frac{a^2\tau n R_a}{2} (\langle x \rangle + (n - 1)\langle xx' \rangle_1) - \frac{(a\tau n R_a \langle x \rangle)^2}{1 + \tau(R_r + R_a)}\tag{2.2}$$

Here, correlations in vesicle release from synchrony between cells is neglected, but correlations arising from multiple release sites remain. Similarly, variance arising from uncertain release is neglected, but variance from uncertain spike arrival and restock events remain. This reduced case produces qualitatively similar behaviour to the full model. We seek R_a such that

$$0 = \frac{R_r}{R_r + R_a} + (n-1) \frac{2R_r^2}{(2R_r + R_a)(R_r + R_a)} - \frac{R_a R_r}{(R_r + R_a)^2} - (n-1) \frac{2R_a R_r^2 (3R_r + 2R_a)}{(R_r + R_a)^2 (2R_r + R_a)^2} - 2\tau n \frac{R_a R_r^3 (\tau R_a^2 + 3\tau R_a R_r + 2R_r(1 + \tau R_r))}{(R_r + R_a)^3 (1 + \tau(R_r + R_a))^2} \quad (2.3)$$

Even solving the reduced model is equivalent to solving a sixth-order polynomial in R_a ; a final assumption is necessary to produce a tractable result. A useful assumption is that the postsynaptic membrane time constant is very small, $\tau \ll 1$. This means individual EPSPs decay very rapidly. Then, we can linearise Eq. (2.2) in terms of τ so that

$$\text{Var}(V) \approx \frac{a^2 \tau n R_a}{2} (\langle x \rangle + (n-1) \langle x x' \rangle_1) \quad (2.4)$$

and the maximum occurs when R_a satisfies

$$0 = \frac{R_r}{R_r + R_a} + (n-1) \frac{2R_r^2}{(2R_r + R_a)(R_r + R_a)} - \frac{R_a R_r}{(R_r + R_a)^2} - (n-1) \frac{2R_a R_r^2 (3R_r + 2R_a)}{(R_r + R_a)^2 (2R_r + R_a)^2} \quad (2.5)$$

This is equivalent to a quadratic equation in R_a

$$0 = (3-2n)R_a^2 + 4R_r R_a + 4(2n-1)R_r^2 \quad (2.6)$$

with positive solution (in the interesting case with multiple release sites, $n \geq 2$)

$$R_a = \frac{2R_r}{2n-3} \left(1 + \sqrt{1 + (2n-1)(2n-3)} \right) \quad (2.7)$$

This result holds for a reduction of the full model with no uncertainty in vesicle release ($p = 1$), only one presynaptic neuron ($n = 1$), and very fast decay of voltage transients ($\tau \ll 1$). Nevertheless, it retains sources of stochasticity in uncertain spike arrival and vesicle restock, as well as correlated vesicle release from different active sites. The feature of a non-monotonic variance response to increasing presynaptic firing rates still holds for the reduced model and the above gives some insight into what influences the location of the peak. The presynaptic rate R_a that gives the highest variance response is an increasing function of restock rate R_r , showing that resilience to the greater depression

induced by high firing rates is key. It is also a decreasing function of release-site number n , showing that stronger potential correlations increase the sensitivity to depression at higher values of R_a .

2.8.3 Validity of the low n approximation

In Figure 5, the low release site number n approximation (blue dashed line) appears to provide a relatively poor fit to the simulated firing rates. The major reason for this is that non-zero firing rates in the low n regime depend on on shot-noise finite-size fluctuations that are not captured by the long-term steady-state variance. The gaussian firing rate provides a better estimate as the long-term variance becomes a better descriptor of the short-term voltage behaviour when the firing rate increases, for example when synchrony is higher ($S = 25$ curve).

2.8.4 The limit $R_r \rightarrow \infty$

The major qualitative result of this paper, the non-monotonic postsynaptic response to presynaptic correlation, can arise even when synaptic depression is absent. As the vesicle restock rate R_r increases the left-hand side of the firing rate tuning curves will get taller, tending to a limiting curve as $R_r \rightarrow \infty$. In this case the amount of neurotransmitter released is limited only by the presynaptic activity, but the postsynaptic rate still displays a tuning curve response to changing presynaptic correlations. There are a number of reasons to use the more complex depressing model discussed here over a static synaptic model in this context. The first is physiological relevance: depression occurs at real synapses and the shape and location of the tuning curves depend on the parameter R_r . The machinery introduced here allows the tuning curve to be fixed for realistic synaptic parameter sets. Secondly, the results discussed do depend on quantal correlations and finite-size effects. A major contribution of this paper is to develop the mathematics necessary to treat these factors together and variable restock is an important component of the variance of the quantal synaptic model. Finally, in the absence of depression, the postsynaptic firing rate could be taken to an arbitrarily high value by increasing the presynaptic firing rate R_a . It is important to note the interaction of the correlation-dependent tuning curve (Figs 5 and 6) with the rate-dependent tuning curve seen by de la Rocha and Parga (2005) and further explained by the non-monotonic variance curve (Fig. 3). Increasing the presynaptic rate R_a has the effect of reducing neurotransmitter release correlations by leaving greater numbers of release sites empty, flattening out the correlation tuning curves. Without a consideration of depression, there would be no scope to study this further effect.

2.8.5 Setting tuning curves with release probability p

The location of the correlation tuning curves are also set by the release probability p . For lower release probabilities, stronger correlations are necessary to synchronously release the same amount of neurotransmitter, but release sites do not depress as much. All else being equal, reducing p pushes the tuning curves to the right and flattens them. Increasing p has the opposite effect.

Chapter 3

Synaptic transmission of spike trains with arbitrary interspike interval statistics

3.1 Overview

THIS chapter quantifies how well spike trains with arbitrary ISI statistics activate depressing synapses. Approximating spike trains as a Poisson process is a common approach; however, research has shown that approximating the sum of several non-Poisson spike trains as a Poisson spike train is unsound (Lindner 2006) and that the feedforward properties of non-Poisson trains can be qualitatively different to the Poisson case (Cateau and Reyes 2006). A more recent numerical study combined spike train analysis with plastic synapses, finding that regular spike trains are better at crossing depressing synapses than ‘bursty’ trains (Reich and Rosenbaum 2013).

I now extend the models and methods introduced in Chapter 2 to consider non-Poisson spike trains and derive exact results for the correlations in neurotransmitter release when the spike train is a renewal process. Regular spike trains are shown to cause stronger synaptic responses, and this is verified experimentally. However, when the release probability is low, ‘bursty’ trains are able to cause larger deviations in the postsynaptic voltage. I accurately approximate the postsynaptic firing rate in the renewal and weakly-correlated ISI case, allowing the future incorporation of temporally structured spiking activity into studies of networks with dynamic synapses.

Note that the application of this theory to networks driven with a non-constant rate requires a very careful consideration of the timescales involved: it is, for example, hard to distinguish between a ‘bursty’ neuron and one that rapidly transitions between high and low firing rates. A number of caveats are needed to extend this theory to non-constant, non-Poisson, rates; discussion of such results is beyond the scope of this chapter.

3.1.1 Author contributions

Conceived the study: MJER and ADB. Derived and solved equations: ADB and MJER. Conducted experiments: MRF and MJW. Wrote code for simulations: ADB. Prepared figures: ADB. Wrote the paper: ADB and MJER.

The majority of the first draft was written by ADB. The major exceptions to this are the two experimental sections of the Methods, *Preparation of neocortical slices* and *Patch-clamp recordings from excitatory cells*, which follow standard lab protocols. All equations used in the final results were initially derived by ADB. The auto- and crosscorrelations in vesicle release (Eqs (3.19) and (3.32)) were initially written as an infinite series of convolution integrals. The idea of writing these as inverse Fourier transforms, which substantially simplifies the later voltage variance result, was introduced by MJER and the correct Fourier form was derived by ADB.

Synaptic transmission of spike trains with arbitrary interspike interval statistics

Alex D. Bird^{1,2,3}, Michael R. Fisher², Mark J. Wall², and Magnus J. E. Richardson³

¹ Warwick Systems Biology Doctoral Training Centre, ² School of Life Sciences, and ³

Warwick Systems Biology Centre,
University of Warwick, CV4 7AL, United Kingdom.

Abstract Short-term synaptic depression, caused by depletion of releasable neurotransmitter vesicles, modulates the strength of neuronal connections in a history-dependent manner. Quantifying the statistics of synaptic transmission therefore requires the development of stochastic models linking probabilistic neurotransmitter release with the spike-train statistics of the presynaptic population. A common approach has been to model the presynaptic spike train as either regular or a memory-less Poisson process: few analytical results are available that describe the behaviour of a depressing synapse when the afferent spike train has more complex, temporally correlated statistics. We have derived a series of results that allow for the fraction of occupied release sites and the neurotransmitter release probability to be calculated for a presynaptic spike train with arbitrary interspike interval (ISI) statistics and verified these with paired-cell recordings. The results take a particularly compact form when the presynaptic spike times are generated by a renewal process, i.e. when the ISIs are independent. This encompasses a broad range of models that are currently used for circuit and network analyses, including the class of integrate-and-fire models. Our approach allows for the postsynaptic voltage mean and variance to be calculated, which in turn gives an accurate approximation of the firing rate of a neuron driven by depressing synapses from non-Poissonian presynaptic neurons. These results allow for the incorporation of more complex and physiologically relevant firing patterns into future analytic studies of neuronal circuits and networks.

Key words: Synaptic depression, non-Poisson, renewal, adaptation, firing rate

3.2 Introduction

Variability in the nervous system arises from unreliability in processes ranging in scale from ion channel dynamics to neurotransmitter vesicle release (Verveen et al. 1967; Steinmetz et al. 2000; White et al. 2000; Faisal et al. 2008; Ribrault et al. 2011). The activity of a cortical neuron is therefore stochastic; dependent on the statistical properties of the incoming drive (Kuhn 2004; de la Rocha and Parga 2005). A common

approach to treating this stochasticity analytically assumes that neuronal firing is uncorrelated, with a Poisson process used to model spike times (Stein 1965; Kuhn et al. 2003; Rosenbaum et al. 2012).

However, non-Poisson activity is regularly observed *in vivo* (Fellous et al. 2003; Reyes 1999; Buzsaki and Draguhn 2004; Shinomoto et al. 2009) and can have a substantial effect on the propagation of activity (Lindner 2006; Cateau and Reyes 2006; Pipa et al. 2013; Dummer et al. 2014). The impact of non-Poisson spiking is compounded when considered alongside vesicle-depletion depression, where synaptic transmission becomes weaker and less reliable as the available packaged neurotransmitter is released (Eccles et al. 1941; Tsodyks and Markram 1997; Zucker and Regehr 2002; Südhof 2004). Whilst average rate effects under the influence of depression are well-known (Abbott 1997; Tsodyks et al. 1998; Cortes et al. 2013), a recent study by Reich and Rosenbaum (2013) has shown that a renewal firing pattern more regular than Poisson slightly increases the rate of vesicle release, enhancing the fidelity and efficiency of signal transmission.

We present an analysis for quantifying synaptic transmission when the presynaptic action potential train is a renewal process with an arbitrary interspike interval distribution (ISI). This covers a wide variety of spiking neuron models such as the leaky, quadratic and exponential integrate-and-fire receiving noisy drive with temporal correlations shorter than the shortest ISI (Fourcaud-Trocmé et al 2003; Ostojic 2011), and is often used to fit experimental data (Bennett and Kearns 2000; Fellous et al. 2003; Barbieri 2007; Shinomoto et al. 2009). The resulting predictions for levels of vesicle occupancy under renewal firing patterns are verified by paired-cell recordings from cortical layer-V pyramidal cells. We highlight the applications of our results in two situations: when the ISIs are gamma-distributed, with a single parameter α continuously varying the regularity of the spike train, and when the spikes are generated by white Gaussian and shot noise drive to the presynaptic cell. Finally, we show that the results allow for an accurate estimation of postsynaptic firing rates, allowing consideration of correlated behaviour in studies of larger systems.

3.3 Methods and Models

Ethics statement. All experiments were performed in accordance with the UK Animals (Scientific Procedures) Act (1986).

Synapse and neuron. A quantal model of synaptic dynamics is used. The binary variable x represents the occupancy of an active site, taking the value 1 when a neurotransmitter vesicle is present and 0 otherwise. As x is a binary variable taking only the values 0 and 1, $x^2 \equiv x$

and so $\text{var}(x) = \langle x \rangle - \langle x \rangle^2$. Empty sites are restocked as a Poisson process with rate R_r . On arrival of an action potential at the site, a present vesicle will fuse and release neurotransmitter with probability p . The train of neurotransmitter release events from a site is denoted χ . The neurotransmitter contained in a single vesicle causes an increase in the postsynaptic voltage of magnitude a . We initially consider the behaviour of a single release site, before looking at a synapse consisting of n release sites receiving the same presynaptic train, but with independent restock processes.

Neurons are treated as leaky integrators with time constant τ with the addition of a threshold-reset mechanism to account for firing: when the membrane voltage V reaches a voltage V_{th} a spike is recorded and the voltage is reset to V_{re} . The voltage therefore obeys

$$\frac{dV}{dt} = \frac{E_0 - V}{\tau} + a \sum_k \delta(t - t_k) \quad (3.1)$$

where δ is a Dirac delta and t_k are the times of vesicle release at synapses onto the neuron.

Renewal processes. The firing of the presynaptic neuron is modelled as a renewal process with an arbitrary distribution f of interspike intervals. This means that there is no correlation between successive interspike intervals, although the shape of the ISI distribution will cause correlations in the spike times themselves. The overall firing rate of the presynaptic neuron is the reciprocal of the mean ISI μ_f . ‘Bursty’ neurons have positively autocorrelated, whereas periodic neurons have negatively autocorrelated, spike trains. Integrate-and-fire neurons (LIF, EIF, QIF) receiving short-time correlated drive will fire as a renewal process, with the degree of burstiness constrained by the difference between resting and reset values. If $V_{re} > E_0$, irregular activity will emerge with positively correlated spike times and if $V_{re} < E_0$ the firing will be more regular. The drive can be either a Gaussian process modelling relatively weak drive at high rates (Gerstein and Mandelbrot 1964; Brunel and Hakim 1999), or a shot-noise process (Stein 1965; Wilbur and Rinzel 1983; Richardson and Swarbrick 2010) capturing finite size effects.

Gamma distributed ISIs provide a useful illustration of the results presented here as a single shape parameter α continuously varies the ‘burstiness’ of the train.

$$f(t) = \frac{(\alpha R_a)^\alpha}{\Gamma(\alpha)} t^{\alpha-1} e^{-\alpha R_a t} \quad (3.2)$$

for $\Gamma(\alpha) = \int_0^\infty x^{\alpha-1} e^{-x} dx$ the gamma function. When $\alpha = 1$ this reduces to an exponential distribution and the neuron fires as a Poisson process. For $0 < \alpha < 1$, firing is more irregular, or ‘bursty’, than Poisson and for $\alpha > 1$ it is more regular (see Figure 1).

Preparation of neocortical slices. Parasagittal slices of somatosensory neocortex ($300 \mu\text{m}$) were prepared from male Wistar rats, at postnatal day **14-16**. Rats were kept on a 12 hour light-dark cycle with slices made 90 minutes after entering the light cycle. In accordance with the UK Animals (Scientific Procedures) Act (1986), rats were killed by cervical dislocation and then decapitated. The brain was rapidly removed, cut down the midline and the two sides of the brain stuck down. The brain was angled at 15° so that planar slices could be obtained with the dendritic structure of the excitatory neurons intact. Slices were cut with a Microm HM

650 V micro-slicer (Carl Zeiss) in cold (2-4°C) high Mg^{2+} low Ca^{2+} artificial cerebrospinal fluid (aCSF) consisting of 127 mM NaCl, 1.18 mM KH_2PO_4 , 2.14 mM KCl, 26 mM $NaHCO_3$, 8 mM $MgCl_2$, 0.5 mM $CaCl_2$ and 10 mM glucose. Slices were stored at 34°C for 1 hour in standard aCSF (1 mM Mg^{2+} and 2 mM $CaCl_2$) and then at room temperature for 1-6 hours.

Patch-clamp recordings from excitatory cells. A slice was transferred to the recording chamber and perfused at 2 ml/min with aCSF at 32°C. Slices were visualised using an Olympus BX51W1 microscope with IR-DIC optics and a Hitachi CCD camera (Scientifica, Bedford, UK). Whole-cell recordings were made with patch pipettes (5-8 m Ω) manufactured from thick walled glass (Harvard Apparatus Edenbridge UK) containing 135 mM K-gluconate, 7 mM NaCl, 10 mM HEPES, 0.5 mM EGTA, 2 mM ATP, 0.3 mM GTP, and 10 mM phosphocreatine (290 mOSM, pH 7.2). Voltage recordings were obtained using an Axon Multiclamp 700B amplifier and digitised at 20 kHz with a Digidata 1440A (Molecular Devices, Sunnyvale, CA). Pyramidal neurons were identified based on their location in the layered neocortex, somata size and dendritic extent. During recording, neurons were labelled either with the fluorescent dye Alexa Fluor® 488 hydrazide (12.5 mM, Life Technologies, Paisley, UK) or with biocytin (1 mg/mL, Sigma-Aldrich, Dorset, UK) to allow confirmation of the cell type and to ensure an intact apical dendrite.

Stimulation protocols. Presynaptic cells were stimulated with square-pulse currents of 5ms duration and magnitude sufficient to reliably induce a single action potential without causing bursting. Stimulation protocols were 8s long with stochastic activity from 0.5s to 4.5s and a recovery spike at 7.75s. A rest period of 15s was applied between presentations of the stimulus. Spike times in the stochastic portion were generated as a renewal process with interspike intervals following a gamma distribution with mean 0.2s and various shape parameters α . Additional constraints to allow for consistent results were that spikes must be more than 5ms apart and that the same number (19) must occur between 0.5s and 4.5s. Stimulation protocols that did not satisfy these constraints were discarded and replaced. Four α values were used: 1/3, 2/3, 1, and 10. A protocol was generated for each α value and these were successively applied to the presynaptic cell until 30 repetitions of each were obtained.

EPSP amplitude analysis. EPSP magnitudes were extracted from the averaged postsynaptic traces using the deconvolution method of Richardson and Silberberg (2008), so that each EPSP represents the average over 30 repetitions of the same stimulus. Most traces exhibited a ‘sag’ due to I_h currents and it was necessary to account for this. Amplitudes were normalised to the size of the first EPSP in each trace to allow for comparison between connections. Steady-state was taken to be the period between the fourth and nineteenth EPSPs.

Parameter comparison between cells. Comparing mean EPSP amplitudes between different synapses required normalisation of their dynamic parameters: release probability p and restock rate R_r . These were extracted from the first three EPSPs in each trace, which were not used to estimate the steady-state mean EPSP amplitude. Estimates for p and R_r were obtained by minimising the squared difference between each EPSP and that predicted by Tsodyks-Markram depression model (Tsodyks and Markram 1997). For the five synapses studied, this gives release probability estimates of $p = 0.65, 0.63, 0.59, 0.62$, and 0.62 . The corresponding restock rates are found to be $R_r = 2.64, 2.39, 1.56, 3.18$, and 1.89 Hz. The mean parameters across all sites

Parameter	Interpretation	Value
a	amplitude of EPSP induced by neurotransmitter released from a single docked vesicle	0.25mV
a_e	mean amplitude of a presynaptic impulse	
E_0	resting membrane voltage	−70mV
n	number of vesicle release sites per presynaptic neuron	Varies
N	number of presynaptic neurons	Varies
p	probability of spike arrival inducing neurotransmitter release at a site with a vesicle present	0.66
R_a	rate of presynaptic spiking	10Hz
R_e	rate of excitatory shot noise drive to presynaptic cell	
R_r	rate at which empty vesicles are replaced at release sites	2Hz
V	postsynaptic membrane voltage	Varies
V_{re}	voltage membrane resets to after an action potential	Varies
V_{th}	threshold at which action potentials are initiated	−55mV
α	shape parameter of gamma ISIs	Varies
μ_f	mean ISI	0.1s
σ_v	strength of gaussian white noise to presynaptic cell	
τ	membrane time constant	10ms

Table 3.1: Typical parameter values used for figures.

are therefore release probability $\bar{p} = 0.62$ and restock rate $\bar{R}_r = 2.33\text{Hz}$. To allow for comparison, EPSPs from the five different synapses were scaled so that the mean EPSP amplitude under Poisson drive ($\alpha = 1$) was equivalent to the mean EPSP amplitude predicted by these parameters.

3.4 Results

First, we present the formulae detailing the moments of vesicle occupancy for an arbitrary ISI distribution, before demonstrating applications to the cases when presynaptic firing is given by a renewal process with gamma-distributed interspike intervals and by the response of an LIF neuron to white-noise Gaussian- and shot-noise drive. The predicted spike-triggered occupancies are validated experimentally for cortical layer-V pyramidal cells. The autocorrelation in neurotransmitter release is derived exactly and used to calculate the postsynaptic voltage variance. Crosscorrelations in release are used to demonstrate that vesicle release probability underpins how far changing synaptic strength can tune synapses to respond to signals encoded with different temporal correlations. Finally, it is shown that the voltage mean and variance alone can be used to accurately approximate the postsynaptic firing rate.

3.4.1 Prespike and overall occupancy means for a renewal process

To determine the mean vesicle occupancy under an arbitrary pattern of spike times $\{t_1, t_2, \dots, t_m\}$, consider the expected occupancy x_m immediately before the m th spike at time t_m as a function of the occupancy x_{m-1} immediately before the $m-1$ th spike. x_m satisfies the recursion equation

$$x_m = [(1-p) + p(1 - e^{-R_r(t_m - t_{m-1})})]x_{m-1} + [1 - e^{-R_r(t_m - t_{m-1})}](1 - x_{m-1}) \quad (3.3)$$

giving

$$x_m = 1 - \frac{p}{1-p} \sum_{k=1}^m (1-p)^k e^{-R_r(t_m - t_{m-k})} \quad (3.4)$$

under the initial condition $x_1 = 1$. Taking expectations as m goes to infinity gives

$$\langle x \rangle_\infty = 1 - \frac{p}{1-p} \sum_{k=1}^{\infty} (1-p)^k \langle e^{-R_r T_k} \rangle \quad (3.5)$$

where T_k is the k th ISI before $\langle x \rangle_\infty$. If $\{t_1, t_2, \dots, t_m\}$ are generated by a renewal process, this simplifies to

$$\begin{aligned} \langle x \rangle_\infty &= 1 - \frac{p}{1-p} \sum_{k=1}^{\infty} (1-p)^k \langle e^{-R_r T} \rangle^k \\ \langle x \rangle_\infty &= \frac{1 - \langle e^{-R_r T} \rangle}{1 - (1-p) \langle e^{-R_r T} \rangle} \end{aligned} \quad (3.6)$$

$\langle x \rangle_\infty$ is the expected value of x immediately before a presynaptic spike; the mean occupancy in terms of spike times. The mean occupancy over all time $\langle x \rangle$ can be found by integrating the expected occupancy $\langle x(T) \rangle$ at a time T since the last spike over the probability that another spike has not arrived by time T . This entails integrating over the complement of the ISI cumulative distribution $P(T)$

$$\langle x \rangle = \frac{1}{\mu_f} \int_0^\infty \langle x(T) \rangle P(T) dT \quad (3.7)$$

where μ_f is the mean of the ISI distribution f . The overall time-mean is then given by

$$\langle x \rangle = 1 - \frac{p \int_0^\infty e^{-R_r T} \int_T^\infty f(\sigma) d\sigma dT}{\mu_f (1 - (1-p) \langle e^{-R_r T} \rangle)} \quad (3.8)$$

The variances of the prespike occupancy and overall occupancy follow from the binary-variable result $\langle x^2 \rangle \equiv \langle x \rangle$ as described in Methods.

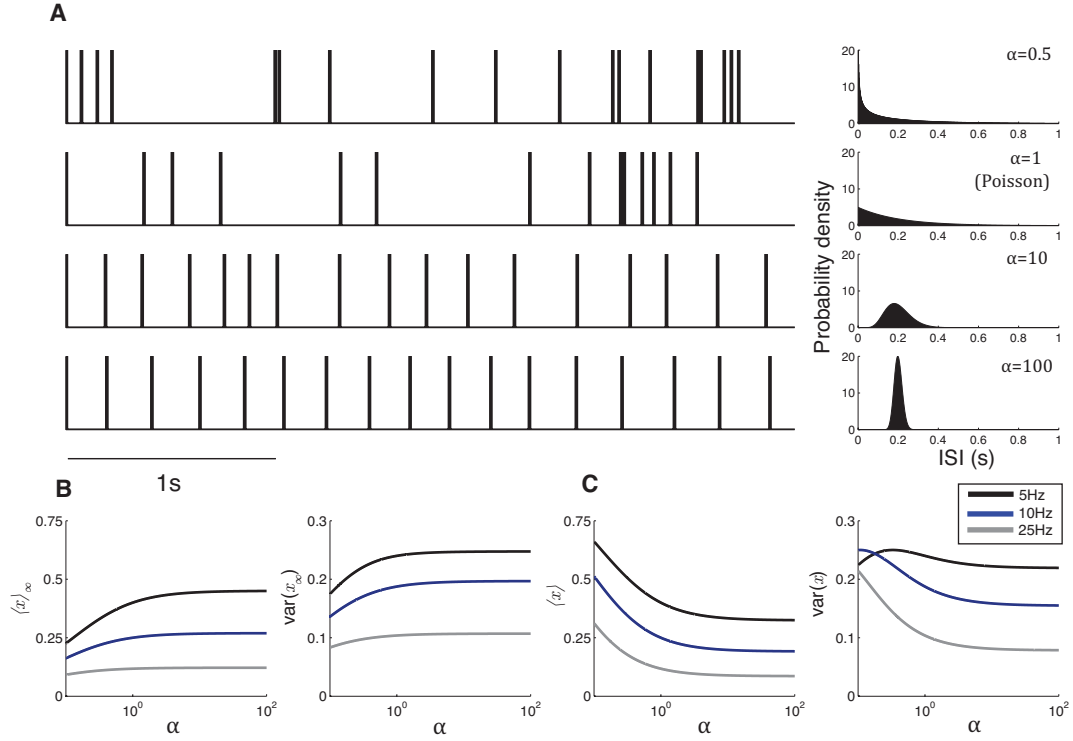


Figure 3.1: Gamma interspike intervals demonstrate the effects of regularity on theoretical vesicle occupancy. **(A)** Example spike trains and ISI distributions (inset) for $R_a = 5\text{Hz}$ and different values of α . From top to bottom $\alpha = 0.5$ (‘bursty’), $\alpha = 1$ (Poisson), $\alpha = 10$ (regular), and $\alpha = 100$ (very regular). **(B, C)** Mean (Eq. (3.9)) and variance (Eq. (3.10)) of prespike occupancy $\langle x \rangle_\infty$ **(B)** and overall occupancy $\langle x \rangle$ **(C)**. Note that the curves for $\langle x \rangle_\infty$ and $\langle x \rangle$ for each instance of R_a take the same value when $\alpha = 1$. Parameters as in Table 3.1 unless otherwise specified.

3.4.2 Gamma ISIs

When we consider ISIs drawn from a gamma distribution with mean $\frac{1}{R_a}$, the degree of regularity in the presynaptic spike train is governed by the shape parameter α . Varying α continuously allows a visualisation of the implications of Eqs (3.6) and (3.8) in relation to the regularity of firing (see Figure 3.1). In addition, the occupancy results can be written without integrals as

$$\begin{aligned}\langle x \rangle_\infty &= \frac{1 - \Lambda}{1 - (1 - p)\Lambda} \\ \langle x \rangle &= \frac{R_r(1 - (1 - p)\Lambda) - pR_a(1 - \Lambda)}{R_r(1 - (1 - p)\Lambda)}\end{aligned}\tag{3.9}$$

where $\Lambda = (\frac{\alpha R_a}{\alpha R_a + R_r})^\alpha$. Λ approaches $e^{-\frac{R_r}{R_a}}$ in the limit $\alpha \rightarrow \infty$ (perfectly periodic spiking). In the limit of extreme bursting $\alpha \rightarrow 0$, $\langle x \rangle$ behaves as $-\frac{\alpha}{p}\log(\alpha)$, losing its dependence on R_r and R_a .

Using the binary variable result $\langle x^2 \rangle \equiv \langle x \rangle$, the variances in x_0 and x can similarly be written.

$$\begin{aligned} \text{var}(x_\infty) &= \frac{p\Lambda(1-\Lambda)}{(1-(1-p)\Lambda)^2} \\ \text{var}(x) &= \frac{pR_a(1-\Lambda)(R_r(1-(1-p)\Lambda) - pR_a(1-\Lambda))}{R_r^2(1-(1-p)\Lambda)^2} \end{aligned} \quad (3.10)$$

Note that $\text{var}(x_\infty)$ does not tend to zero as the regularity of the spike train increases, even when release is perfectly reliable with $p = 1$, due to the variability in vesicle restock events.

3.4.3 Experimental validation of predicted $\langle x \rangle_\infty$ values

Paired whole-cell patch-clamp recordings were carried out to verify the predictions made above. Four different α values, 1/3, 2/3, 1 and 10 corresponding to two bursty, one Poisson, and one regular, were used to generate patterns of action potentials at average rate $R_a = 5\text{Hz}$ (Fig. 3.2a). Five connected pairs of cortical layer-V pyramidal cells were identified and each had stimulus protocols applied for all four values of α . The postsynaptic voltage traces were averaged and the EPSP amplitudes were normalised to the size of the first EPSP in each trace to allow for comparison between connections.

The distribution of normalised EPSP amplitudes in the steady-state has a pronounced skew towards higher values, which is more noticeable for lower α (Fig. 3.2d). Eq. (3.9) provides a good fit to the measured relative EPSP amplitudes for different α values (Fig. 3.2e).

3.4.4 Fluctuation-driven ISIs

If the external drive to an LIF presynaptic neuron is modelled by Gaussian white noise of strength σ_v , the Fourier transform \hat{f} of the ISI distribution f of the presynaptic cell is (Richardson and Swarbrick 2010)

$$\hat{f}(w) = \frac{\int_0^\infty x^{iw\tau} \frac{d}{dx} [e^{xx_{re}-x^2/2}] dx}{\int_0^\infty x^{iw\tau} \frac{d}{dx} [e^{xx_{th}-x^2/2}] dx} \quad (3.11)$$

with $x_{th} = \frac{V_{th}-E_0}{\sigma_v}$ and $x_{re} = \frac{V_{re}-E_0}{\sigma_v}$. Now, as we have by definition that

$$\hat{f}(w) = \int_{-\infty}^\infty e^{-iws} f(s) ds \quad (3.12)$$

we can proceed by analogy between the above and equation (3.8). Noting that f is 0 for negative arguments, we can directly substitute this result into equations (3.6) and (3.8)

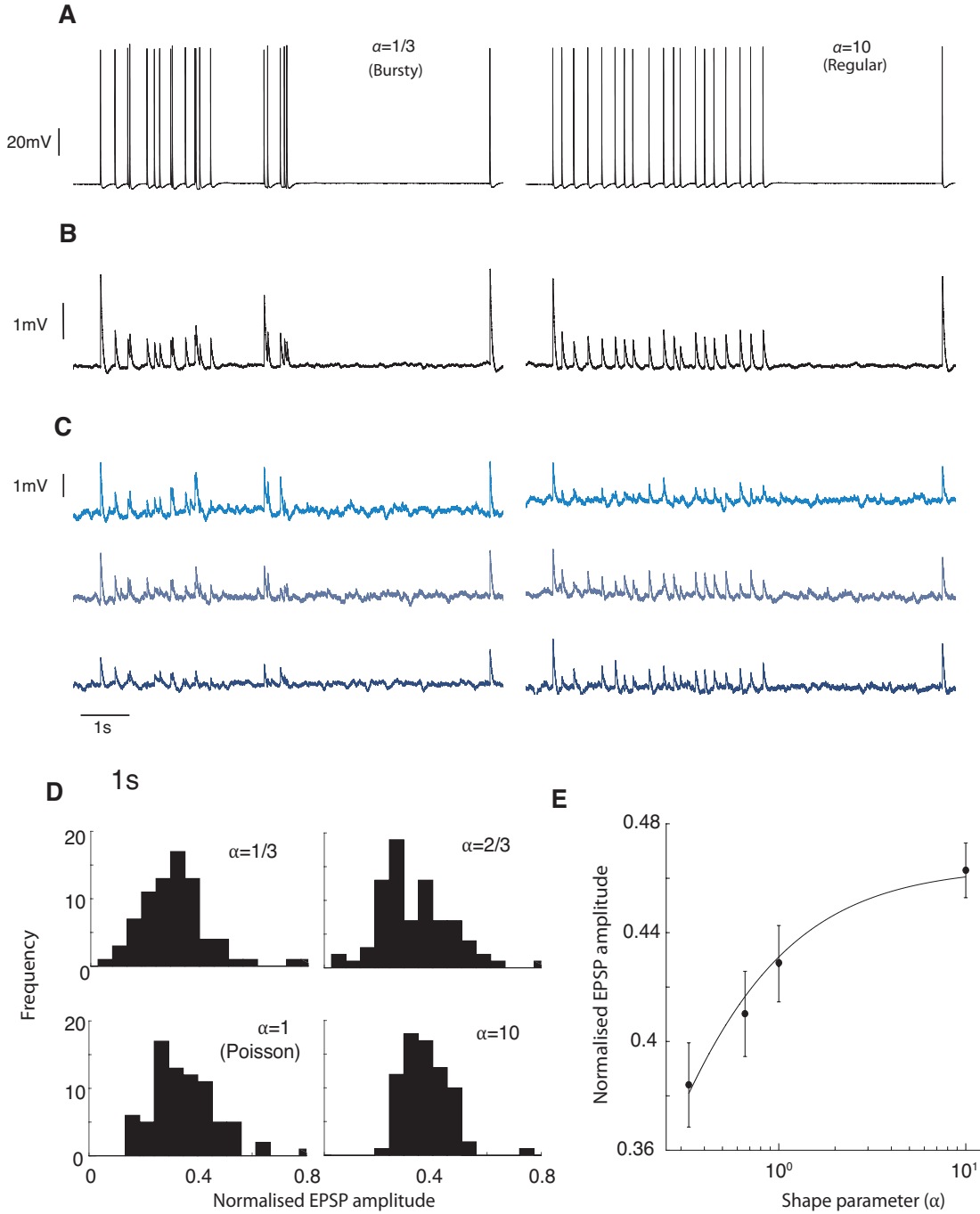


Figure 3.2: Changes in mean EPSP amplitude for experimental paired-cell recordings. **(A)** Irregular and regular presynaptic voltages with gamma-distributed interspike intervals with shape parameter $\alpha = 1/3$ (left, irregular) and $\alpha = 10$ (right, regular). **(B)** Averaged postsynaptic voltages for the above presynaptic traces. The steady-state is considered to be the period from the fourth EPSP onwards, excluding the recovery spike. **(C)** Representative individual postsynaptic voltage traces. **(D)** Distribution of steady-state amplitudes for the fourth to nineteenth EPSPs in five stimulus protocols (normalised to the value of the first EPSP) for four different shape parameters (from top-left $\alpha = 1/3$, $\alpha = 2/3$, $\alpha = 1$, and $\alpha = 10$) **(E)** Mean steady-state EPSP amplitude as a function of spike-train regularity α . Dots give mean normalised EPSPs; error bars show standard error of the mean. Solid line gives fit from Eq. (3.9), with mean parameters of $\bar{p} = 0.62$, $\bar{R}_r = 2.33\text{Hz}$ (see Methods).

(Fig. 3.3). The prespike vesicle occupancy $\langle x \rangle_\infty$ for a Gaussian white-noise driven LIF neuron is then

$$\langle x \rangle_\infty = \frac{\int_0^\infty x^{\tau R_r} e^{-\frac{x^2}{2}} (e^{xx_{th}} - e^{xx_{re}}) dx}{\int_0^\infty x^{\tau R_r} e^{-\frac{x^2}{2}} (e^{xx_{th}} - (1-p)e^{xx_{re}}) dx} \quad (3.13)$$

The distance between E_0 and V_{re} determines the shape of the ISI distribution, with negative values giving rise to regular and positive values to irregular firing (Ostojic 2011). The presynaptic firing rate can be kept constant by reducing the strength of the noise σ_v as V_{re} increases above E_0 , allowing the effect of changing regularity to be plotted (Fig. 3.3a and b).

A similar result applies to shot-noise drive, where excitatory impulses arrive at the presynaptic neuron as a Poisson process with rate R_e and exponentially distributed magnitude with mean a_e

$$\langle x \rangle_\infty = \frac{\int_0^{\frac{1}{a_e}} s^{\tau R_r + 1} (1 - a_e s)^{\tau R_e} \left(\frac{e^{sv_{th}}}{1 - a_e s} - e^{sv_{re}} \right) ds}{\int_0^{\frac{1}{a_e}} s^{\tau R_r + 1} (1 - a_e s)^{\tau R_e} \left(\frac{e^{sv_{th}}}{1 - a_e s} - (1-p)e^{sv_{re}} \right) ds} \quad (3.14)$$

where $v_{th} = V_{th} - E_0$ and $v_{re} = V_{re} - E_0$. To calculate the overall mean $\langle x \rangle$ in this case note that μ_f , the inverse of the neuron's firing rate, is given by Richardson and Swarbrick (2010) as

$$\mu_f = \tau \int_0^{1/a_e} \frac{1}{s} \left(\frac{e^{sv_{th}}}{1 - a_e s} - e^{sv_{re}} \right) (1 - a_e s)^{\tau R_e} ds \quad (3.15)$$

To keep the presynaptic firing rate $\frac{1}{\mu_f}$ constant, the rate of arrival of excitatory impulses R_e is adjusted as V_{re} changes. The mean impulse size a_e is kept constant to maintain the shot-noise finite-size effects. Figure 3.3 shows the effect of changing the threshold-reset distance for different values of a_e . Vesicle occupancy is less sensitive to the threshold-reset distance in this case as shot-noise effects dominate.

3.4.5 Autocorrelations in vesicle release

To consider the postsynaptic voltage effects arising from non-Poisson presynaptic behaviour, we first derive the autocorrelation in vesicle release χ , $\langle \chi(T)\chi(0) \rangle - \langle \chi \rangle^2$. Let $A(T)$ be the probability density of a spike arriving whilst a vesicle is present at time T given that there was a release at time 0. Let $S(T)$ be the probability density of a spike arriving at time T given that there was a spike at time 0. Let $R(T) = 1 - e^{-R_r T}$ be the probability that a vesicle is restocked in the interval $(0, T)$. Then $S(T)$ satisfies

$$S(T) = f(T) + \int_0^T S(t) f(T-t) dt \quad (3.16)$$

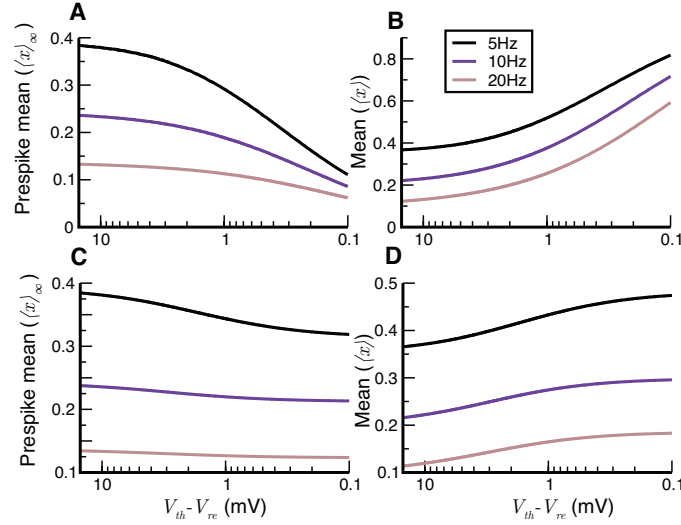


Figure 3.3: Theoretical vesicle occupancy for noise-driven neurons. **(A)** Prespike vesicle occupancy as a function of the distance between V_{th} and V_{re} for mean presynaptic firing rates 5Hz, 10Hz, and 20Hz when the presynaptic cell receives Gaussian drive (Eq. (3.13)). The resting voltage E_0 lies 10mV below V_{th} in all cases. **(B)** Overall mean vesicle occupancy. Note that in this case the two curves for each firing rate take the same value when $V_{re} = E_0$ mV (reset and rest coincide). **(C, D)** Prespike and overall mean vesicle occupancy respectively as a function of the distance between V_{th} and V_{re} when the presynaptic cell receives shot-noise drive (Eq. (3.14)). Parameters as in Table 3.1 unless otherwise specified.

where the first term accounts for the case of no spikes in the interval $(0, T)$ and the second accounts for any non-zero number of spikes in the interval $(0, t)$ for all $0 < t < T$. Similarly, $A(T)$ satisfies

$$\begin{aligned}
 A(T) &= f(T)R(T) \\
 &+ \int_0^T A(t)[pf(T-t)R(T-t) + (1-p)f(T-t)]dt \\
 &+ \int_0^T (S(t) - A(t))f(T-t)R(T-t)dt
 \end{aligned} \tag{3.17}$$

where the first two terms mirror those in the equation for $S(T)$ and the third accounts for the penultimate spike arriving at the site whilst it is unstocked. Taking a Fourier transform $S(T) \rightarrow \hat{S}(\omega)$, $A(T) \rightarrow \hat{A}(\omega)$ of the two equations gives

$$\begin{aligned}
 \hat{S}(\omega) &= \frac{\hat{f}(\omega)}{1 - \hat{f}(\omega)} \\
 \hat{A}(\omega) &= \frac{\hat{f}(\omega) - \hat{f}(\omega - iR_r)}{(1 - \hat{f}(\omega))(1 - (1-p)\hat{f}(\omega - iR_r))}
 \end{aligned} \tag{3.18}$$

$\hat{A}(\omega)$ can be inverted to give $A(t)$. The autocorrelation in vesicle release at lag T is then given by the probability that a spike arrives whilst the site is stocked and induces vesicle release at time T given that neurotransmitter was released from the site at time

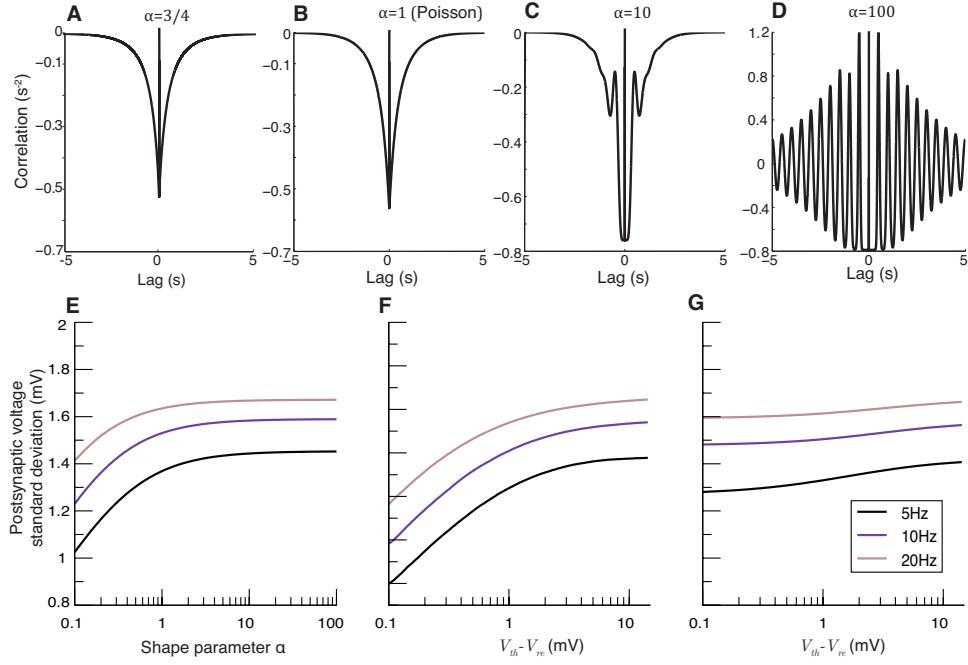


Figure 3.4: Theoretical release autocorrelations and voltage variances. **(A-D)** Vesicle release autocorrelations for gamma-distributed interspike intervals with shape parameters **A** $\alpha = 0.75$, **B** $\alpha = 1$ (Poisson), **C** $\alpha = 10$ and **D** $\alpha = 100$ (Eq. 3.19). **(E)** Postsynaptic voltage standard deviation for gamma ISIs as a function of α for different presynaptic firing rates R_a (Eq. 3.24). **(F, G)** Voltage standard deviations as a function of the distance between V_{th} and V_{re} under presynaptic Gaussian **(F)** and shot **(G)** noise drive for different mean presynaptic firing rates. Parameters as in Table 3.1 unless otherwise specified.

0. As χ is a train of delta pulses, it is necessary to account for $T = 0$ with an additional delta term.

$$\text{Autocorr}(\chi) = \frac{p\langle x \rangle_\infty}{\mu_f} \delta(T) + \frac{(p\langle x \rangle_\infty)^2}{\mu_f} A(T) \quad (3.19)$$

Figures 3.4a-d show the autocorrelation in release for gamma-distributed ISIs with different values of α . For the Poisson case $\alpha = 1$, the autocorrelation decays exponentially (Fig. 3.4b) as the presynaptic spike train itself is uncorrelated (with a flat autocorrelation) but neurotransmitter cannot be released until a fresh vesicle is trafficked to the site. For the ‘bursty’ case $\alpha < 1$, the presynaptic spike-train autocorrelation is positive at short lags and negative for longer lags; but the positive region of spike train autocorrelation will typically overlap with the region where the site is unstocked. This produces a shallower but broader negative release autocorrelation than the Poisson case (Fig. 3.4a). For regular spike trains $\alpha > 1$ the spiking autocorrelation is periodic, and the release autocorrelation inherits this property with a larger initial decrease due to depression (Fig. 3.4c and d).

3.4.6 The postsynaptic response

We now consider the effect that non-Poisson spiking has on the postsynaptic voltage. A postsynaptic neuron receives excitatory synaptic input from N independent presynaptic cells, each initially with one release site, firing with the same ISI distribution given by $f(t)$. Then the subthreshold transmembrane voltage obeys

$$\frac{dV}{dt} = \frac{E_0 - V}{\tau} + a \sum_{i=1}^N \chi_i(t) \quad (3.20)$$

where $\chi_i(t) = \sum_{Rel} \delta(t - t_{Rel}^i)$ is the train of neurotransmitter release events from the i^{th} neuron and a is the magnitude of the voltage change induced by a single vesicle. The steady-state voltage mean $\langle V \rangle$ is given by

$$\langle V \rangle = E_0 + \frac{ap\tau N}{\mu_f} \langle x \rangle_\infty \quad (3.21)$$

This is an increasing function of the prespike occupancy $\langle x \rangle_\infty$ and so increases with the regularity of the presynaptic spike train. The second moment is

$$\langle V^2 \rangle = a^2 e^{-\frac{2t}{\tau}} \int_{-\infty}^t \int_{-\infty}^t e^{\frac{s}{\tau}} e^{\frac{s'}{\tau}} \langle (\sum_{i=1}^N \chi_i(s)) (\sum_{i=1}^N \chi_i(s')) \rangle ds' ds \quad (3.22)$$

As individual neurons are independent $\langle \chi_i(s) \chi_j(s') \rangle = 0$ for $i \neq j$ and Eq. 3.22 can be reduced to the form

$$\langle V^2 \rangle = 2a^2 N \int_0^\infty e^{-\frac{2t'}{\tau}} \int_0^\infty e^{-\frac{t''}{\tau}} \langle \chi(t'') \chi(0) \rangle dt'' dt' \quad (3.23)$$

where the variables $t' = t - s$, $t'' = t - s'$ allow introduction of the form of neurotransmitter release autocorrelation derived above (Eq. 3.19). Noting that the inner integral corresponds to a Fourier transform on the autocorrelation allows us to use Eq. 3.18 to write the voltage variance as

$$\begin{aligned} \text{var}(V) &= \frac{a^2 N \tau}{2} \left[\frac{px_0}{\mu_f} - \hat{A}(-i/\tau) \right] \\ \text{var}(V) &= \frac{a^2 N \tau}{2} \left[\frac{px_0}{\mu_f} - \frac{\langle e^{-T/\tau} \rangle - \langle e^{-(1/\tau + R_r)T} \rangle}{(1 - \langle e^{-T/\tau} \rangle)(1 - (1-p)\langle e^{-(1/\tau + R_r)T} \rangle)} \right] \end{aligned} \quad (3.24)$$

$\langle e^{-T/\tau} \rangle$ and $\langle e^{-(1/\tau+R_r)T} \rangle$ can be evaluated in both the gamma and white-noise driven cases. For gamma ISIs (Fig. 3.4e),

$$\langle e^{-T/\tau} \rangle = \left(\frac{\alpha R_a}{\frac{1}{\tau} + \alpha R_a} \right)^\alpha, \quad \langle e^{-(1/\tau+R_r)T} \rangle = \left(\frac{\alpha R_a}{\frac{1}{\tau} + R_r + \alpha R_a} \right)^\alpha \quad (3.25)$$

and for neurons driven by Gaussian white noise with strength σ_v (Fig. 3.4f) with a presynaptic membrane time constant τ' and a postsynaptic membrane time constant τ ,

$$\begin{aligned} \langle e^{-T/\tau} \rangle &= \frac{\int_0^\infty x^{-\frac{\tau'}{\tau}} \frac{d}{dx} [e^{xx_{re}-x^2/2}] dx}{\int_0^\infty x^{-\frac{\tau'}{\tau}} \frac{d}{dx} [e^{xx_{th}-x^2/2}] dx} \\ \langle e^{-(1/\tau+R_r)T} \rangle &= \frac{\int_0^\infty x^{-(\frac{1}{\tau}+R_r)\tau'} \frac{d}{dx} [e^{xx_{re}-x^2/2}] dx}{\int_0^\infty x^{-(\frac{1}{\tau}+R_r)\tau'} \frac{d}{dx} [e^{xx_{th}-x^2/2}] dx} \end{aligned} \quad (3.26)$$

with $x_{th} = \frac{V_{th}-E_0}{\sigma_v}$ and $x_{re} = \frac{V_{re}-E_0}{\sigma_v}$. Similarly for shot noise driven neurons with presynaptic membrane time constant τ' and excitatory impulses of mean size a_e and rate R_e (Fig. 3.4g)

$$\begin{aligned} \langle e^{-T/\tau} \rangle &= \frac{\int_0^{1/a_e} s^{-\frac{\tau'}{\tau}} \frac{d}{ds} [(1-a_e s)^{\tau' R_e} e^{s v_{re}}] ds}{\int_0^{1/a_e} s^{-\frac{\tau'}{\tau}} \frac{d}{ds} [(1-a_e s)^{\tau' R_e - 1} e^{s v_{th}}] ds} \\ \langle e^{-(1/\tau+R_r)T} \rangle &= \frac{\int_0^{1/a_e} s^{-(\frac{1}{\tau}+R_r)\tau'} \frac{d}{ds} [(1-a_e s)^{\tau' R_e} e^{s v_{re}}] ds}{\int_0^{1/a_e} s^{-(\frac{1}{\tau}+R_r)\tau'} \frac{d}{ds} [(1-a_e s)^{\tau' R_e - 1} e^{s v_{th}}] ds} \end{aligned} \quad (3.27)$$

where $v_{th} = V_{th} - E_0$ and $v_{re} = V_{re} - E_0$. Note that these only hold when $\tau' R_e > 1$, where excitatory impulses arrive more regularly than the membrane time constant, and this is where shot noise driven neurons display interesting behaviour (Richardson and Swarbrick 2010).

The voltage variance increases with the regularity of the presynaptic spike train for single release sites (Fig. 3.4e-g).

3.4.7 Effect of multiple release sites

A single presynaptic neuron will typically have multiple vesicle release sites onto a postsynaptic cell, with estimates of this parameter n varying from around 10 to 100 (Loebel et al. 2009). It is conceivable that, as a ‘burst’ of presynaptic activity would release many more vesicles from a single neuron in a short time than an isolated spike, large values of n would counteract the reduced overall synaptic transmission caused by irregular spiking shown by Eqs 3.21 and 3.24. This would particularly be the case for low release probabilities.

To investigate this, we expanded our model to consider multiple release sites per neuron. As each of these sites will receive all of the neuron's action potentials, there will be correlations in vesicle release. In particular, the cross-correlation $\langle \chi(T)\chi'(0) \rangle$ between release from different sites will impact upon the postsynaptic response. The first quantity to consider here is the joint prespike occupancy $\langle xx' \rangle_\infty$, the probability that both of a pair of sites are occupied when a spike arrives. This can be calculated in a similar way to $\langle x \rangle_\infty$ (Eqs 3.3 to 3.6); the expected joint occupancy xx'_m of two sites before the m th spike in a train at time t_m in terms of the joint occupancy xx'_{m-1} immediately before the $(m-1)$ th spike at time t_{m-1} obeys the recursion relation

$$\begin{aligned} xx'_m = & xx'_{m-1} [(1-p)^2 + 2p(1-p)(1 - e^{-R_r(t_m - t_{m-1})}) + p^2(1 - e^{-R_r(t_m - t_{m-1})})^2] \\ & + 2(x_{m-1} - xx'_{m-1}) [(1-p)(1 - e^{-R_r(t_m - t_{m-1})}) + p(1 - e^{-R_r(t_m - t_{m-1})})^2] \\ & + (1 - x_{m-1})^2 [1 - e^{-R_r(t_m - t_{m-1})}]^2 \end{aligned} \quad (3.28)$$

The first term on the right hand side accounts for the situation where both sites are stocked at time t_{m-1} , the second where only one is, and the third where neither is. Rearranging and taking expectations as $m \rightarrow \infty$, as in the case of $\langle x \rangle_\infty$, gives

$$\langle xx' \rangle_\infty = \frac{1 + 2((1-p)\langle x \rangle_\infty - 1)\langle e^{-R_r T} \rangle - (2(1-p)\langle x \rangle_\infty - 1)\langle e^{-2R_r T} \rangle}{1 - (1-p)^2 \langle e^{-2R_r T} \rangle} \quad (3.29)$$

To compute the full cross-correlation, Eq. (3.17) can be adapted to describe $A'(T)$, the probability density that a spike arrives whilst a vesicle is present at time T given that the site was stocked immediately after a spike at time 0

$$\begin{aligned} A'(T) = & f(T) \\ & + \int_0^T A'(t) [pf(T-t)R(T-t) + (1-p)f(T-t)]dt \\ & + \int_0^T (S(t) - A'(t))f(T-t)R(T-t)dt \end{aligned} \quad (3.30)$$

Then

$$\hat{A}'(\omega) = \frac{\hat{f}(\omega)(1 - \hat{f}(\omega - iR_r))}{(1 - \hat{f}(\omega))(1 - (1-p)\hat{f}(\omega - iR_r))} \quad (3.31)$$

The crosscorrelation in vesicle release is then a sum of $A(T)$ and $A'(T)$ weighted respectively by the probabilities that the second site is unstocked and stocked immediately

after the first releases

$$\begin{aligned} \text{Crosscorr}(\chi, \chi') = & \\ & \frac{p^2 \langle xx' \rangle_\infty}{\mu_f} \left[\delta(T) + (p \langle xx' \rangle_\infty + (1 - \langle xx' \rangle_\infty)) A(T) \right. \\ & \left. + (1 - p) \langle xx' \rangle_\infty A'(T) \right] \end{aligned} \quad (3.32)$$

Cross-correlated vesicle release can be included in the calculation of the voltage variance (Bird and Richardson 2014). The term $\langle (\sum_{i=1}^N \chi_i(s)) (\sum_{i=1}^N \chi_i(s')) \rangle$ in Eq. 3.22 is replaced by $\langle (\sum_{i=1}^N \sum_{j=1}^n \chi_{ij}(s)) (\sum_{i=1}^N \sum_{j=1}^n \chi_{ij}(s')) \rangle$ as each neuron has n release sites. Then there will be Nn autocorrelations given by Eq. 3.19 and $Nn(n-1)$ cross-correlations given by Eq. 3.32, giving the voltage variance as

$$\begin{aligned} \text{var}(V) = & \frac{a^2 N \tau}{2} \left[\frac{p \langle x \rangle_\infty}{\mu_f} + (n-1) \frac{p^2 \langle xx' \rangle_\infty}{\mu_f} \right. \\ & - (1 + (n-1)(1 - (1-p) \langle xx' \rangle_\infty)) \frac{\langle e^{-T/\tau} \rangle - \langle e^{-(1/\tau + R_r)T} \rangle}{(1 - \langle e^{-T/\tau} \rangle)(1 - (1-p) \langle e^{-(1/\tau + R_r)T} \rangle)} \\ & \left. - (n-1)(1-p) \langle xx' \rangle_\infty \frac{\langle e^{-T/\tau} \rangle - \langle e^{-T/\tau} \rangle \langle e^{-(1/\tau + R_r)T} \rangle}{(1 - \langle e^{-T/\tau} \rangle)(1 - (1-p) \langle e^{-(1/\tau + R_r)T} \rangle)} \right] \end{aligned} \quad (3.33)$$

This formula represents the incorporation of novel details into the voltage variance including: stochastic transmission, quantal effects, short-term plasticity, multiple contacts, and non-Poisson input. Figure 3.5 shows the standard deviation in postsynaptic voltage as a function of both the release site number n and gamma ISI shape parameter α for different release probabilities p . For intermediate and high values of p , the standard deviation increases as function of n for all values of α . However, if p is low, the standard deviation decreases with α and the effect is stronger as n increases. This quantifies the intuitive phenomenon of irregular trains driving stronger voltage deviations when n is high and p is low as the vesicles are released temporally close together and can induce relatively large fluctuations.

3.4.8 Postsynaptic firing rates estimated by the matched-variance method

It has been shown that the postsynaptic firing rate is relatively insensitive to temporal correlations as long as the subthreshold mean and variance can be matched (Alijani and Richardson 2011). Using the mean μ and variance σ^2 derived above, the firing rate of an LIF neuron is given by the reciprocal of (Brunel and Hakim 1999)

$$\tau \int_0^\infty \frac{dz}{z} e^{-z^2/2} (e^{zz_{th} - e^{zz_{re}}}) \quad (3.34)$$

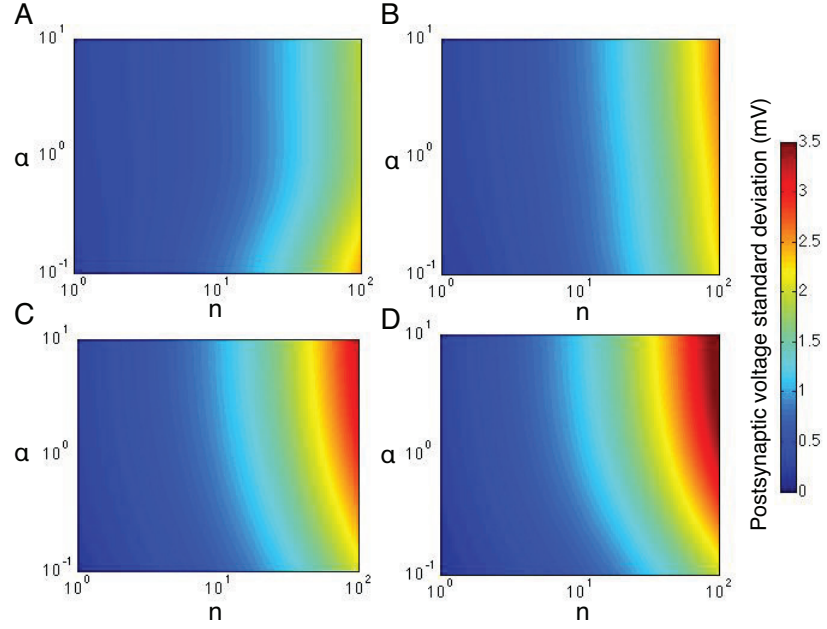


Figure 3.5: The theoretical effect of multiple release sites per presynaptic neuron. Postsynaptic voltage standard deviation as a function of the number of release sites n and gamma ISI shape parameter α for different release probabilities (**A**) $p = 0.25$, (**B**) $p = 0.5$, (**C**) $p = 0.75$, and (**D**) $p = 1$ (Eq. 3.33). The number of release sites is scaled down in proportion to the release probability to maintain the same voltage mean. Parameters as in Table 3.1 unless otherwise specified.

with $z_{th} = (V_{th} - E - \mu)/\sigma$ and $z_{re} = -\mu/\sigma$. Figure 3.6 shows the firing rates predicted by this method compared to simulations.

The matched-variance method can underestimate the simulated result when n is large and the presynaptic train is particularly bursty, as in this case the postsynaptic voltage distribution can be notably non-Gaussian. In the gamma ISI case when $n = 25$ the estimate only holds well for $\alpha > 0.3$ (Fig. 3.6a). For shot-noise driven neurons with a low firing rate (Fig. 3.6c, black line) a similar underestimation can occur. In general the approximation provides a good estimate of the postsynaptic firing rate in the majority of situations.

3.5 Discussion

We have presented a series of results which will allow for non-Poisson effects to be incorporated into studies of neuronal populations and networks. Non-Poisson activity is commonly seen *in vivo* and can have a substantial effect on neuronal activity. We have derived exact results for the key properties of synaptic transmission when the spike train can be modelled as a renewal process, with particular attention to the cases where the ISIs form a gamma distribution or are generated by filtered Gaussian or shot noise.

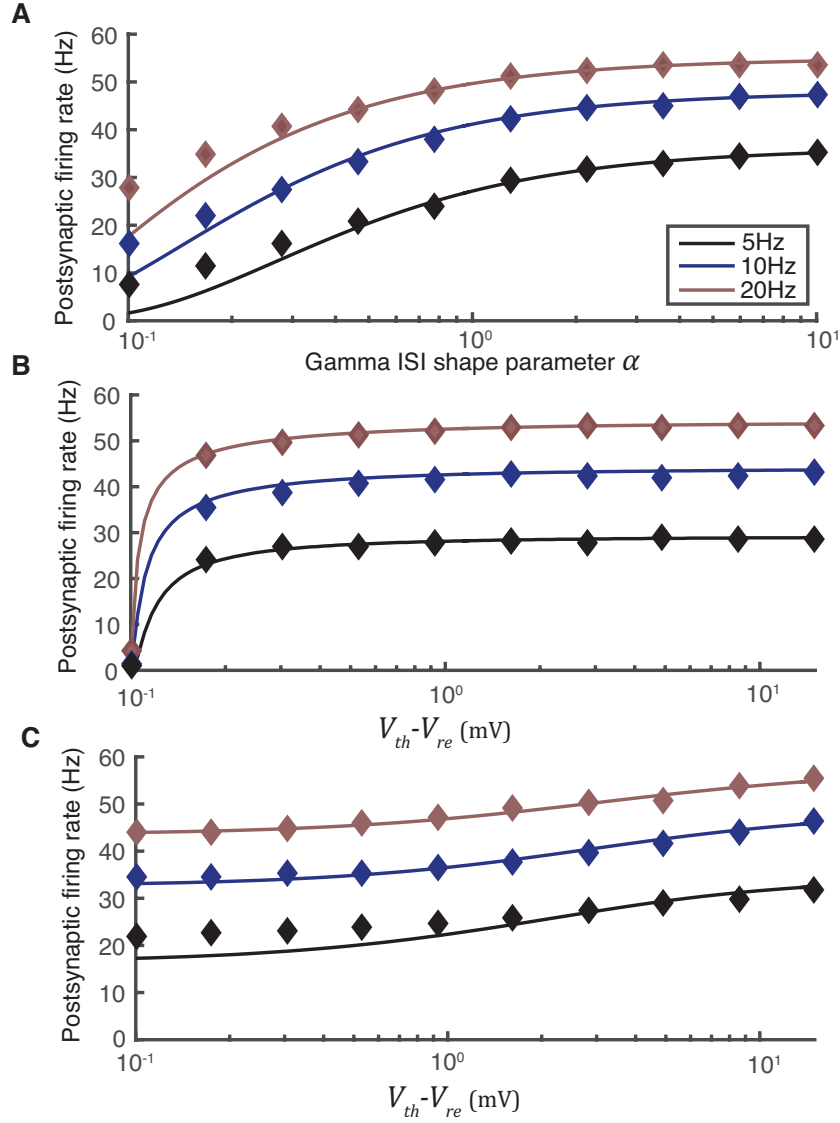


Figure 3.6: Simulated postsynaptic firing rates are well-approximated by the matched-variance method. **(A)** Simulations (diamonds) against predictions (lines) of postsynaptic firing rate as a function of the presynaptic ISI shape parameter α for different presynaptic firing rates R_a with 25 release sites per presynaptic neuron. **(B, C)** Simulations against predicted rates for Gaussian- **(B)** and shot- **(C)** noise driven presynaptic firing. Parameters as in Table 3.1 unless otherwise specified.

Exact results for the voltage variance in the renewal case confirm that irregular firing across depressing synapses typically causes weaker transmission (Ramcharan et al. 2000; Reich and Rosenbaum 2013), although this is counteracted to some extent in strong, mature synapses (Sherman 2001; Shinomoto et al. 2009; Jacob et al 2012); both aspects can be captured by the theory introduced here. It is important to note that the effect of spike train regularity on postsynaptic response are typically entirely dependent on synaptic depression. Low release probability p and fast vesicle replenishment R_r can reverse the phenomenon of reduced synaptic efficacy under irregular trains, leading to qualitatively different behaviour. The developmental reduction in release probability

(Reyes and Sakmann 1999; Frick et al. 2007; Kerr et al. 2013; Nakamura et al. 2015) means that synaptic strength, mediated by changes in the release-site number n , will become a better discriminator of temporal codes in spike trains with age.

The accuracy of the matched-variance method in estimating postsynaptic firing rates will allow for a straightforward incorporation of complex spike-patterns into circuits and feed-forward networks.

3.5.1 Extensions

To complete the incorporation of temporal spike-train structure into recurrent networks, it would be necessary to obtain the output statistics of the postsynaptic spike train beyond the firing rate. This is currently a problem of great interest (Ostojic 2011; Dummer et al. 2014) given the strong effects non-Poissonian behaviour is acknowledged to have even across static synapses (Cateau and Reyes 2006). To include the negative components of vesicle-release autocorrelation arising from short-term depression would increase physiological relevance and bring studies in this area into line with much of the literature on neuronal networks (Abbott 1997; Tsodyks et al. 1998; Brunel and Wang 2003; Cortes et al. 2013).

Adaptation currents are present across the nervous system (Benda and Herz 2003) and can modulate responses to persistent activity by high-pass filtering and response selectivity (Wang 1998; Benda et al 2005; Peron and Gabbiani 2009). These functional roles overlap with those attributed to synaptic depression (Furukawa et al. 1982; Abbott and Regehr 2004; Hallermann and Silver 2013), and there have been a number of recent studies on the interactions of short-term synaptic plasticity with slow adaptation mechanisms (Peterson et al. 2014; Moezzi et al. 2014; Nagel et al. 2015). A key feature of adaptation currents is the creation of correlations between interspike intervals (Schwalger et al. 2010), generating non-renewal spike trains. These correlations have recently been shown to take the form of a geometric series (Schwalger and Lindner 2013) and Eq. (3.5) presents a way of deriving approximate results for the synaptic transmission of weakly correlated ISIs. This would link two key short-term adaptive processes in neural circuits (Furukawa et al. 1982; Wang 1998; Abbott and Regehr 2004; Benda et al 2005; Peron and Gabbiani 2009; Hallermann and Silver 2013).

Another area of interest would be relating the precise forms of spike-frequency adaptation to short-term plasticity in experimental studies (Peterson et al. 2014; Moezzi et al. 2014; Nagel et al. 2015). As there is redundancy between the effects of these two phenomena, it is likely that there will be relationships between neuronal adaptation and

synaptic plasticity in systems displaying both. Describing these relationships would help to elucidate the different functions of the two adaptation mechanisms across the brain.

Acknowledgements

We acknowledge funding through a Warwick Systems Biology Doctoral Training Centre fellowship to Alex D. Bird, funded by the UK EPSRC and BBSRC funding agencies, and funding to Magnus J. E. Richardson under BBSRC Grant No. BB/J015369/1.

Chapter 4

Bayesian inference for the quantal parameters of dynamic synapses

4.1 Overview

IN this chapter I apply Bayesian inference to estimate synaptic parameters from paired-cell patch-clamp data. Bayesian inference allows quantification of the probability that model parameters will take certain values given a set of data. Two recent studies have also taken a Bayesian approach to inferring synaptic parameters. Bhumbra and Beato (2013) focussed on the static quantal properties of isolated vesicle release and did not attempt to infer dynamic properties. Costa et al. (2013) considered synaptic plasticity explicitly, defining optimal experimental stimulus protocols and identifying pre- and postsynaptic cell classes from the dynamic parameters of the synapse; their method used a Gaussian approximation to EPSP amplitudes and so does not account for stochastic quantal effects, particularly at weak synapses, or for the negative correlations between subsequent EPSPs arising from a quantal model.

The method introduced here allows computation of an exact likelihood function for both dynamic and quantal properties and so allows direct estimation of the physiological parameters for four of the most commonly used models of synaptic function. The approach is tested with simulated and real data.

4.1.1 Author contributions

Conceived the study: MJER and ADB. Derived and solved equations: ADB and MJER. Conducted experiments: MRF, MK (Michael Kerr), and MJW. Wrote code for simulations: ADB and MJER. Prepared figures: ADB. Wrote the paper: ADB and MJER.

The majority of the first draft was written by ADB. The major exceptions to this are the three experimental sections of the Methods, *Preparation of neocortical slices*, *Patch-clamp recordings from excitatory cells*, and *Adenosine application*, which follow standard lab protocols. All equations were initially derived by ADB.

Bayesian inference for the quantal parameters of dynamic synapses

Alex D. Bird^{1,2,3}, Michael R. Fisher², Mark J. Wall², and Magnus J. E. Richardson³

¹Systems Biology Doctoral Training Centre, ²School of Life Sciences, and ³Warwick Systems Biology Centre, University of Warwick, CV4 7AL, United Kingdom.

Abstract. Synapses mediate communication between neurons, but respond to activity in a way that is both stochastic and plastic: varying between presentations of the same stimulus and due to the immediate history of transmission. This complicates attempts to infer the parameters behind synaptic transmission and a number of different approaches have been proposed to quantify the properties of synaptic connections. Recently, Bayesian approaches have been applied to make better use of the data collected in paired-cell experiments and provide estimates of the probability distributions of the parameters involved. Though these approaches considered either isolated stimulation or a regime in which synaptic strength is large and can be well-approximated by a Gaussian, they have demonstrated considerably increased accuracy when compared to existing non-Bayesian techniques. Here we have extended these methods and present a Bayesian inference method with an exact likelihood function that allows estimation of quantal and dynamic parameters at a synapse of any strength. Four common models of synaptic dynamics are treated explicitly: vesicle-depletion depression, facilitation, augmented vesicle recovery, and release-independent depression; the physiological parameters are directly estimated in each case.

Key words: Bayesian inference, EPSP data, synaptic depression, quantal, stochastic

4.2 Introduction

The dynamics of synaptic function are crucial to communication between neurons. An action potential in the presynaptic cell triggers an influx of Ca^{2+} into synaptic terminals, causing probabilistic release of neurotransmitter from vesicles docked at active sites on the presynaptic membrane. The neurotransmitter binds to the postsynaptic cell, causing a change in the membrane conductance that allows current to flow and the postsynaptic neuron to depolarise with an excitatory postsynaptic potential (EPSP). Depletion of vesicles available at active sites can cause an activity-dependent reduction in synaptic efficacy, whilst a build-up of Ca^{2+} can increase the probability that docked vesicles release neurotransmitter, causing an increase in efficacy. Synaptic transmission is thus both fundamentally stochastic (Fatt and Katz 1954; del Castillo and Katz 1954; Stein

1965) and plastic (Eccles et al. 1941; Furukawa et al. 1982; Abbott 1997; Tsodyks and Markram 1997; Zucker and Regehr 2002).

A single EPSP is ‘built up statistically of small all-or-none units which are identical in size with the spontaneous ‘miniature’ postsynaptic potentials (del Castillo and Katz 1954) caused by the neurotransmitter released from individual vesicles. Initial analyses of paired-cell data used the amplitude distribution of EPSPs to identify quantal ‘peaks’ corresponding to sums of similar ‘mini’ amplitudes (Boyd and Martin 1956; Liley 1956; Bennett and Florin 1974; Kuno 1964; Kuno and Weakly 1972; Bekkers 1994) (see Bennett and Kearns, 2000, for a review). Whilst very effective for neuromuscular synapses, such as those considered by del Castillo and Katz (1954), the greater variation in ‘mini’ amplitudes at central synapses (Hanse and Gustafsson 2001; Franks et al. 2003; Hardingham et al. 2010) necessitated different techniques to recover robust results in the central nervous system.

Mean-variance analysis was developed to produce reliable estimates of the maximum number of vesicles that can be released by a single stimulus (Silver et al. 1998; Clements 2003; Silver 2003). Initial applications relied on conducting experiments under a variety of conditions, in particular varying the extracellular Ca^{2+} concentration to alter the vesicle release probability (Foster and Regehr 2004; Birò et al. 2005). Brémaud et al. (2007) and Loebel et al. (2009) increased the practicality of the method by exclusively using short-term vesicle depletion to vary the effective release probability under a single experimental condition. Their analysis shows that multiquantal release is the key to the wide range of EPSP amplitudes observed (Song et al. 2005; Lefort et al. 2009); it is in general not sufficient to consider the number of distinct anatomical contacts as being the maximum number of vesicles that could be released under the ‘single-vesicle hypothesis’ (Kuno 1971; Korn et al. 1981).

More recent approaches have introduced techniques from Bayesian inference to better estimate synaptic parameters. Bayesian inference determines how far experimental evidence supports a given set of model parameters. This relies on the fact that the probability of a certain model being correct given observed data is proportional to the probability of observing that data given that the model is correct. As such it makes better use of data, including every observation rather than extracting moments as in previous approaches. This framework was first applied to neurophysiological synaptic data by Turner and West (1993) to extract the number of components in a unitary EPSP, but their approach was not readily applicable to standard experimental protocols and was not widely adopted (Bekkers 1994). A more influential Bayesian analysis was that by McGuinness et al. (2010) to measure presynaptic Ca^{2+} concentrations. Bhumbra and Beato (2013) used a Bayesian approach to analyse the quantal parameters underpinning

isolated EPSPs, finding that accurate parameter estimates could be made from less data than with existing mean-variance methods.

Inference on isolated EPSPs, however, does not allow recovery of the parameters behind short-term plasticity. Costa et al. (2013) addressed this issue in a Bayesian framework using the Tsodyks-Markram model of short-term plasticity (Tsodyks et al. 1998). This proved accurate and informative, using a ‘slice’ sampling method (Neal 2003) to approximate high-dimensional distributions and revealing experimental protocols that maximised the effectiveness of the inference procedure. The amplitude of observed EPSPs was assumed to follow a Gaussian distribution. This makes the method unsuitable for weak synapses where quantal effects from a small number of release sites and correlations between subsequent EPSPs are significant (del Castillo and Katz 1954; Thomson et al. 1993; Fuhrmann et al. 2002).

Here we extend these methods of Bayesian inference to extract quantal synaptic parameters from plastic synaptic connections with arbitrary vesicle release-site number. This is an extension and continuation of previous Bayesian work (Bhumbra and Beato 2013; Costa et al. 2013) in that it allows recovery of both quantal synaptic parameters and those governing short-term plasticity. The main barrier to this approach is that the number of correlations between neurotransmitter releases from active sites grows exponentially with the number of EPSPs; we use a Markovian property to compute the exact likelihood function with a complexity that grows only linearly with EPSP number. We demonstrate the application of our approach to common models of depression and facilitation. We apply the analysis to a variety of experimental datasets and describe possible generalisations to other models of plasticity.

4.3 Methods

Ethics statement. All experiments were performed in accordance with the UK Animals (Scientific Procedures) Act (1986).

Preparation of neocortical slices. Parasagittal slices of somatosensory neocortex ($300\mu\text{m}$) were prepared from male Wistar rats, at postnatal day **16-18**. Rats were kept on a 12 hour light-dark cycle with slices made 90 minutes after entering the light cycle. In accordance with the UK Animals (Scientific Procedures) Act (1986), rats were killed by cervical dislocation and then decapitated. The brain was rapidly removed, cut down the midline and the two sides of the brain stuck down. The brain was angled at 15° so that planar slices could be obtained with the dendritic structure of the excitatory neurons intact. Slices were cut with a Microm HM 650 V micro-slicer (Carl Zeiss) in cold ($2-4^\circ\text{C}$) high Mg^{2+} low Ca^{2+} artificial cerebrospinal fluid (aCSF) consisting of 127 mM NaCl, 1.18 mM KH_2PO_4 , 2.14 mM KCl, 26 mM NaHCO_3 , 8 mM

MgCl₂, 0.5 mM CaCl₂ and 10 mM glucose. Slices were stored at 34°C for 1 hour in standard aCSF (1 mM Mg²⁺ and 2 mM CaCl₂) and then at room temperature for 1-6 hours.

Patch-clamp recordings from excitatory cells. A slice was transferred to the recording chamber and perfused at 2 ml/min with aCSF at 32°C. Slices were visualised using an Olympus BX51W1 microscope with IR-DIC optics and a Hitachi CCD camera (Scientifica, Bedford, UK). Whole-cell recordings were made with patch pipettes (5-8 mΩ) manufactured from thick walled glass (Harvard Apparatus Edenbridge UK) containing 135 mM K-gluconate, 7 mM NaCl, 10 mM HEPES, 0.5 mM EGTA, 2 mM ATP, 0.3 mM GTP, and 10 mM phosphocreatine (290 mOSM, pH 7.2). Voltage recordings were obtained using an Axon Multiclamp 700B amplifier and digitised at 20 kHz with a Digidata 1440A (Molecular Devices, Sunnyvale, CA). Pyramidal neurons were identified based on their location in the layered neocortex, somata size and dendritic extent. During recording, neurons were labelled either with the fluorescent dye Alexa Fluor® 488 hydrazide (12.5 mM, Life Technologies, Paisley, UK) or with biocytin (1 mg/mL, Sigma-Aldrich, Dorset, UK) to allow confirmation of the cell type and to ensure an intact apical dendrite.

Adenosine application. All drugs were prepared as concentrated stock solutions (1000 mM), stored frozen and then thawed and diluted in aCSF immediately before use. Adenosine, 8-cyclopentyl-theophylline (8CPT; A1R antagonist) was purchased from Sigma (Poole, UK). Adenosine acts via A1, A2 and A3 receptors, A1Rs being the principal neocortical subtype. Initial experiments confirmed this by comparing transmission in 8CPT + adenosine and 8CPT only, where any difference would be due to A2 or A3 activation. No significant difference was found, with a mean ratio of 8CPT + adenosine/8CPT of 0.93 (SEM, 0.08).

Stimulation protocols. Presynaptic cells were stimulated with square-pulse currents of 5 ms duration and magnitude sufficient to reliably induce a single action potential without causing bursting. Stimulation consisted of either 8 – 10 spikes at 20 – 50 Hz with 10 s between traces or 20 spikes generated by a Poisson process with a mean rate of 5 Hz.

Data for the Bayesian algorithm. For each presentation of the presynaptic stimulus, the amplitudes and times of the individual EPSPs are extracted from the postsynaptic voltage trace using the voltage deconvolution method (Richardson and Silberberg 2008). The standard deviation of external noise σ_D is extracted from a baseline period of the original individual traces. This gives two vectors for each presentation: one of EPSP times and one of EPSP amplitudes. Note that spike times do not have to be constant between trials, allowing usage of this method *in vivo* when spiking is uncontrolled but monitored.

Bayesian principle. We seek to obtain an estimate of the probability that the synaptic parameters take a particular value given the observed postsynaptic response. If the space of parameters is Θ , then the probability of a set of parameter values $\theta \in \Theta$ being true given an observed set of EPSP times and amplitudes **Data** is proportional to the likelihood of that data being observed if θ were the true parameter set:

$$P[\Theta = \theta | \text{Data}] \propto P[\text{Data} | \Theta = \theta] P[\Theta = \theta] \quad (4.1)$$

Model	Description	Inferred parameters
DEP	Vesicle depletion depression	n, p_0, τ_D, μ_a , and σ_a
FAC	Facilitation	$n, p_0, \tau_D, p_1, \tau_f, \mu_a$, and α_a
DAR	Depression with augmented recovery	$n, p_0, \tau_D, R_1, R_\infty, \tau_R, \mu_a$, and σ_a
FAR	Facilitation with augmented recovery	$n, p_0, \tau_D, R_1, R_\infty, \tau_R, p_1, \tau_f, \mu_a$, and σ_a
RID	Release independent depression	$n, p_0, \tau_D, p_1, \tau_{I_0}, \mu_a$, and σ_a
FDR	Release independent depression and frequency dependent recovery	$n, p_0, \tau_D, p_1, \tau_{I_0}, \tau_{I_1}, \tau_{\tau_I}, \mu_a$, and σ_a

Table 4.1: Table of synaptic models used and their inferred parameters. Note that the standard deviation of external noise σ_D is fixed from the raw traces.

Likelihoods are computed with respect to a synapse model. The models discussed here are described below and summarised in Table 4.1. The probability $P[\Theta = \theta]$ on the right-hand side is the prior distribution, which is initially uniform but is updated with each presentation of the presynaptic stimulus. This is often referred to as ‘Posterior \propto Likelihood \times Prior’. Defining Data_i to be the set of response times and amplitudes to the i th independent repeat (from N in total), the probability of $\theta \in \Theta$ given all of the data is

$$P[\Theta = \theta | \{\text{Data}_i\}_{i=1}^N] \propto \prod_{i=1}^N \left(P[\text{Data}_i | \Theta = \theta] \right) \quad (4.2)$$

The prior distribution is taken to be flat (uninformative) in all cases over some range (Table 4.2). This could be adapted in future studies if stereotypical parameter distributions can be established.

Synaptic models. It is possible to treat a broad class of synaptic models using the inference presented here. The synapses this inference can be applied to are assumed to have a number n of vesicle release sites to which neurotransmitter vesicles can dock. On arrival of a presynaptic spike neurotransmitter is released independently from each docked vesicle with probability p . This probability p can differ between spikes, but for a given spike should be identical across all release sites; it should not depend on the history of release at individual sites but only on the presynaptic action potential train. The ‘mini’ quantal amplitude, the influence on the voltage of the postsynaptic cell from the neurotransmitter released by a single vesicle, should be modelled by a random variable, with independent identical distribution between different vesicles. The contribution from different vesicles should sum linearly. The ‘mini’ amplitude distribution could differ between spikes. In an interval between spikes, empty release sites are independently stocked with vesicles with a certain probability which depends on the length of the interval.

The models discussed below all display these properties. We explicitly consider cases where facilitation (Varela et al. 1997; Tsodyks et al. 1998) and release-independent depression (Fuhrmann 2004) alter the vesicle release probability between spikes, or augmented recovery (Hosoi et al. 2007) alters the rate of vesicle replenishment, but do not vary the ‘mini’ quantal amplitude distribution. This covers the most common models of short-term plasticity in the cortex.

(i) *Depression*. A synaptic connection between two cells consists of a number n of vesicle release sites. When the presynaptic cell spikes, each vesicle present at a release site is released with probability p_0 . The neurotransmitter in a single vesicle causes a voltage increase in the postsynaptic cell treated as a gamma-distributed amplitude with mean μ_a (mV) and standard deviation σ_a (mV). Between pulses, empty release sites are stocked with vesicles as a Poisson process with rate $1/\tau_D$ (Hz) so that the probability of an empty site being restocked in an interval of length T is $(1 - e^{-\frac{T}{\tau_D}})$. This model is abbreviated to DEP in Table 4.1 and the basic five-dimensional parameter space has ranges given in Table 4.2 (Tsodyks and Markram 1997).

(ii) *Facilitation*. The release probability p_0 is at some synapses dependent on the history of activity and is then a dynamic variable $p(t)$. This model (Varela et al. 1997; Fuhrmann et al. 2002) includes facilitation: the influx of calcium into the synaptic terminal induced by an action potential increases the release probability $p(t)$ for subsequent spikes, this facilitation decays with time constant τ_f (s). The magnitude of increase caused by a single spike saturates as p approaches 1 and the release probability immediately after the first spike is denoted p_1 . A special case is when the release probability doubles after the first spike and so $p_1 = 2p_0$ (Tsodyks et al. 1998).

$$\frac{dp}{dt} = \frac{p_0 - p}{\tau_f} + \frac{(p_1 - p_0)(1 - p)}{1 - p_0} \sum \delta(t_{\text{Spike}}) \quad (4.3)$$

The parameter space is now 7-dimensional (Varela et al. 1997; Fuhrmann et al. 2002), or 6-dimensional in the case of the original Tsodyks model (Tsodyks et al. 1998). The model is abbreviated to FAC in Table 4.1.

(iii) *Augmented recovery*. It has also been observed at some synapses that the rate at which empty sites are restocked is increased by presynaptic activity (Wang 1998; Kittelmann et al. 2013; Hallermann and Silver 2013). The mechanism behind this is also related to calcium influx. The model (Hosoi et al. 2007) used to describe this process augments the base restock rate $\frac{1}{\tau_D}$ (Hz) with a dynamic component $R_a(t)$ so that the total rate of recovery at time t is $\frac{1}{\tau_D} + R_a(t)$, matching the double exponential recovery observed experimentally. R_a is increased to R_1 after an isolated spike, saturates to a maximum of R_∞ and decays back to zero with time constant τ_R (s).

$$\frac{dR_a}{dt} = -\frac{R_a}{\tau_R} + \frac{R_1(R_\infty - R_a)}{R_\infty} \sum \delta(t_{\text{Spike}}) \quad (4.4)$$

Augmented recovery is observed at both purely depressing and facilitating synapses; modelling it adds three additional parameters. The depression with augmented recovery and facilitation with augmented recovery are denoted DAR and FAR respectively in Table 4.1.

(iv) *Release-independent depression (RID)*. This model (Fuhrmann 2004) is appropriate for synapses that do not display facilitation and considers a different form of depression which is uncorrelated with the preceding EPSP amplitudes. RID is a reduction in release probability p caused by spiking activity which decays on a timescale τ_{I_0} . The release probability immediately after an isolated pulse is p_1 , but in contrast to facilitation $p_1 < p_0$.

$$\frac{dp}{dt} = \frac{p_0 - p}{\tau_{I_0}} - \frac{p}{p_0}(p_0 - p_1) \sum \delta(t_{\text{Spike}}) \quad (4.5)$$

The parameter space is again 7-dimensional. The model is abbreviated to RID in Table 4.1.

(v) *Release-independent depression (RID) with frequency dependent recovery (FDR)*. RID is often accompanied by frequency-dependent recovery (Fuhrmann 2004), a reduction in the timescale of recovery from RID. The timescale $\tau_I(t)$ is a dynamic variable with initial value τ_{I_0} , magnitude after an isolated spike τ_{I_1} , and decay timescale τ_{τ_F}

$$\begin{aligned}\frac{dp}{dt} &= \frac{p_0 - p}{\tau_I} - \frac{p}{p_0}(p_0 - p_1) \sum \delta(t_{\text{Spike}}) \\ \frac{d\tau_I}{dt} &= \frac{\tau_{I_0} - \tau_I}{\tau_{\tau_F}} - \frac{\tau_I}{\tau_{I_0}}(\tau_{I_0} - \tau_{I_1}) \sum \delta(t_{\text{Spike}})\end{aligned}\tag{4.6}$$

The parameter space is now 9-dimensional. The model is abbreviated to FDR in Table 4.1.

(v) *Possible extensions*. Any synaptic model with (potentially inhomogeneous) Poisson vesicle replenishment and a release probability (dynamic or otherwise) that depends purely on the presynaptic action potentials could be studied using this inference. A possible extension not dealt with explicitly in this study, but that meets these criteria, is to consider postsynaptic receptor desensitisation, where the ‘mini’ amplitude distribution is affected by the history of the process (Otis et al. 1996; Jones and Westbrook 1996).

Sampling parameter space. It is possible to exhaustively search a discretisation of the parameter space in a number of cases. This allows an exact calculation of the likelihood function evaluated at a grid of points spanning the parameter space. Marginals and joint marginals for each parameter and parameter pair can be found by successively integrating over the other dimensions.

In some cases, exhaustive computation of likelihoods is too computationally expensive time- and memory-wise, necessitating use of a suitable Markov Chain Monte Carlo sampling method. A Metropolis-Hastings sampler (Metropolis et al. 1953; Hastings 1970) is used here as a simple and robust way of traversing parameter space. Convergence is optimised by tuning the step-size during ‘burn-in’ as in Roberts et al. (1997).

Convergence of the sampler to the true distribution is determined (and computation speeded) by running a number of samplers in parallel and comparing the resultant likelihoods.

Information gain. Information gain is measured by the Kullback-Leibler divergence D_{KL} of a posterior from a prior (Kullback and Leibler 1951). If $f(x)$ is the posterior and $g(x)$ is the prior, then the Kullback-Leibler divergence quantifies the additional bits added by the posterior f compared to the prior g

$$D_{\text{KL}} = \int_{-\infty}^{\infty} f(x) \log_2 \left(\frac{f(x)}{g(x)} \right) dx\tag{4.7}$$

For discrete distributions (for example regarding the number of vesicle release sites n), the integrals are replaced by sums.

Goodness of fit. To determine how well a posterior distribution matches a dataset, it is necessary to measure the goodness of fit G_{Θ} . Here we use a measure of how well a posterior distribution of parameters allows reproduction of a given dataset. G_{Θ} is determined by a bootstrapping procedure. Model parameters are sampled independently from their posterior distributions and used to simulate a set of EPSPs with the same stimulation times and number of repeats as the original data. The goodness of fit G_{θ} of this parameter set θ is given by the inverse root of the

Parameter	Interpretation	Range (units)
n	Number of release sites	1 to 100
τ_D	Timescale of recovery from depression	0 to 1 (s)
p_0	Initial release probability from a single site (given that a vesicle is present)	0 to 1
μ_a	Mean voltage response to neurotransmitter from a single vesicle	0 to 0.5 (mV)
α_a	Shape parameter of voltage response distribution to neurotransmitter contained in a single vesicle	0 to 0.25 (mV)
τ_f	Timescale at which facilitation decays	0 to 0.25 (s)
p_1	Release probability after a single isolated spike	p_0 to 1 (facilitation) or 0 to p_0 (RID)
R_1	Additional vesicle recovery rate after a single isolated spike	0 to 10 (Hz)
R_∞	Maximum additional vesicle recovery rate	R_1 to 100 (Hz)
τ_R	Timescale at which augmented recovery decays	0 to 0.25 (s)
τ_{I_0}	Initial recovery timescale from RID	0 to 0.5 (s)
τ_{I_1}	Recovery timescale from RID after a single isolated pulse	0 to τ_{I_0} (s)
τ_{τ_I}	Decay timescale from FDR	0 to 0.5 (s)
σ_D	Standard deviation in postsynaptic voltage trace due to external noise (fixed by raw traces)	0 to 0.2 (mV)
p	Dynamic release probability	0 to 1
R_a	Augmented component of vesicle restock rate	0 to R_∞ (Hz)
τ_I	Dynamic RID recovery timescale	0 to 0.2 (s)

Table 4.2: Table of inferred (top), fixed (middle), and dynamic (bottom) synaptic parameters used in the model and their ranges. Usual ranges can be expanded on a case-by-case basis.

sum of the squared differences between the simulated and observed mean EPSPs, weighted by the variance of the measured sample mean, and the sum of the squared differences between the simulated and observed variance in EPSPs, weighted by the variance of the experimental sample variance.

$$G_\theta = N_{\text{EPSPs}}^4 \left[\sum_{\text{EPSPs}} \left[\left(\frac{\mu_{\text{Data}} - \mu_{\text{Sim}}}{\sigma_\mu^2} \right)^2 + \left(\frac{\sigma_{\text{Data}}^2 - \sigma_{\text{Sim}}^2}{\sigma_{\sigma^2}^2} \right)^2 \right] \right]^{-\frac{1}{2}} \quad (4.8)$$

where N_{EPSPs} is the number of EPSPs, μ_{Data} is the measured mean EPSP, μ_{Sim} is the simulated mean EPSP, σ_{Data} is the measured EPSP standard deviation, σ_{Sim} is the simulated EPSP standard deviation, σ_μ is the standard deviation of the sample mean for the measured EPSPs, and σ_{σ^2} is the standard deviation of the sample variance for the measured EPSPs. Higher values indicate a better agreement between posterior and data.

This gives the goodness of fit for a single parameter set θ . Repeating the process and averaging over a set of G_θ s allows estimation of the goodness of fit of the model, G_Θ . In practice, 10^5

parameter sets are sampled to allow estimation of G_Θ , and estimates are quoted \pm the standard error of the mean.

4.4 Results

We first describe a technique for the computation of the likelihood function for a single trace occurring given a set of synaptic parameters, as required for the Bayesian inference procedure. This is an important step as a naive likelihood calculation quickly becomes intractable due to the number of correlations between release sites growing exponentially with the number of presynaptic spikes. We have used the Markovian property of the vesicle occupancy before a spike to substantially reduce the computational complexity of this calculation so that the number of calculations grows linearly with the number of spikes. We provide an illustrative example calculation with three spikes and two release sites.

We then discuss the effects of different quantal parameters on identifiability for simulated data and how this compares with previous approaches. We apply the technique to experimental data for depressing juvenile synapses in control and in the presence of the neuromodulator adenosine, which is implicated in altering synaptic dynamics (Kerr et al. 2013).

4.4.1 Computing exact likelihoods

A key component of the exact likelihood is the probability that a number k_i of vesicles are released at the i th spike. The number of probabilities $P[k_1 \& k_2 \& \dots \& k_m]$ of releases from n release sites with m spikes grows as $(n+1)^m$ and therefore quickly becomes intractable. To resolve this issue it is possible to use the fact that $P[k_i]$ is only dependent on the probability distribution of the number of vesicles present before the i th spike and the current release probability p . This Markovian property means that the number of calculations can be reduced to only $m(n+1)^2$. The procedure for doing this makes exact computation practical and is now outlined (Fig. 4.1).

(i) *Release probabilities.* To determine the probabilities of releasing each possible number of vesicles (from 0 to n) in response to a stimulus, note that if there are y vesicles present beforehand then the number released k is binomially distributed $k \sim B(y, p)$. This is true for all values of y from 0 to n . Thus the probability that k vesicles are released by

a stimulus is given by

$$\begin{aligned} P[k] &= \sum_{y=k}^n P[k|y]P[y] \\ &= \sum_{y=k}^n \binom{y}{k} p^k (1-p)^{y-k} P[y] \end{aligned} \quad (4.9)$$

The black line in Figure 4.1b illustrates the probability distribution of vesicles released k by each spike in a train.

(ii) *Occupancy after a spike.* The probability of the number of vesicles present taking a value y_{\oplus} immediately after an observed release of size k is given by

$$\begin{aligned} P[y_{\oplus}] &= P[k|y_{\oplus} + k]P[y_{\oplus} + k] \\ &= \binom{y_{\oplus} + k}{k} p^k (1-p)^{y_{\oplus}} P[y_{\oplus} + k] \end{aligned} \quad (4.10)$$

The brown line in Figure 4.1b illustrates the distribution of vesicles present immediately after each spike y_{\oplus} in a train.

(iii) *Recovery between spikes.* Between spikes, empty release sites are restocked as a Poisson process. The probability that an individual empty site is restocked in an interval of length T is $(1 - e^{-T/\tau_D})$. Given that the number of empty sites after the last spike is $n - y_{\oplus}$, the number that restock in an interval of length T is binomially distributed $\sim B(n - y_{\oplus}, 1 - e^{-T/\tau_D})$. This is true for all postspike occupancies y_{\oplus} and so the probability $P[y]$ that there are y vesicles present before the next spike is

$$\begin{aligned} P[y] &= \sum_{y_{\oplus}=0}^y P[y|y_{\oplus}]P[y_{\oplus}] \\ &= \sum_{y_{\oplus}=0}^y \binom{n - y_{\oplus}}{y - y_{\oplus}} (1 - e^{-T/\tau_D})^{y - y_{\oplus}} e^{-T/\tau_D(n - y)} P[y_{\oplus}] \end{aligned} \quad (4.11)$$

The green line in Figure 4.1b illustrates the distribution of vesicles present immediately before each spike y in a train.

(iv) *Matching amplitudes.* The probability of each possible number m of vesicles released matching the i th measured EPSP amplitude A_i is dependent on μ_a , σ_a , and the background noise strength σ_D . The distribution of the voltage changes induced by a single vesicle is modelled by a gamma random variable. The gamma distribution for individual vesicles is preferred over a Gaussian as the coefficient of variation of ‘mini’ amplitudes is often large enough to otherwise imply that individual vesicles would regularly have a hyperpolarising effect (Robinson 1976; Hanse and Gustafsson 2001; Bhumbra and Beato 2013). This is unphysiological and introduces the potential for the model to assign

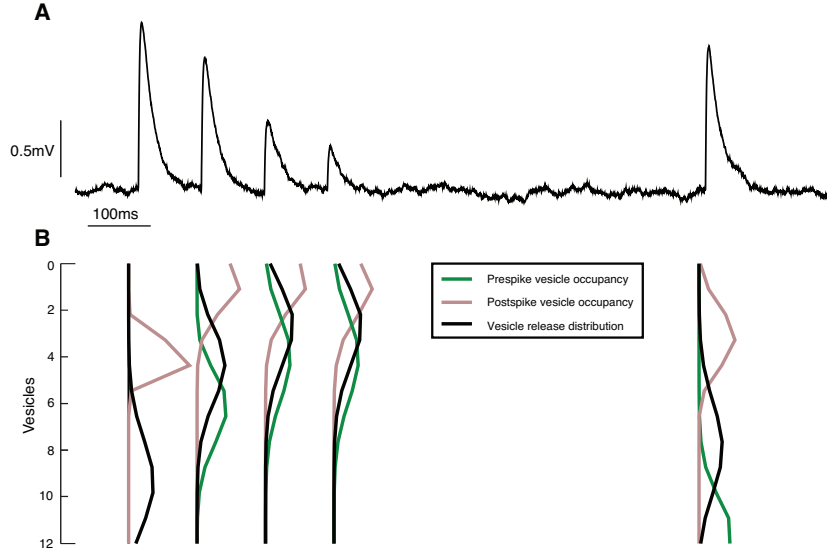


Figure 4.1: An illustration of the procedure for calculating exact likelihoods. **(A)** Simulated postsynaptic voltage trace. **(B)** Inferred distributions of vesicles leading to observed EPSPs. The green line gives the distribution of y , the number of vesicles present immediately before each spike (initially all release sites are stocked), the black line gives the distribution of k , the number of vesicles released by each spike, and the brown line gives the distribution of y_{\oplus} , the number of vesicles present immediately after each spike. The likelihoods in **B** are calculated with the same parameters used to simulate postsynaptic trace in **A**.

some portion of variability in total EPSP size to such ‘negative’ vesicles and so reduce the robustness of the estimation. In addition, variability in response between different anatomical contacts is likely to induce a skewed distribution that is best fit by a gamma density (Markram et al. 1997; Franks et al. 2003).

Considering first the gamma case without background noise,

$$\begin{aligned}
 P[A_i] &= \sum_{k=0}^n P[A_i|k]P[k] \\
 P[A_i] &= \sum_{k=0}^n \frac{\left(\frac{\mu_a}{\sigma_a^2}\right)^k \frac{\mu_a^2}{\sigma_a^2}}{\Gamma(k \frac{\mu_a^2}{\sigma_a^2})} A_i^{k \frac{\mu_a^2}{\sigma_a^2} - 1} e^{-\frac{\mu_a A_i}{\sigma_a^2}} P[k]
 \end{aligned} \tag{4.12}$$

where $P[k]$ comes from the release probabilities discussed above and Γ is the gamma function $\Gamma(t) = \int_0^\infty r^{t-1} e^{-r} dr$. To include the external noise requires convolution of the density $P[A_i|k]$ with the Gaussian $N(0, \sigma_D)$.

$$P[A_i] = \sum_{k=0}^n \frac{\left(\frac{\mu_a}{\sigma_a^2}\right)^k \frac{\mu_a^2}{\sigma_a^2}}{\Gamma(k \frac{\mu_a^2}{\sigma_a^2})} \frac{1}{\sqrt{2\pi}\sigma_D} \int_0^\infty s^{k \frac{\mu_a^2}{\sigma_a^2} - 1} e^{-\frac{\mu_a s}{\sigma_a^2}} e^{-\frac{(A_i - s)^2}{2\sigma_D^2}} ds P[k] \tag{4.13}$$

For convenient evaluation, this integral can be mapped onto the range $[0, 1)$ by the transformation $z = \frac{s}{1+s}$.

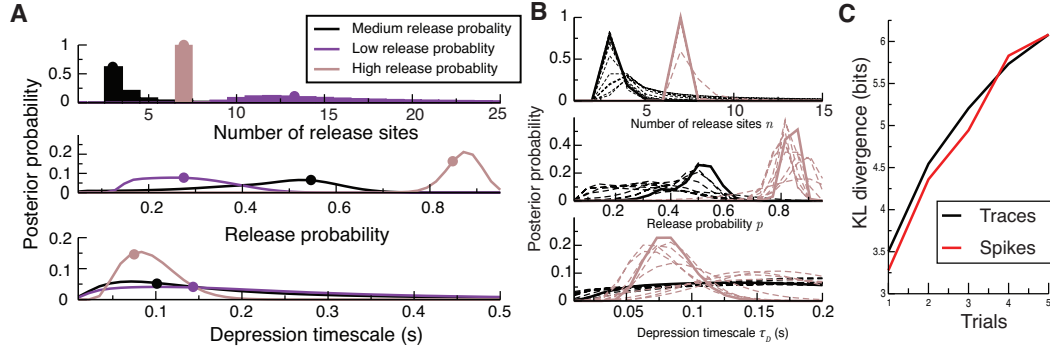


Figure 4.2: Identifiability of parameters in a quantal model with no uncertainty in ‘mini’ quantal size (simulated data). **(A)** Posterior distributions of three quantal parameters under conditions of medium (black), low (purple), and high (brown) release probability p_0 . Inference was conducted on five traces of five spikes, synthetically generated with parameters indicated by dots. **(B)** Convergence of posterior distributions in the medium (black) and high (brown) release probability p cases. Intermediate posteriors are indicated by dashed lines. Inference was conducted on ten traces of five spikes, synthetically generated with the same parameters as in **A**. **(C)** Kullback-Leibler (KL) divergence of posterior of n from a flat prior for different inference methods. The black line corresponds to a method where each trial adds an additional trace of five spikes; the red line corresponds to an alternative procedure where each trial adds an additional spike to each of five traces with originally one spike each and so initially doesn’t account for the correlation between EPSPs. Plotted lines are the mean KL divergences after 1000 inferences on sets of EPSP amplitudes simulated with parameters generated uniformly from the ranges in Table 4.2.

(v) *Matrix formulation.* The structure of the likelihood allows the above steps to be written as a matrix product. Write \mathbf{R}^i for the matrix determining vesicle release from the i th presynaptic spike, $\mathbf{M1}^i$ for the matrix determining the distribution of vesicles remaining after the i th spike, and $\mathbf{M2}^i$ for the matrix determining the number of vesicles that recover in the interval following the i th spike. \mathbf{R}^i depends on the release probability p_i at the i th spike, $\mathbf{M1}^i$ depends on the release probability p_i and observed amplitude A_i of the i th spike, and $\mathbf{M2}^i$ depends i th interspike interval T_i . Elements in the three matrices are given by

$$\begin{aligned}\mathbf{R}_{j,l}^i(p_i) &= \mathbb{P}[k_i = j + 1 | y = l + 1] \\ \mathbf{M1}_{j,l}^i(p_i, A_i) &= \mathbb{P}[A_i | k_i] \mathbb{P}[k_i = j + 1 | y_{\oplus} = l + 1 - k_i] \\ \mathbf{M2}_{j,l}^i(T_i) &= \mathbb{P}[y = j + 1 | y_{\oplus} = l + 1]\end{aligned}\tag{4.14}$$

where the probabilities on the right-hand side correspond to the probabilities defined in the sections above. As every release site is assumed to be initially fully stocked, the vector \mathbf{x} giving the probability of any number site being occupied is given first by a column vector of zeros except for the $n + 1$ th (final) entry, which is equal to one. The

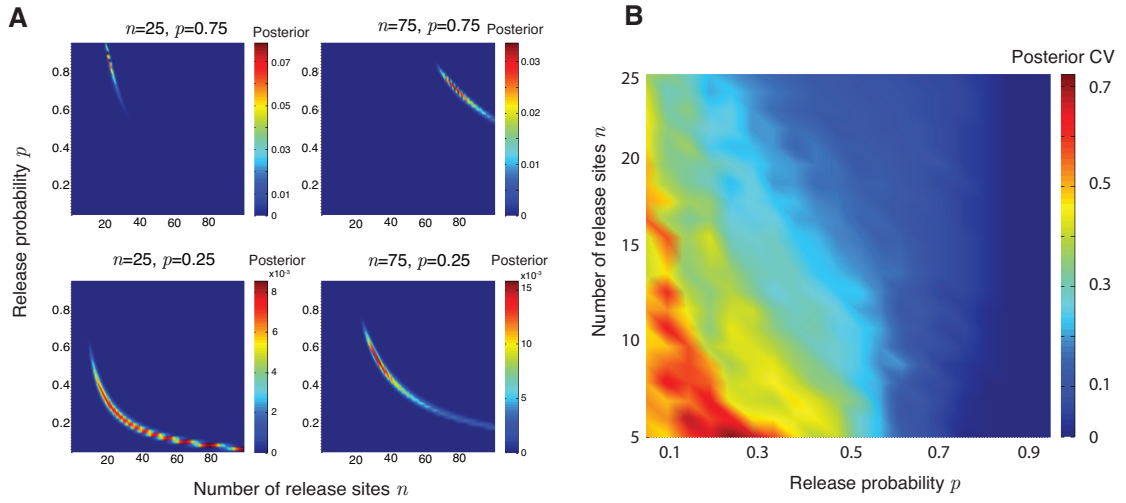


Figure 4.3: Joint distribution of release-site number n and release probability p_0 (Simulated data). **(A)** Joint marginal distributions of release site number n and release probability p for low and high values of both parameters for ten traces of five spikes with $\tau_D = 0.1$ s. **(B)** Coefficient of variation (standard deviation divided by mean) of the posterior distribution of the number of release sites n for different values of n and release probability p with trials and τ_D as in **A**.

distribution of release probabilities \mathbf{k}^i , for the i th spike is then given by

$$\mathbf{k}^i = \begin{cases} \mathbf{R}^1 \mathbf{x} & \text{if } i = 1 \\ \mathbf{R}^i \prod_{j=1}^{i-1} [\mathbf{M}^j \mathbf{M}^j] \mathbf{x} & \text{if } i > 1 \end{cases}$$

The likelihood of a trace of m measured amplitudes being generated by a parameter set $\theta \in \Theta$ is then the product $\prod_{i=1}^m P[A_i]$ where each $P[A_i]$ is computed from the probability vector \mathbf{k}^i using Eq. (4.13).

4.4.2 Example likelihood calculation

To illustrate the procedure above, we will calculate the likelihood that EPSP amplitudes $[0.67, 0.23, 0.34]$ mV were observed for spikes at times $[0, 0.1, 0.2]$ s under the DEP model given that $n = 2$, $\tau_D = 0.1$ s, $p_0 = 0.6$, $\mu_a = 0.3$ mV, $\sigma_a = 0.1$ mV, and $\sigma_D = 0.05$ mV. As both sites are initially stocked the initial occupancy vector \mathbf{x} is given by

$$\mathbf{x} = \begin{pmatrix} 0 \\ 0 \\ 1 \end{pmatrix} \quad (4.16)$$

In the DEP model, the release probability is fixed at $p_0 = 0.6$ for each spike and so the release matrix for each spike is given by

$$\mathbf{R}^1 = \mathbf{R}^2 = \mathbf{R}^3 = \begin{pmatrix} 1 & 0.6 & 0.36 \\ 0 & 0.4 & 0.48 \\ 0 & 0 & 0.16 \end{pmatrix} \quad (4.17)$$

The first release distribution \mathbf{k}^1 and likelihood $P[A_1]$ of the first spike having the observed amplitude of 0.67mV (to four decimal places) are therefore

$$\mathbf{k}^1 = \begin{pmatrix} 0.16 \\ 0.48 \\ 0.36 \end{pmatrix} \quad P[A_1] = 0.2018 \quad (4.18)$$

Given the observed amplitude of the first spike and the probability that an empty release site being restocked in the interval $[0, 0.1]$ is $1 - e^{-\frac{0.1}{0.1}} = 0.6321$, the postspike occupancy $\mathbf{M1}^1$ and restock $\mathbf{M2}^1$ matrices can be written

$$\mathbf{M1}^1 = \begin{pmatrix} 1 & 0.4280 & 0.2199 \\ 0 & 0.5720 & 0.3920 \\ 0 & 0 & 0.3880 \end{pmatrix} \quad \mathbf{M2}^1 = \begin{pmatrix} 0.1353 & 0 & 0 \\ 0.4651 & 0.3679 & 0 \\ 0.3996 & 0.6321 & 1 \end{pmatrix} \quad (4.19)$$

The second release distribution \mathbf{k}^2 and likelihood $P[A_2|A_1]$ of the second spike having amplitude 0.23mV can be written

$$\mathbf{k}^2 = \begin{pmatrix} 0.3030 \\ 0.4961 \\ 0.2009 \end{pmatrix} \quad P[A_2|A_1] = 0.5032 \quad (4.20)$$

As the second interspike interval is the same as the first, the restock matrices $\mathbf{M2}^2$ and $\mathbf{M2}^1$ are the same, and $\mathbf{M1}^2$ is given by

$$\mathbf{M1}^2 = \begin{pmatrix} 1 & 0.4560 & 0.2502 \\ 0 & 0.5440 & 0.3980 \\ 0 & 0 & 0.3518 \end{pmatrix} \quad (4.21)$$

The final release distribution can be calculated as above to give the final amplitude probability $P[A_3|A_2, A_1]$ and trace likelihood $P[A_1, A_2, A_3]$

$$P[A_3|A_2, A_1] = 0.3447 \quad P[A_1, A_2, A_3] = 0.0350 \quad (4.22)$$

4.4.3 Identifiability of number of release site number n and release probability p_0

A major difficulty with estimating synaptic parameters is in distinguishing between the number of release sites n when the release probability p_0 is low. Considering a case where there is no uncertainty in the size of a ‘mini’ EPSP so as to focus on the parameters n , p_0 and τ_D , Bayesian inference allows quantification of this difficulty (Fig. 4.2). When p_0 is low, the relatively broad spread of the posterior distribution for all parameters (Fig. 4.2a) and slower convergence (Fig 4.2b) are in line with results seen in Bhumbra and Beato (2013) and Costa et al. (2013); the additional consideration of synaptic dynamics and correlated binomial release statistics in this paper do not substantially alter this constraint.

Despite this, considering the correlations between spikes within a train is more informative than conducting an analysis on isolated spikes. Figure 4.2c shows the Kullback-Leibler (KL) divergence between the posterior and prior of the marginal distribution of the number of release sites n as a function of the number of trials used in the inference. The black line shows the effect of adding an additional trace of five spikes for each trial, whereas the red line shows the effect of adding an additional spike to each of five traces for each trial. The former method, which accounts for the correlations between EPSPs in earlier trials, has a higher divergence and so provides more information from the same amount of data. The latter method also produces a KL divergence that fluctuates more, revealing the artificial sensitivity to noise that comes from ignoring correlations.

A further issue with identifiability comes from dependencies between parameters. To quantify this, Bayesian inference allows the full joint posterior distribution $P[n, p_0]$ to be calculated (Fig. 4.3a). In cases of low p_0 , the joint distribution takes a characteristic concave shape and it is difficult to infer one parameter without constraining the other.

If the release probability p_0 is low, it is possible to reliably distinguish the release site number n more easily if this number is large. Figure 4.3b plots the coefficient of variation of the posterior marginal in n as a function of n and p_0 , giving a measure of precision by measuring the relative width of the posterior. Whilst, in this case, it is always possible to perfectly distinguish n when p_0 is high (above 0.8), lower values of p_0 require higher values of n to achieve an equivalent precision.

4.4.4 Depression at juvenile synapses for noisy connections

Juvenile layer-V cortical synapses in juveniles are strongly depressing (Reyes and Sakmann 1999). A connection was stimulated with a Poisson train of action potentials to

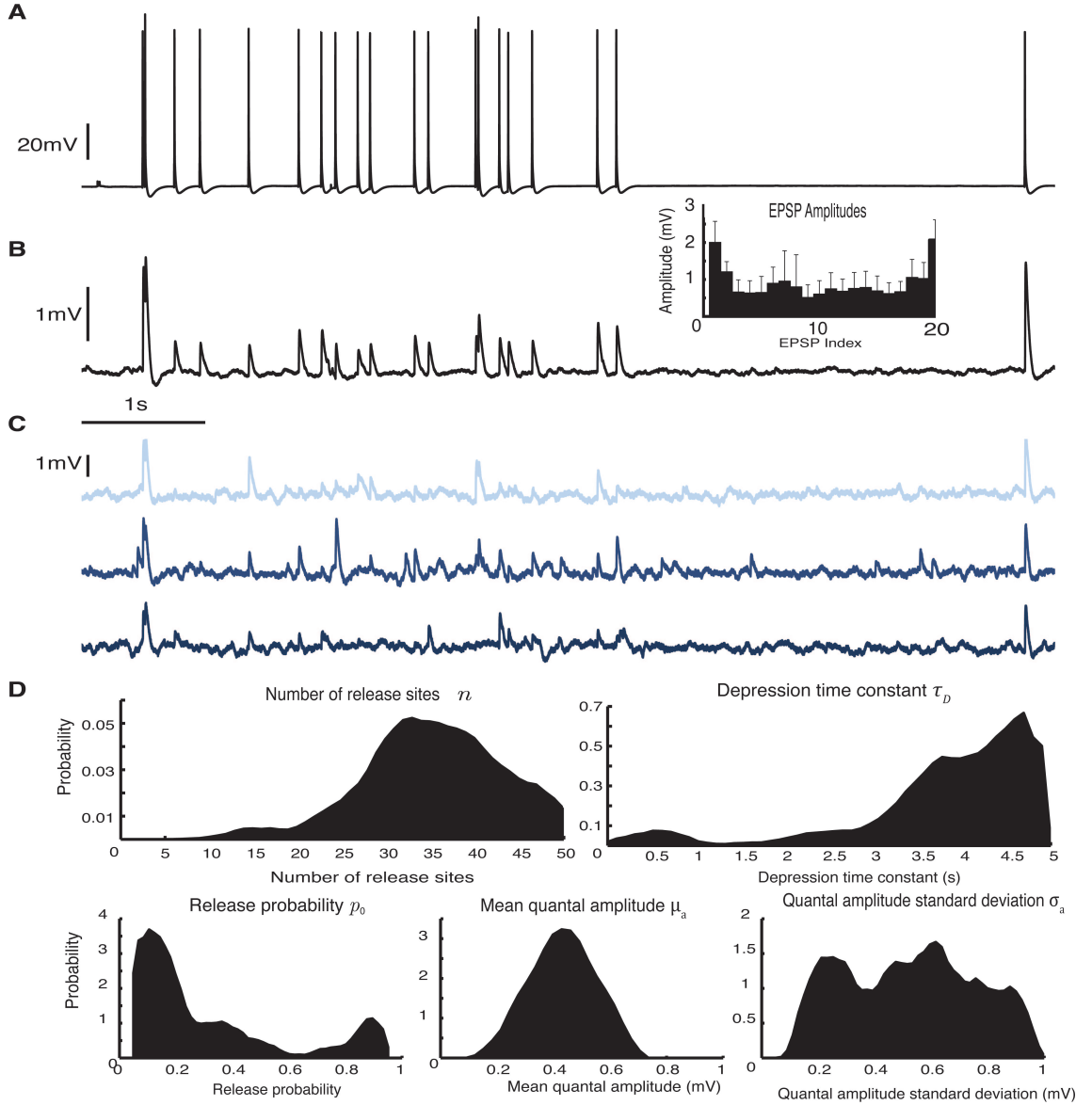


Figure 4.4: DEP model applied to a noisy juvenile synapse (experimental data). (A) Poisson spike train in the presynaptic neuron. (B) Mean postsynaptic voltage over 30 traces with mean and standard deviation of individual EPSP amplitudes (inset bar graph). (C) Example individual postsynaptic traces showing a high baseline variance. (D) Posterior distributions for the DEP model parameters after 5000 Metropolis-Hastings samples.

test the inference procedure for the DEP model (Fig. 4.4). The connection was relatively noisy (Fig. 4.4c), with a standard deviation in the baseline voltage of $\sigma_D = 0.68\text{mV}$. This made interpretation difficult, and gave a particularly broad spread to the posterior for the standard deviation in the ‘mini’ amplitude σ_a . The posteriors for release site number n and, particularly, mean ‘mini’ amplitude μ_a are relatively well-constrained (Fig 4.4d). The depression appears to be badly captured by the DEP model, however, with the synapse depressing strongly at first, but then reaching a relatively stable state with very slow recovery. This leads to a bimodal posterior for the release probability p_0

and high inferred values of the depression time constant τ_D (a factor of ten higher than commonly reported). The low signal-to-noise ratio of this data makes more detailed discussion difficult.

4.4.5 Adenosine at juvenile synapses

The neuromodulator adenosine is implicated in the developmental shift from dominant depression at juvenile synapses to dominant facilitation at mature synapses (Kerr et al. 2013). An initially depressing connection was stimulated with periodic spikes at 20Hz and the postsynaptic response was recorded as a control (Fig. 4.5a). Adenosine was applied to the slice as described in Methods and the stimulus protocol was repeated.

The external voltage noise was much lower in this instance ($\sigma_D = 0.1\text{mV}$ for control and $\sigma_D = 0.08\text{mV}$ under adenosine), making parameter inference more robust. Fitting the DEP model to the data gathered under adenosine led to a broad spread in the posteriors of most parameters (Fig. 4.5b, red line, $G_\Theta = 0.9377 \pm 0.0133$), although it should be noted that the parameters of the control are not particularly well-constrained by the data either (Fig. 4.5b, blue line, $G_\Theta = 1.5980 \pm 0.0268$). The parameters of the FAC model are a good fit to the adenosine data ($G_\Theta = 2.1068 \pm 0.0331$).

The inferred mean quantal amplitude μ_a changes substantially under application of adenosine in Figure 4.5b and between the DEP and FAC models applied to the adenosine data (Figs 4.5b and c). This is largely due to the inaccuracy of the DEP model applied to a facilitating synapse: the posterior of μ_a shifts as the model is unable to account for the true dynamic release probability. Note that the predicted quantal amplitudes of the control data under the DEP model (Fig. 4.5b, blue line) and the adenosine data under the FAC model (Fig. 4.5c, red line) are similar, in the region of 0.7mV.

The estimates for the number of release sites n and mean ‘mini’ amplitude μ_a appear consistent between the DEP model of the control data and the FAC model of the adenosine data.

The Bayesian inference reveals the changes in synaptic parameters after application of adenosine, showing the major effect on initial release probability p_0 .

4.5 Discussion

We have presented a method for producing parameter distributions from single-vesicle run-down experiments using an exact calculation of the quantal likelihood for a dynamic

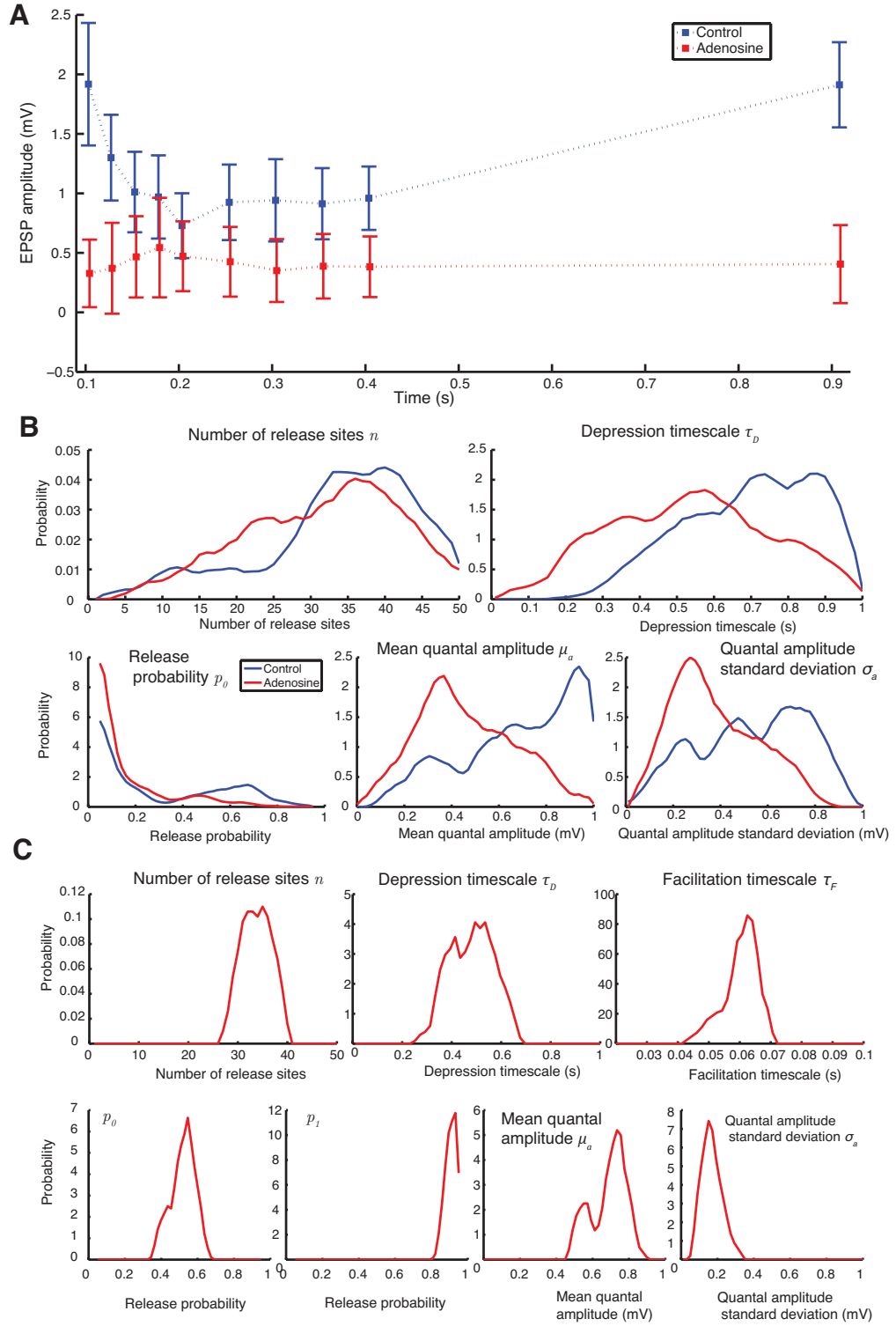


Figure 4.5: Change in synaptic dynamics after application of adenosine (experimental data). **(A)** Mean and variance of EPSPs as a function of stimulus time in control (blue) and after application of adenosine (red). **(B)** Posterior distributions of synaptic parameters under the DEP model in control (blue) and under adenosine (red). **(C)** Posterior distributions under the FAC model after the application of adenosine. All with 10000 Metropolis-Hastings samples.

synapse; the method is not dependent on repeated stimulus patterns and so is suitable for situations *in vivo* where presynaptic firing is uncontrolled, but monitored. Calculation of the exact likelihood function described here allows for Bayesian determination of the distributions of the physiological parameters underpinning a synapse, extending the recent work of Bhumbra and Beato (2013) and Costa et al. (2013). The major contribution of our study is the consideration of correlations between EPSPs; these will be most significant when the number of release sites n is low and release is most variable ($p \approx \frac{1}{2}$). We have shown that the issues of parameter identifiability when release probability is low highlighted by the two previous studies are not resolved by accounting for EPSP correlations with an exact quantal likelihood function. We have also used the joint posterior distribution of release site number n and release probability p_0 to quantify the relationship between these two parameters when it comes to identifiability. The method has been applied to experimental data from a juvenile connection, where the high level of external noise leads to relatively broad posterior distributions and makes inference difficult for any method. Finally, we have applied the technique to a synapse before and after the application of the neuromodulator adenosine, which is believed to mediate the developmental shift in synaptic dynamics from depressing to facilitating (Kerr et al. 2013). The inference is shown to capture the shift in synaptic properties between control and adenosine states.

Inference of synaptic parameters is complex (Clements 2003; Silver 2003), and we believe that a Bayesian approach, which allows quantification of the uncertainty in an estimate is the best way to handle this complexity. Our work, alongside that of Bhumbra and Beato (2013) and Costa et al. (2013), provides a principled way to infer physiological parameters at a synaptic connections.

4.5.1 Extensions

To further demonstrate the practicality of the inference procedure described here it would be necessary to apply it to a greater array of experimental data, allowing comparison of the many synaptic models described.


Acknowledgements

We acknowledge funding through a Warwick Systems Biology Doctoral Training Centre fellowship to Alex D. Bird, funded by the UK EPSRC and BBSRC funding agencies, and funding to Magnus J. E. Richardson under BBSRC Grant No. BB/J015369/1. Data under adenosine was gathered by Michael Kerr.

Chapter 5

Optimal current transfer in dendrites

5.1 Overview

 IN this chapter I study how far dendrites are optimised to passively propagate synaptic currents. This follows from a previous numerical study on dendritic optimality that found a quadratic profile optimised current transfer (Cuntz et al. 2007). I derive an accurate asymptotic approximation is made to the voltage in a passive cable with arbitrary radius profile using the fact that voltage will change more quickly than radius in a typical neurite. This analytical result allows derivation of the optimal taper profile to propagate voltages proximally, matching the earlier non-parametric result. The quadratic form is seen to predict the structure of dendrites from a variety of cell classes, implying that passive propagation is an important factor in dendritic function.

5.1.1 Author contributions

Conceived the study: HC and ADB. Derived and solved equations: ADB. Wrote code for simulations: ADB and HC. Prepared figures: ADB and HC. Wrote the paper: ADB and HC.

The first draft was entirely written by ADB. All equations were initially derived by ADB. The figure panels were generated using MATLAB scripts written by ADB and finalised by HC.

Optimal current transfer in dendrites

Alex D. Bird^{1,2,3} and Hermann Cuntz^{4,5}

¹Systems Biology Doctoral Training Centre, ²School of Life Sciences, and ³Warwick Systems Biology Centre, University of Warwick, CV4 7AL, United Kingdom.

⁴Ernst Strüngmann Institute for Neuroscience in cooperation with Max Planck Society and ⁵Frankfurt Institute for Advanced Studies, Frankfurt-am-Main, Germany.

Abstract. Integration of synaptic currents across an extensive dendritic tree is a prerequisite for computation in the brain. Dendritic tapering away from the soma has been suggested to both equalise contributions from synapses at different locations and maximise the current transfer to the soma. To find out how this is achieved precisely, an analytical solution for the current transfer in dendrites with arbitrary taper is required. We derive here an asymptotic approximation that accurately matches results from numerical simulations. From this we then determine the diameter profile that maximises the current transfer to the soma. We find a simple quadratic form that matches diameters obtained experimentally indicating a fundamental architectural principle of the brain that links dendritic diameters to signal transmission.

Key words: neuron, dendrite, taper, voltage, optimal

5.2 Optimal current transfer in dendrites

Integration of synaptic inputs relies on the propagation of currents arising from sources across the dendritic tree. Whilst active processes strongly contribute to current flow in most neurons (Llinás 1988; Stuart and Sakmann 1994; London and Häusser 2005), understanding the passive backbone to transmission is key to an intuitive grasp of dendritic function; the results of Wilfrid Rall in highlighting the properties of cylindrical dendrites (Rall 1959; Rall 1969; Rall and Rinzel 1973) are of foundational importance in compartmental modelling and computational neuroscience. Dendrites are, however, not generally cylindrical. The distal taper seen in the majority of all cases appears to both increase passive current flow towards the soma (Jaffe and Carnevale 1999; Williams and Stuart 2002; Cuntz et al. 2007), thus reducing the energy requirements of active compensatory processes, and contributes to the phenomenon of dendritic democracy, where somatic voltage amplitudes are equalised between different synaptic sites (Magee and Cook 2000; Häusser 2001; Rumsey and Abbott 2006).

Common approaches to modelling taper treat a dendritic cable as a series of cylinders or linearly tapering frusta (Rall 1969; Butz and Cowan 1974; Koch et al. 1983; Holmes

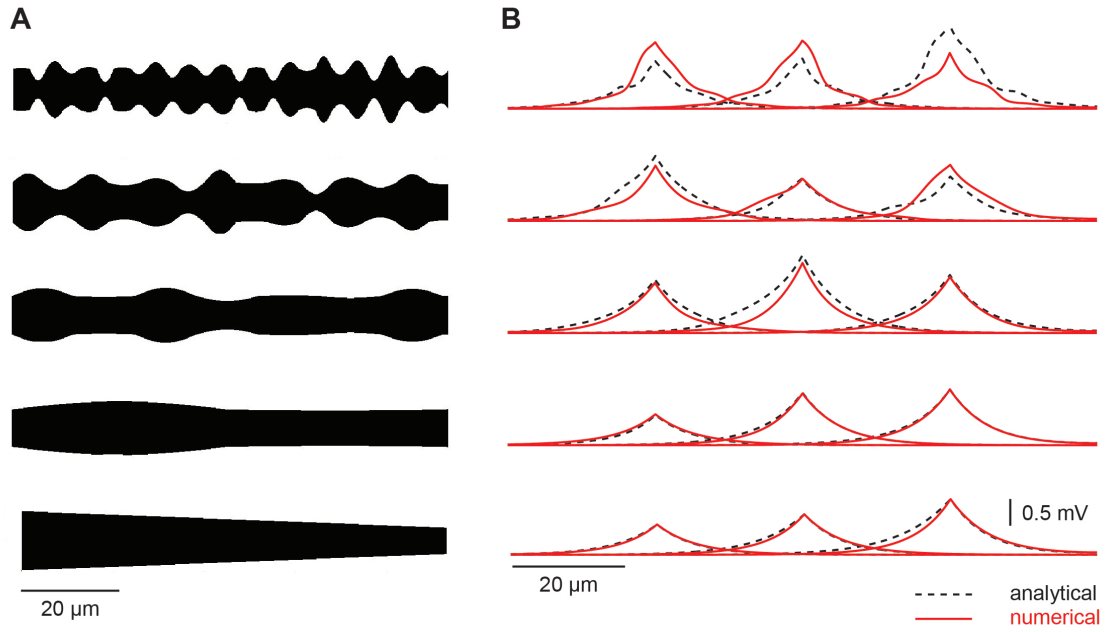


Figure 5.1: Cable theory with arbitrary diameters: Accuracy of the asymptotic approximation. **(A)** Sample radius profiles illustrating the accuracy of the analytical approximation. **(B)** Comparison of numerical (red solid lines) and analytical (black dashed lines) voltages in dendrites with varying radius profiles for currents injected at three points. As the radius changes more slowly, the first-order approximation becomes more accurate (from top to bottom).

and Rall 1992; Zador et al. 1995; Hines and Carnevale 1997; Cuntz et al. 2010). Whilst these techniques are accurate and powerful, there is still much to be gained from an analytical solution to the voltage in terms of intuition and computational speed. A number of solutions for the voltage in non-uniform cables exist (Goldstein and Rall 1974; Poznanski 1991; London et al. 1999), but these involve either the more tractable cases of varying electrotonic properties with constant radius or are limited to a few forms of radius taper.

We present an asymptotic approximation to the voltage in dendrites with an arbitrary taper profile using the insight that voltage attenuation is substantially faster than radius change in realistic morphologies. A particularly appealing prospect for such an approach is that the optimal taper profile to transmit distal synaptic currents to the soma can then be derived using variational calculus.

A length of passive dendrite tapers with radius at distance x given by $r(x)$. The leak conductance per unit area is denoted g_l , the axial resistance r_a , and the membrane time constant τ . Then the voltage above equilibrium $v(x, t)$ at location x and time t obeys

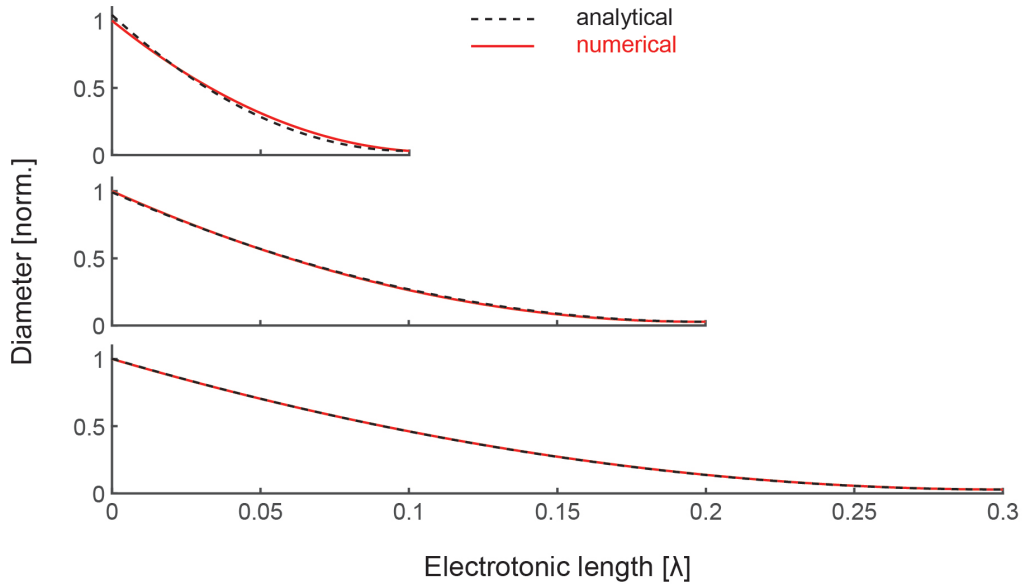


Figure 5.2: Diameter profiles to optimise current transfer. Comparison of non-parametrically optimised (red solid lines) and theoretical (black dashed lines) radius profiles for different electrotonic lengths of dendritic branch. The theoretical profile is less strongly tapering in the shortest case as it neglects the increase in distal input resistance from the sealed end.

the generalised cable equation (see Section 5.4)

$$\tau \frac{\partial v}{\partial t} = -v + \frac{1}{2r_{ag}r(x)} \frac{1}{\sqrt{1 + (r'(x))^2}} \frac{\partial}{\partial x} \left[r^2(x) \frac{\partial v}{\partial x} \right] \quad (5.1)$$

The rate of voltage attenuation is generally significantly steeper than the rate of change of dendritic radius, allowing use of the method of multiple scales (Hinch 1991) to accurately approximate the voltage evolution. We introduce $X = \epsilon x$ as the ‘slow’ taper variable and treat it as independent of x . Large regions of most dendritic trees admit small values of ϵ (~ 0.001 , Fig. 5.4).

Expanding in ϵ (see Section 5.5), gives the first-order steady-state solution

$$v(x) = \sqrt{\lambda(x)} \left[A e^{\int^x \frac{1}{\lambda(s)} ds} + B e^{-\int^x \frac{1}{\lambda(s)} ds} \right] \quad (5.2)$$

for $\lambda(x) = \sqrt{\frac{r(x)}{2r_{ag}}}$ the location-dependent electrotonic length and constants A and B determined by the boundary constraints. This provides an accurate approximation to the voltage in real dendritic cables (Fig. 5.1).

The simple form seen here allows for the usual features of cable theory to be reconstructed. In particular, standard analytic results for voltage propagation in complex dendritic structures and time-dependence have easy analogies in tapering cables. Greater

accuracy can also be achieved, up to a point, by taking higher-order terms in ϵ . These results are shown in the Supplementary Information.

This form of the first-order voltage allows for study of the optimal dendritic radius profile to propagate synaptic currents towards the soma. Previous work in this direction lacked a continuous representation of the voltage profile and used numerical methods to explore optimality (Cuntz et al. 2007). Calculus of variations provides a framework in which to define the optimal profile (for the leading-order component of the voltage) continuously.

Given a dendritic cable of length L with volume Vol and distal (minimal) radius r_L , the goal is to maximise the voltage at the proximal end of a dendritic cable for synaptic currents arising at all points along the cable. This means maximising the functional

$$J = \int_0^L \frac{1}{\lambda^{\frac{7}{2}}(x')} e^{-\int_{x'}^0 \frac{1}{\lambda(s)} ds} dx' \quad (5.3)$$

where the effect of ‘reflected’ current at the distal end has been neglected due to the relatively fast time course of excitatory potentials.

The maximisation gives an optimal radius profile of (see Section 5.8)

$$r(x) = \alpha(L - x)^2 + r_L \quad (5.4)$$

where α is fitted to match the volume of a segment. This profile matches the results of numerical optimisation (Fig. 5.2).

Having found the optimal single cable for voltage propagation, it remains to be shown how far real dendritic trees correspond to this optimality. Rall (Rall 1959) showed that if the diameters of cylindrical sections at dendritic branch points satisfied the relationship $d_p^{3/2} = d_{c1}^{3/2} + d_{c2}^{3/2}$, then the entire dendritic tree could be collapsed to a single cylinder; the same relationship would allow for a tapering tree to be collapsed to a continuous quadratically tapering cable. Rall’s relationship is rarely satisfied in real dendrites (Poznanski 1991; Whitehead and Rosenberg 1993; Lindsay et al. 2003). Using a Rallian diameter ratio at a branch, however, allows us ensure that the transition between parent and daughter branches obeys the quadratic optimality condition. This makes it possible to map quadratic radii onto complex dendritic morphologies by constraining dendrites to locally obey optimality. The resulting predicted morphologies show how far dendritic trees are globally optimised to transmit and equalise current transfer.

We have selected a number of neuronal classes with a broad array of functions to examine the validity of our predictions (Fig. 5.3c). It should be noted here that obtaining reliable measurements of dendritic radius is experimentally very challenging and this

makes exact comparisons difficult. Different cell types satisfy the equivalent quadratic criterion to different degrees. Of the cell classes studied, the best agreement was for fly neurons, which might be considered genetically more hardwired. In terms of mammalian neurons, the best agreement was found for dentate gyrus granule cells. These cells are known to both obey Wilfrid Rall's branching criterion (Desmond and Levy 1984) and undergo continuous replacement throughout life (Cameron and McKay 2001). These results suggest that our model might best match cells with a stereotypic morphology and therefore an initially optimal passive backbone.

The diameter profiles of apical and basal dendrites in cortical pyramidal cells match optimality to different degrees. The apical tree appears well described in terms of quadratic equivalent taper, despite differences specifically at the trunk of the apical dendrite. As the apical trunk might be more strongly specialised in propagating dendritic spikes, deviations might not be surprising. The predicted diameter profile for the basal dendrites was less accurate. Here there appear to be sections of the reconstruction that are much more voluminous than their length relative to other branches would suggest. This might imply that the relationship between nearby cells exerts a stronger influence than is seen elsewhere and that local cortical microcircuits display preferential connections in some directions.

No agreement was found for cerebellar Purkinje cells, where the general taper profile is much shallower than would be expected and dendrites often exhibit alternate bulges and narrower regions. The distinctive layered structure of the cerebellum means that excitatory synaptic inputs arrive in distinct locations, strong synapses from climbing fibres proximally and individually weaker, but much more numerous, synapses from parallel fibres distally. These two types of inputs are implicated in different spiking patterns, complex and simple spikes respectively, and the functional relationship between the two is beyond the scope of our general optimality principle.

Structurally, the agreement between ideal and observed morphologies therefore varies with specific function, but the model seems to provide a good fit to large regions of many dendritic trees. We can, however, show how well the quadratic taper performs for all classes studied (Fig. 5.3b). Plotting the current transfer from all nodes to the soma illustrates the advantages of quadratic taper against a constant diameter and provides a slight advantage over observed morphologies. Our results highlight the importance of a specific form of taper in maximising current transfer and equalising synaptic inputs.

Dendrites perform an array of non-linear computations involving active processes and local inhibition. The general principle of global passive optimality does not explain every facet of dendritic function, but does provide a new intuition. Interestingly, for the dendrites where current transfer loss was largest because of either the size (the apical

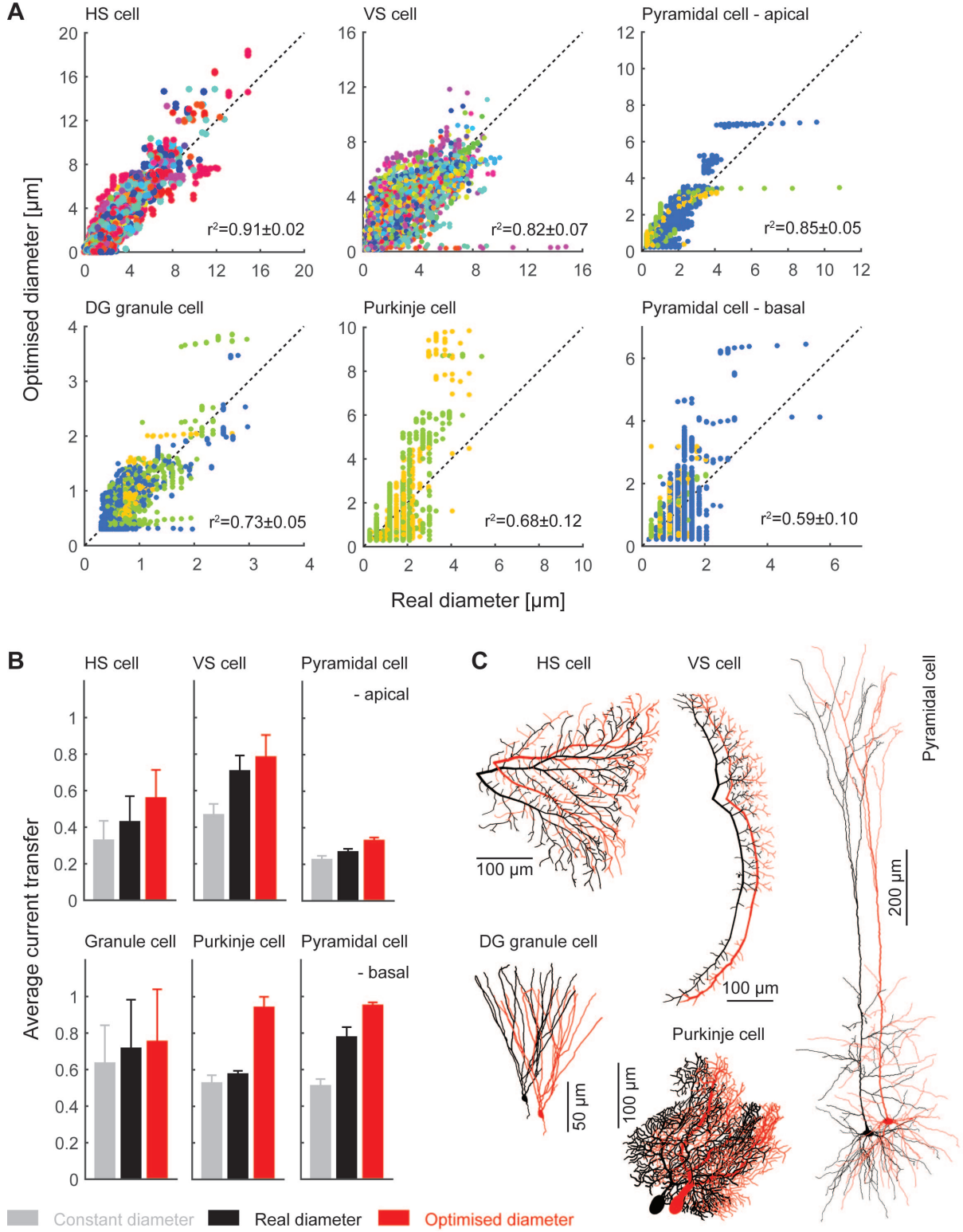


Figure 5.3: Real dendrites are constrained by current transfer optimality. **(A)** Scatter plots of measured radius against optimal radius and correlation coefficients for different cell classes. **(B)** Average current transfer to the root from different cell classes with (from left to right) constant, measured, and optimal radii. **(C)** Examples of reconstructed sample morphologies (black) and the same morphologies with optimal diameter profiles (red). The neurons shown in this figure are two types of fly neurons (HS cell and VS cell with specific membrane conductance of $g_l = 5 \times 10^{-4} \text{ S cm}^{-2}$) and three mammalian neurons (dentate gyrus granule cells with $g_l = 4 \times 10^{-5} \text{ S cm}^{-2}$, and cerebellar Purkinje cells and neocortical Layer V neurons with $g_l = 5 \times 10^{-5} \text{ S cm}^{-2}$).

dendrite of the pyramidal cell) or because of a high membrane conductivity (as was the case in the fly neurons), the diameters tended to be better predicted by optimal current transfer. Where cells deviate substantially from passive optimality, for example specifically along the trunk of the apical dendrite of a pyramidal cell or across a Purkinje cell, there is evidence that these sections of dendrite favour functions other than the unidirectional propagation of excitatory synaptic currents towards the soma. Furthermore, in active tissue distal inputs may be additionally filtered by the membrane conductance changes induced by activation of proximal excitatory and inhibitory synapses. A full study of temporal effects would account for this and may be able to explain more aspects of dendritic optimality.

We have used the fact that voltages in dendrites typically decay much more quickly than radii to make a simple and accurate approximation to the propagation of currents across real dendritic trees. The compact form of the voltage approximation allows for a straightforward reproduction of the standard results of cable theory (Rall 1959; Rall 1969; Rall and Rinzel 1973). Further, this result allows the continuous optimum taper profile for transmitting synaptic currents to the soma to be deduced. The optimal voltage profile tallies with notions of both dendritic democracy (Magee and Cook 2000; Häusser 2001; Timofeeva et al. 2008) and energy optimisation (Cuntz et al. 2007) and provides a close match to reconstructed dendritic morphologies across a range of cell classes. The simple forms of both voltage and optimal radius allow a clearer intuitive understanding of the function of dendritic trees.

Acknowledgements

This research was supported by a Warwick Systems Biology DTC fellowship to ADB funded by the UK EPSRC and BBSRC funding agencies, and by a BMBF grant (No. 01GQ1406 - Bernstein Award 2013) to HC. The cell morphologies used are freely available as described in online methods. The authors report no conflicts of interest.

5.3 Supplementary material: Overview

The body of the paper gives the key results and their implications, the derivations and justifications are given below. Firstly, we give a derivation of the cable equation for an arbitrary radius profile. The resulting generalised cable equation is well known, but this derivation is rarely stated. We then define the multiple scales approximation allowing a solution in steady state and derive the approximate response to an injected synaptic current in a cable with a closed boundary. We discuss the regions of real dendrites where this approximation holds and demonstrate that is a general phenomenon.

We demonstrate the utility of the approximation in more general situations: showing how to produce a higher-order approximation, resolve transients and compute the voltage in a complex dendritic structure. The penultimate section gives the derivation of the optimal radius profile as a perfect-square quadratic taper and describes the algorithm for constructing a quadratic equivalent cable from a real dendritic morphology. Finally, we describe the data and numerical techniques used.

5.4 Derivation of the cable equation for an arbitrary dendritic radius profile

Consider a section of dendrite with continuously varying radius $r(x)$. Take a section of cable from x to $x + \Delta$ with voltages $V(x)$ and $V(x + \Delta)$ at the respective ends. Then Ohm's Law gives that the current I flowing through this segment obeys

$$V(x + \Delta) - V(x) = -IR \quad (5.5)$$

where the resistance R is the resistance of the segment given by

$$R = \frac{r_a \Delta^2}{\int_x^{x+\Delta} A_c(s) ds} \quad (5.6)$$

for r_a the axial resistance and $A_c(x) = \pi r^2(x)$ the cross-sectional area of the dendrite at x . Rearranging the first equation to solve for I gives

$$I = -\frac{\int_x^{x+\Delta} A_c(s) ds}{r_a \Delta} \frac{V(x + \Delta) - V(x)}{\Delta} \quad (5.7)$$

and taking the limit $\Delta \downarrow 0$ gives the current-voltage relationship

$$I(x) = -\frac{A_c(x)}{r_a} \frac{\partial V}{\partial x} \quad (5.8)$$

The capacitative and leak currents over the region $(x, x + \Delta)$ obey respectively

$$\begin{aligned} I_C(x) &= CA_s(x, x + \Delta) \frac{\partial V}{\partial t} \\ I_l(x) &= g_l A_s(x, x + \Delta)(V - E_l) \end{aligned} \quad (5.9)$$

for C the capacitance and g_l the conductance per unit area and

$$A_s(x, x + \Delta) = 2\pi \int_x^{x+\Delta} r(s) \sqrt{1 + (r'(s))^2} ds \quad (5.10)$$

the surface area of the region. Using conservation of current, we have

$$I_C + I_l = I(x) - I(x + \Delta) \quad (5.11)$$

So

$$\begin{aligned} C \frac{\partial V}{\partial t} &= g_l(E_0 - V(x)) - \frac{\Delta}{A_s(x, x + \Delta)} \frac{I(x + \Delta) - I(x)}{\Delta} \\ C \frac{\partial V}{\partial t} &= g_l(E_0 - V(x)) - \frac{1}{2\pi r(x) \sqrt{1 + (r'(x))^2}} \frac{\partial I}{\partial x} \end{aligned} \quad (5.12)$$

where in the second equation we have again taken the limit $\Delta \downarrow 0$. Combining this with the axial current equation Eq (5.8) (and dividing by the conductance g_l) gives

$$\tau \frac{\partial V}{\partial t} = E_0 - V + \frac{1}{2r_a g_l r(x) \sqrt{1 + (r'(x))^2}} \frac{\partial}{\partial x} \left[r^2(x) \frac{\partial V}{\partial x} \right] \quad (5.13)$$

This is the cable equation for an arbitrary radius function $r(x)$. Sealed end boundary conditions with non-negligible terminal area (at $x = L$) imply

$$\left(V + \tau_l \frac{\partial V}{\partial t} + \frac{1}{r_a g_l} \frac{\partial V}{\partial x} \right) \Big|_{x=L} = 0 \quad (5.14)$$

At the proximal end, assume that an isopotential soma gives

$$V|_{x=0} = E_0 \quad (5.15)$$

or we allow the cable to be semi-infinite with voltages decaying as $x \rightarrow -\infty$. The cable is initially at rest, with

$$V_{t=0} = E_0 \quad (5.16)$$

We seek to consider the propagation of a δ current injection at any point x' proximally towards the somatic end.

5.5 First-order multiple scales approximation

5.5.1 Homogenous solution

Consider the homogeneous steady-state equation for $v = V - E_l$

$$\frac{d}{dx} \left[r^2(x) \frac{dv}{dx} \right] - 2r_a g_l r(x) \sqrt{1 + (r'(x))^2} v = 0 \quad (5.17)$$

with

$$\left. \frac{dv}{dx} \right|_{x=L} = 0 \quad \lim_{x \rightarrow -\infty} v = 0 \quad (5.18)$$

r changes more slowly as a function of x than v does, specifically $r(x) = \rho(\epsilon x)$ for $\epsilon \ll 1$. It is possible to treat the ‘fast’ voltage length variable x and the ‘slow’ radius length variable ϵx as independent using the method of multiple scales. Then $\frac{dr}{dx} = \epsilon \frac{d\rho}{dx}$ and the steady-state voltage equation becomes

$$0 = \rho^2 \frac{d^2 v}{dx^2} + 2\epsilon \rho \rho' \frac{dv}{dx} - 2r_a g_l \rho \sqrt{1 + (\epsilon \rho')^2} v \quad (5.19)$$

Introducing the new variable

$$w = \rho^\epsilon v \quad (5.20)$$

allows us to write the voltage equation as

$$\begin{aligned} 0 &= \frac{d^2 w}{dx^2} - \left(2r_a g_l \frac{\sqrt{1 + (\epsilon \rho')^2}}{\rho} + \frac{\epsilon^2 (\rho^2 \rho''' - 3\rho \rho' \rho'' + 2(\rho')^3)}{2\rho^3} + \frac{(\epsilon \rho')^2}{4\rho^2} \right) w \\ 0 &= \frac{d^2 w}{dx^2} - f(\epsilon x) w \end{aligned} \quad (5.21)$$

Note that $\sqrt{1 + (\epsilon \rho')^2} \approx 1 + \frac{(\epsilon \rho')^2}{2}$ and that f , the coefficient of w , will always be positive, making the solution appropriately non-oscillatory. We seek solutions of the form

$$w(x) = \mu(\epsilon x) e^{\int^x \sigma(\epsilon s) ds} \quad (5.22)$$

for μ and σ real. Substituting this into the above equation gives at first order

$$w(x) = \frac{\rho(x)^{1/4}}{(2r_a g_l)^{1/4}} \left[A e^{\int^x \sqrt{\frac{2r_a g_l}{\rho(s)}} ds} + B e^{-\int^x \sqrt{\frac{2r_a g_l}{\rho(s)}} ds} \right] \quad (5.23)$$

for some constants A and B . Then $v(x)$ is given by

$$v(x) = \frac{\rho(x)^{1/4-\epsilon}}{(2r_a g_l)^{1/4}} \left[A e^{\int^x \sqrt{\frac{2r_a g_l}{\rho(s)}} ds} + B e^{-\int^x \sqrt{\frac{2r_a g_l}{\rho(s)}} ds} \right] \quad (5.24)$$

Writing $\lambda(x) = \sqrt{\frac{\rho(x)}{2r_a g_l}}$ as the distance-dependent electrotonic length gives the leading-order form

$$v(x) \approx \sqrt{\lambda(x)} \left[A e^{\int^x \frac{1}{\lambda(s)} ds} + B e^{-\int^x \frac{1}{\lambda(s)} ds} \right] \quad (5.25)$$

5.5.2 Current injection

We will take an approach analogous to Green's functions to determine the response to a current injection of magnitude I_{app} at site x' . The Green's function $g(x, x')$ solves the equation

$$\frac{d}{dx} \left[r^2(x) \frac{dg}{dx} \right] - 2r_a g_l r(x) \sqrt{1 + (r'(x))^2} g = \delta(x - x') \quad (5.26)$$

with a given set of boundary conditions. Away from x' , the solution is given by the homogenous voltage above (Eq. 5.25), namely for $x < x'$

$$g(x, x') = \sqrt{\lambda(x)} B_1 e^{-\int_x^{x'} \frac{1}{\lambda(s)} ds} \quad (5.27)$$

using the fact that voltages are required to decay towards the soma. For $x > x'$, the sealed-end condition gives the constants as

$$B_2 = A_2 \left[\frac{2 + \lambda'(L)}{2 - \lambda'(L)} \right] e^{2 \int_{x'}^L \frac{1}{\lambda(s)} ds} \quad (5.28)$$

Continuity of voltage at x' ensures

$$B_1 = A_2(1 + k) \quad (5.29)$$

for k the ratio between A_2 and B_2 given by the sealed end condition. Conservation of current at the point of injection gives

$$\begin{aligned} g'_{x < x'}(x') + \frac{r_a}{\pi \rho^2(x')} I_{app} &= g'_{x > x'}(x') \\ B_1 (\lambda'(x') - 2) + \frac{2r_a \sqrt{\lambda(x')}}{\pi \rho^2(x')} I_{app} &= A_2 (\lambda'(x') + 2 + k(\lambda'(x') - 2)) \end{aligned} \quad (5.30)$$

giving the coefficients in terms of the initial parameters as

$$\begin{aligned} B_1 &= \frac{r_a \sqrt{\lambda(x')}}{2\pi \rho^2(x')} \left[1 + \left(\frac{2 - \lambda'(L)}{2 + \lambda'(L)} \right) e^{-2 \int_{x'}^L \frac{1}{\lambda(s)} ds} \right] I_{app} \\ A_2 &= \frac{r_a \sqrt{\lambda(x')}}{2\pi \rho^2(x')} \left[\frac{2 - \lambda'(L)}{2 + \lambda'(L)} \right] e^{-2 \int_{x'}^L \frac{1}{\lambda(s)} ds} I_{app} \\ B_2 &= \frac{r_a \sqrt{\lambda(x')}}{2\pi \rho^2(x')} I_{app} \end{aligned} \quad (5.31)$$

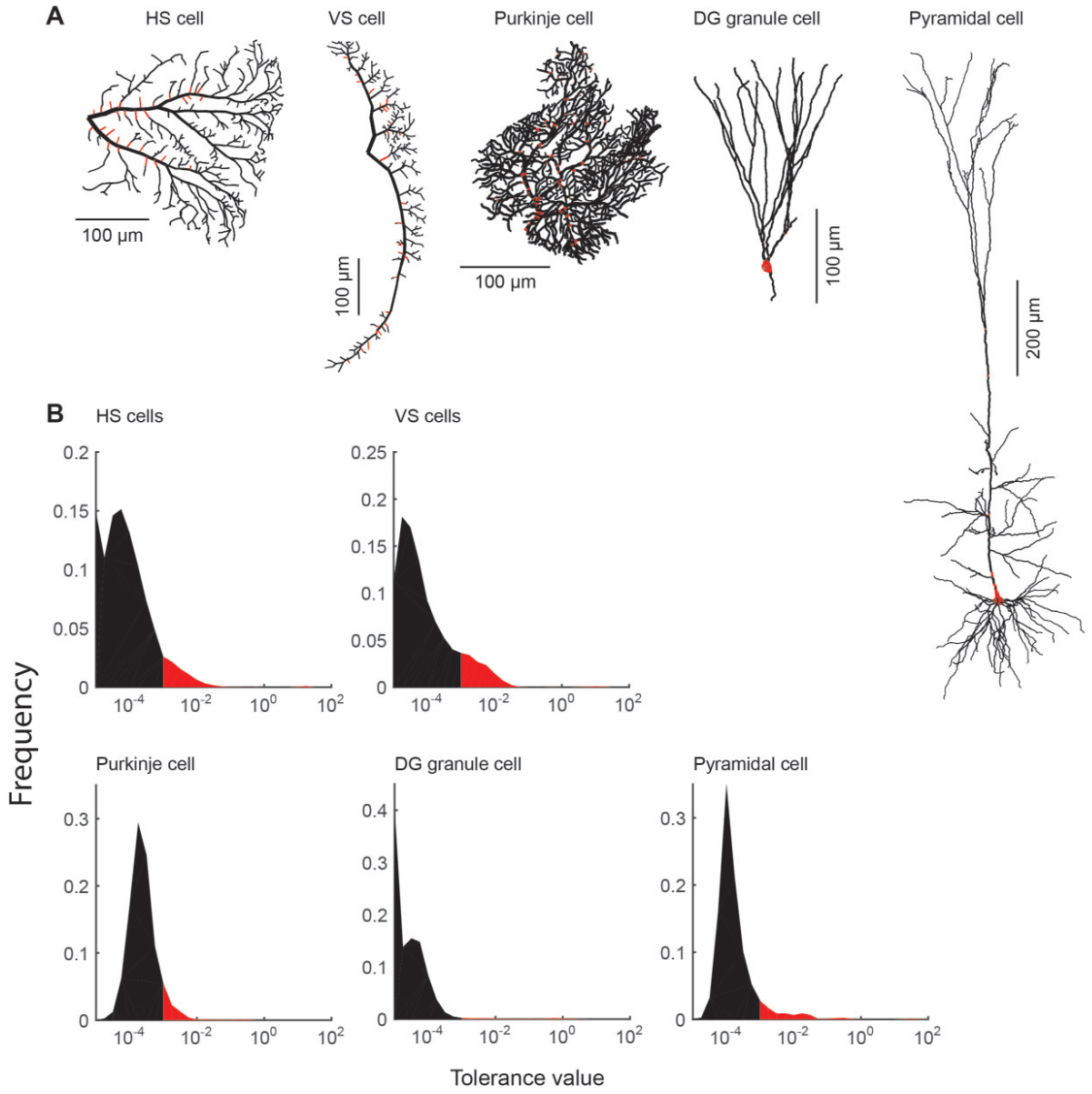


Figure 5.4: Regions of reconstructed dendrites where the asymptotic approximation holds strongly. **(A)** Example reconstructions where $\epsilon > 0.001$ highlighted in red. **(B)** Distribution of ϵ by cell class for the morphologies described in the online material

Note that $B_1(x')$ gives the input resistance at site x' .

5.5.3 Proximal voltage propagation

As we are primarily interested in voltage at the proximal terminal of the dendrite, we focus on the solution in the region $x < x'$ and evaluate the voltage at $x = 0$. The first-order approximation holds for a region of size ϵ^{-1} away from the site of current injection.

5.6 Validity of approximation in real dendrites

We have studied where $\epsilon \ll 1$ in reconstructed dendritic morphologies (Fig. 5.4). Current injection was simulated numerically across the dendritic tree and the highest ratio of voltage change to radius change at each location was determined. The majority of reconstructed dendrites admit very low values of ϵ , although termination points and branch points can have higher values. At branch points the radius can change sharply between a parent and daughter branch, whereas towards the end of dendrites the sealed-end effect can cause shallower voltage attenuation.

5.7 Extending the approximation

5.7.1 Higher-order terms

To obtain approximations valid for larger values of ϵ , it is possible to employ a higher-order approximation. We seek solutions of the form

$$w(x) = \text{Re}\{\mu(\epsilon x)e^{i \int^x \sigma(\epsilon s) ds}\} \quad (5.32)$$

for μ and σ real. Substituting this into the above equation and comparing real and imaginary parts gives

$$\begin{aligned} 2\mu'\sigma + \mu\sigma' &= 0 \\ \epsilon^2\mu'' + \mu(f - \sigma^2) &= 0 \end{aligned} \quad (5.33)$$

The first equation gives $\mu^2\sigma = A$ for some constant A , the second can be solved by expanding μ and σ in powers of ϵ^2 such that $\mu = \mu_0 + \epsilon^2\mu_1$ and $\sigma = \sigma_0 + \epsilon^2\sigma_1$. Similarly, f can be written as $f_0 + \epsilon^2f_1$ where $f_0 = \frac{2r_{ag1}}{\rho}$ and f_1 makes up the rest. Comparing coefficients of ϵ gives

$$\begin{aligned} \sigma_0 &= f_0^{\frac{1}{2}} \\ \mu_0 &= Af_0^{-\frac{1}{4}} \\ \sigma_1 &= \frac{\mu_0'' + \mu_0 f_1}{2\sigma_0\mu_0} \\ \mu_1 &= -\frac{\mu_0\sigma_1}{2\sigma_0} \end{aligned} \quad (5.34)$$

where we have derived the equations for μ from expanding the $\mu^2\sigma = A$ equation in each case. A comes from matching the boundary conditions as above. The second-order approximation can give a substantially better result when ϵ is not very small, for example where there is sharp taper in a narrow region of dendrite (Fig. 5.5).

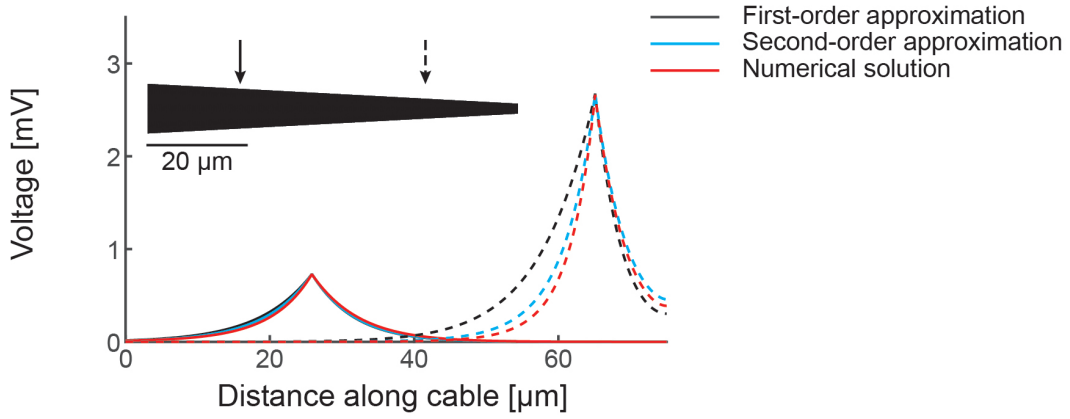


Figure 5.5: Second-order approximation provides better results when ϵ is larger. Simulated (red), leading-order (black), and second-order (blue) voltage profiles for currents injected at two different points (solid and dashed lines respectively) in the linearly tapering cable (inset).

5.7.2 Transient solution

Consider again the full equation

$$\tau_L \frac{\partial v}{\partial t} = -v + \frac{1}{r_{ag} r(x) \sqrt{1 + (r'(x))^2}} \frac{\partial}{\partial x} \left[r^2(x) \frac{\partial v}{\partial x} \right] \quad (5.35)$$

where $v = V - E_0$ is the voltage above rest. The transform $w = \rho^\epsilon v$ gives

$$\tau_L \frac{\partial w}{\partial t} = -w + \frac{1}{f(\epsilon x)} \frac{\partial^2 w}{\partial x^2} \quad (5.36)$$

and introducing θ such that $w = \theta e^{-t/\tau_L}$ gives

$$\tau_L \frac{\partial \theta}{\partial t} = \frac{1}{f(\epsilon x)} \frac{\partial^2 \theta}{\partial x^2} \quad (5.37)$$

Seeking separable solutions of the form $\theta(x, t) = X(x) T(t)$ gives the relationship

$$\frac{\tau_L}{T} \frac{\partial T}{\partial t} = \frac{1}{X f(\epsilon x)} \frac{\partial^2 X}{\partial x^2} = -k^2 \quad (5.38)$$

for some constant k . Then

$$T_k = e^{-\frac{k^2 t}{\tau_L}} \quad W_k \approx \sqrt{\frac{\lambda(x)}{ik}} \left[A_k e^{\int^x \frac{ik}{\lambda(s)} ds} + B_k e^{-\int^x \frac{ik}{\lambda(s)} ds} \right] \quad (5.39)$$

with A_k and B_k determined by the boundary conditions. The voltage profile at different times after current injection into a tapering cable is given in Figure 5.6a.

5.7.3 Complex dendritic structures

It is possible to compute the propagation of voltage in more complex dendritic structures. This can be done recursively from the distal points of the dendritic tree. When two child branches with proximal conductances G_{C1} and G_{C2} respectively meet a parent dendrite at $x = L$, the distal conductance of the parent will be $G_E = G_{C1} + G_{C2}$. To proceed, we require the proximal conductance of the parent dendrite G_0 . The general voltage solution in the parent dendrite can be written in terms of hyperbolic functions as

$$v(x) = \sqrt{\frac{\lambda(x)}{\lambda(L)}} \left[\cosh\left(\int_x^L \frac{1}{\lambda(s)} ds\right) + \left(\lambda(L) \frac{G_E}{G_{\lambda(L)}} - \frac{\lambda'(L)}{2}\right) \sinh\left(\int_x^L \frac{1}{\lambda(s)} ds\right) \right] v_L \quad (5.40)$$

where v_L is the distal voltage and $G_{\lambda(L)} = \frac{\pi \rho^2(L)}{r_a}$ is the cross-sectional conductance of the distal end itself. Then the voltage at the proximal end will be v_0

$$v_0 = \sqrt{\frac{\lambda(0)}{\lambda(L)}} \left[\cosh\left(\int_0^L \frac{1}{\lambda(s)} ds\right) + \left(\lambda(L) \frac{G_E}{G_{\lambda(L)}} - \frac{\lambda'(L)}{2}\right) \sinh\left(\int_0^L \frac{1}{\lambda(s)} ds\right) \right] v_L \quad (5.41)$$

and the current flowing here will be

$$I_0 = \frac{v_L G_{\lambda(0)}}{\sqrt{\lambda(L) \lambda(0)}} \left[\left(\lambda(L) \frac{G_E}{G_{\lambda(L)}} - \frac{\lambda'(L)}{2} + \frac{\lambda'(0)}{2}\right) \cosh\left(\int_0^L \frac{1}{\lambda(s)} ds\right) + \left(\lambda(L) \lambda'(0) \frac{G_E}{2G_{\lambda(L)}} - \frac{\lambda'(L) \lambda'(0)}{4} + 1\right) \sinh\left(\int_0^L \frac{1}{\lambda(s)} ds\right) \right] \quad (5.42)$$

where $G_{\lambda(0)} = \frac{\pi \rho^2(0)}{r_a}$. Then $G_0 = \frac{I_0}{v_0}$, giving

$$G_0 = \frac{G_{\lambda(0)}}{\lambda(0)} \left[\frac{\lambda(L) \frac{G_E}{G_{\lambda(L)}} - \frac{\lambda'(L)}{2} + \frac{\lambda'(0)}{2} + \left(\lambda(L) \lambda'(0) \frac{G_E}{2G_{\lambda(L)}} - \frac{\lambda'(L) \lambda'(0)}{4} + 1\right) \tanh\left(\int_0^L \frac{1}{\lambda(s)} ds\right)}{1 + \left(\lambda(L) \frac{G_E}{G_{\lambda(L)}} - \frac{\lambda'(L)}{2}\right) \tanh\left(\int_0^L \frac{1}{\lambda(s)} ds\right)} \right] \quad (5.43)$$

This allows analytic determination of the conductance across a complex dendritic structure. To determine the corresponding voltage, consider an injection of current I_{app} at a site on some section at $x = x'$. Along this section, the voltage can be determined in terms of hyperbolic functions with constants fixed by the current-voltage relationships at each end of the segment and continuity of voltage and conservation of current at the injection site. This gives

$$\begin{aligned} v_{x>x'}(x) &= \sqrt{\lambda(x)} \left[A_2 \cosh\left(\int_{x'}^x \frac{1}{\lambda(s)} ds\right) + B_2 \sinh\left(\int_{x'}^x \frac{1}{\lambda(s)} ds\right) \right] \\ v_{x<x'}(x) &= \sqrt{\lambda(x)} \left[A_1 \cosh\left(\int_x^{x'} \frac{1}{\lambda(s)} ds\right) + B_1 \sinh\left(\int_x^{x'} \frac{1}{\lambda(s)} ds\right) \right] \end{aligned} \quad (5.44)$$

with

$$\begin{aligned}
A_2 &= \frac{r_a \sqrt{\lambda(x')}}{\pi \rho^2(x')} \left[\frac{1}{\Omega_L - \Omega_0} \right] I_{app} = A_1 \\
B_2 &= \frac{r_a \sqrt{\lambda(x')}}{\pi \rho^2(x')} \left[\frac{\Omega_L}{\Omega_L - \Omega_0} \right] I_{app} \\
B_1 &= \frac{r_a \sqrt{\lambda(x')}}{\pi \rho^2(x')} \left[\frac{\Omega_0}{\Omega_L - \Omega_0} \right] I_{app} \\
\Omega_0 &= \frac{\left(\frac{\lambda'(0)}{2} - \lambda(0) \frac{G_0}{G_{\lambda(0)}} \right) \cosh \left(\int_0^{x'} \frac{1}{\lambda(s)} ds \right) + \sinh \left(\int_0^{x'} \frac{1}{\lambda(s)} ds \right)}{\left(\lambda(0) \frac{G_0}{G_{\lambda(0)}} - \frac{\lambda'(0)}{2} \right) \sinh \left(\int_0^{x'} \frac{1}{\lambda(s)} ds \right) - \cosh \left(\int_0^{x'} \frac{1}{\lambda(s)} ds \right)} \\
\Omega_L &= \frac{\left(\frac{\lambda'(L)}{2} - \lambda(L) \frac{G_E}{G_{\lambda(L)}} \right) \cosh \left(\int_{x'}^L \frac{1}{\lambda(s)} ds \right) + \sinh \left(\int_{x'}^L \frac{1}{\lambda(s)} ds \right)}{\left(\lambda(L) \frac{G_E}{G_{\lambda(L)}} - \frac{\lambda'(L)}{2} \right) \sinh \left(\int_{x'}^L \frac{1}{\lambda(s)} ds \right) - \cosh \left(\int_{x'}^L \frac{1}{\lambda(s)} ds \right)}
\end{aligned} \tag{5.45}$$

The voltage attained at the two ends of the section can be used to provide a simple initial condition for voltages in neighbouring dendrites. The voltage profile in a simple branched morphology is shown in Figure 5.6b.

5.8 Optimality of current transfer

It is possible to use calculus of variations to study the functions $r(x)$ that give extremal values of a functional $J[x, r, r']$. We seek to define the radius profile that maximises current transfer. In this case we seek to maximise the total current transfer to the proximal end $x = 0$ from all injection sites $x' = 0$ to $x' = L$ under constraints of fixed terminal radii or total cable volume. Writing the voltage at 0 due to current injection at x' as $v(0, x')$ such that

$$v(0, x') = \frac{r_a \sqrt{\lambda(x')}}{2\pi \rho^2(x')} \left[1 + \left(\frac{2 - \lambda'(L)}{2 + \lambda'(L)} \right) e^{-2 \int_{x'}^L \frac{1}{\lambda(s)} ds} \right] I_{app} \sqrt{\lambda(0)} e^{-\int_0^{x'} \frac{1}{\lambda(s)} ds} \tag{5.46}$$

We seek to maximise the functional

$$\begin{aligned}
J &= \int_0^L v(0, x') dx' \\
&= \int_0^L K dx'
\end{aligned} \tag{5.47}$$

where J is a functional of the functions $\lambda(x)$ and $\int^x \frac{1}{\lambda(s)} ds$.

It would be possible to consider other functionals here, for example an explicit minimisation of the variance of the proximal voltage induced by current injection at different points. This would be a more direct acknowledgement of dendritic democracy, but would limit the strength of the energy minimisation argument. Another possible extension would be to constrain the total dendritic surface area rather than the volume due to the added metabolic cost of constructing and maintaining neuronal membrane.

It is convenient to write $\Lambda(x) = \int^x \frac{1}{\lambda(s)} ds$ so that $\Lambda'(x) = \frac{1}{\lambda(x)}$ and $K = K[\Lambda, \Lambda']$. For J to take a maximal or minimal value, it is necessary for the integrand K to satisfy the Euler-Lagrange equation

$$0 = \frac{\partial K}{\partial \Lambda} - \frac{d}{dx} \frac{\partial K}{\partial \Lambda'} \quad (5.48)$$

with boundary conditions following from the original constraints. Introducing the constants $C_1 = \frac{r_a \sqrt{\lambda(0)}}{2\pi(2r_a g_l)^2}$ and $C_2 = \frac{2-\lambda'(L)}{2+\lambda'(L)} e^{-2 \int_0^L \frac{1}{\lambda(s)} ds}$ (and noting that this requires the total electrotonic length of the dendrite $\int_0^L \frac{1}{\lambda(s)} ds$ to be conserved) allows us to write

$$K[\Lambda(x), \Lambda'(x)] = \frac{C_1}{\Lambda'(x)^{\frac{7}{2}}} [e^{-\Lambda(x)} + C_2 e^{\Lambda(x)}] \quad (5.49)$$

The Euler-Lagrange equations give that J will not be maximised unless Λ satisfies

$$0 = \frac{9}{7} [C_2 e^{\Lambda(x)} - e^{-\Lambda(x)}] - \frac{9}{2} \frac{\Lambda''(x)}{(\Lambda'(x))^2} [C_2 e^{\Lambda(x)} + e^{-\Lambda(x)}] \quad (5.50)$$

To solve this in terms of elementary functions we introduce a further assumption that current is injected sufficiently far from the distal end for the contribution of ‘reflected’ current to the input resistance to be negligible (This applies more generally when considering responses to transient current injection). This assumption is equivalent to making $C_2 e^{\Lambda(x)}$ vanishingly small, giving the equation

$$\begin{aligned} \frac{\Lambda''(x)}{(\Lambda'(x))^2} &= -\frac{2}{7} \\ \frac{d}{dx} \left[-\frac{1}{\Lambda'(x)} \right] &= -\frac{2}{7} \end{aligned} \quad (5.51)$$

Using the definitions $\Lambda(x) = \int^x \frac{1}{\lambda(s)} ds$, $\lambda(x) = \sqrt{\frac{r(x)}{2r_a g_l}}$, and the boundary conditions gives (for a constant C_3)

$$\begin{aligned} \sqrt{\frac{r(x)}{2r_a g_l}} &= \pm \frac{2}{7} x + C_3 \\ r(x) &= \alpha(L - x)^2 + r_L \end{aligned} \quad (5.52)$$

where r_L is the distal (minimal) radius and α is determined by matching volumes or proximal radii.

5.8.1 Algorithm for optimising an arbitrary dendritic tree

The final comparison of optimal dendritic taper to real morphologies requires an algorithm for mapping a quadratic taper onto complex branched structures. In particular it requires a principled consideration of the way to distribute dendritic radius at branch points. We seek to equalise conductance at branch points using Rall's $\frac{3}{2}$ power relationship; that for a parent radius r_0 , and daughter radii r_1 and r_2 , then $r_0^{\frac{3}{2}} = r_1^{\frac{3}{2}} + r_2^{\frac{3}{2}}$. The ratio between r_1 and r_2 is defined by the lengths l_1 and l_2 of the two daughter branches such that $r_1/l_1^{3/2} = r_2/l_2^{3/2}$. The two daughter branches appear to the parent branch to be a single branch with length $l_0 = (l_1^{3/2} + l_2^{3/2})^{2/3}$. The algorithm for applying these principles to a real dendritic morphology with complex branching structure is described below.

i. Obtaining apparent lengths. Starting at the distal termination points of the tree, path lengths are found to the most distal branch points. The 'apparent length' distal to these branch points is calculated and the process is repeated for every branch point heading towards the root of the tree. This gives an 'apparent length' for the entire tree and for the daughter branches at each branch point.

ii. Distributing radii. The initial radius taper is defined by Eq. (5.52) with L given by the apparent length, r_L by the minimal dendritic radius anywhere on the tree and an initial estimate of the proximal radius from the physiological maximum. At every branch point the parent radius r_0 is already defined by construction and daughter radii r_1 and r_2 are determined using the 'apparent lengths' into each branch. This is continued until radii are assigned everywhere on the tree.

iii. Matching volumes. This procedure may produce a predicted tree with volume higher or lower than the original morphology. The proximal radius is scaled down or up and step 'ii' is repeated until the volumes are matched and an optimal tree with identical volume to the original tree is found.

5.9 Morphological data and numerical methods

5.9.1 Dendritic morphologies and passive parameters

Five cell classes are discussed in the paper, covering an array of functions and species. All morphologies are publicly available. Blowfly *calliphora vicina* HS (25 examples) and VS (30 examples) neuron morphologies are published with the TREES toolbox (Cuntz et al. 2010). The passive parameters used are axial resistance $r_a = 60\Omega\text{cm}$ and

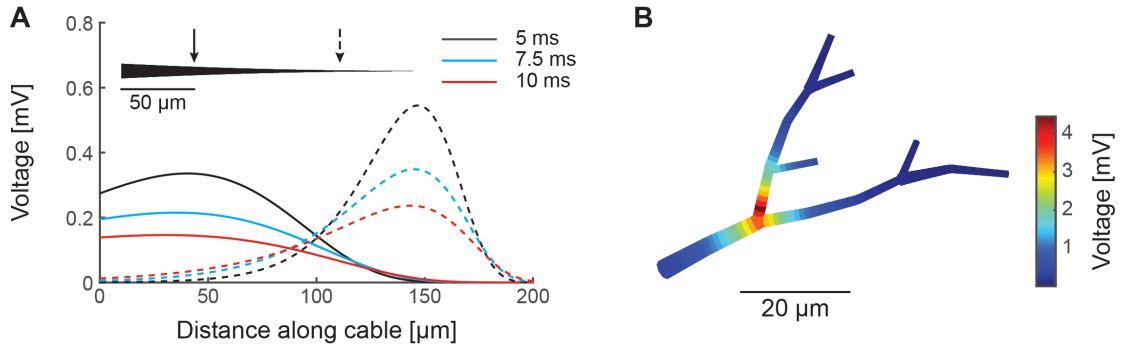


Figure 5.6: Asymptotic approximation allows recovery of classical cable properties. **(A)** Time course of voltage at 5, 7.5, and 10 ms after current injection at two different sites (solid and dashed lines respectively) on a quadratically tapering cable (inset) with $\tau = 20$ ms. **(B)** Steady-state voltage profile in a simple branched structure for current injection at the site with the highest voltage.

membrane conductance $g_l = 5 \times 10^{-4} \text{ S cm}^{-2}$ for both. Mouse dentate gyrus granule cells (3 examples) are published on ModelDB (Accession no. 95960)(Schmidt-Hieber et al. 2007). The passive parameters used are $r_a = 210 \Omega \text{cm}$, $g_l = 4 \times 10^{-5} \text{ S cm}^{-2}$. Rat Purkinje cells (2 examples) are published on NeuroMorpho (IDs NMO_00891 and NMO_0892)(Vetter et al. 2001), with $r_a = 150 \Omega \text{cm}$ and $g_l = 5 \times 10^{-5} \text{ S cm}^{-2}$. Rat Layer V pyramidal cells (3 examples) are published on ModelDB (Accession no. 139653)(Hay et al. 2011), with $r_a = 150 \Omega \text{cm}$ and $g_l = 5 \times 10^{-5} \text{ S cm}^{-2}$ for both basal and apical dendrites.

5.9.2 Numerical methods

Simulations are carried out in MATLAB using the TREES toolbox package (Cuntz et al. 2010). The numerical simulations in Figures 5.1, 5.3, 5.4, and 5.5 use standard functions described in the toolbox. The non-parametric numerical optimisation in Figure 5.2 follows an algorithm adapted from an earlier study (Cuntz et al. 2007). The algorithm assigns radii to seven segments of a cable modelled using the TREES toolbox and uses the MATLAB function ‘fminsearch’ to maximise the current transfer to the proximal end. This is repeated 50 times to produce an overall maximum. The radii of the six distal segments are fitted to a continuous quadratic equation $ax^2 + bx + c$ (as described in Cuntz et al. 2007) to produce the numerical section of Figure 2.

Chapter 6

Discussion



As each results chapter is self-contained with its own discussion, the remarks here will assess links between chapters and the thesis as a whole.

6.1 Introduction

In this thesis I have considered factors affecting synaptic transmission in cortex. Temporal factors in the form of short-term plasticity are shown to have a number of novel effects; the modulation of correlations in neurotransmitter release by both transient synchrony and long-term plasticity leads to a tuning-curve in the postsynaptic firing response. Regular spike trains are able to cross depressing synapses more efficiently than irregular ones, but in conditions of low release probability irregular trains can induce stronger deviations in the postsynaptic voltage. Further, this thesis provides a number of exact analytical results and accurate approximations that clarify the functional effects seen and form a robust foundation for further study of stochastic synaptic transmission. The Bayesian inference described in this thesis allows direct estimation of the quantal and dynamic parameters governing synaptic transmission from data, enabling a more accurate understanding of synaptic function in different physiological situations. I have also derived an accurate analytical approximation to the cable equation for arbitrary radius profile and used this to demonstrate the optimal form of taper to passively maximise and equalise the propagation of synaptic currents towards the soma. That this form predicts the radius profile of a variety of cell classes suggests that maximisation of current transfer is a genuine constraint for the architecture of individual neurons.

The functional results have wider implications for the propagation of signals in neuronal networks. Synchrony in a population can arise either from joint sensory inputs (de

Charms and Merzenich 1996; Baker et al. 2001) or intrinsically, through the connectivity of the neurons (Aertsen et al. 1989). The finding that individual synaptic weights optimally balance synchrony suggests that, alongside being tuned to inputs encoded by synchrony, there will be a trade-off between the degree of clustering in a network and the strength of connections; potentially relating network motifs (Perin et al. 2011) with the known distribution of cortical synaptic weights (Markram et al. 1997). The fact that bursty spike trains are particularly suited to inducing large deviations in the postsynaptic voltage when the initial vesicle release probability is low is intuitive, but the effect is also highly dependent on the release site number. Indeed the developmental decrease in release probability with maturity (Reyes and Sakmann 1999; Frick et al. 2007) means that synapses will become better discriminators of correlations in input statistics with age, making them more ‘tunable’ via long-term plasticity. Together these two sets of results provide a robust analytical description of the effects of long-term plasticity in modulating the postsynaptic response to correlations both between neurons and within spike trains.

The description of synaptic function in these two chapters has a qualitative dependence on the model parameters; n determines the postsynaptic sensitivity to crosscorrelations, p influences the effect of autocorrelations, and a and τ_D determine the sharpness of the tuning. Obtaining accurate and reliable estimates of these parameters is therefore crucial to determining which synaptic features are most salient in different cortical regions and different developmental states. The Bayesian approach presented in this thesis allows recovery of the probability distribution of these parameters given the available data. This allows accurate estimation of the parameters and quantifies the uncertainty in these estimates. The novel derivation of a method for calculating the exact likelihood function means that physiological parameters can be directly inferred for the most common synaptic models (Abbott 1997; Tsodyks et al. 1998; Fuhrmann et al. 2002; Fuhrmann 2004), and extends the overall utility of other Bayesian approaches (Bhumbra and Beato 2013; Costa et al. 2013).

The spatial distribution of anatomical contacts in the postsynaptic dendritic tree is another major factor in understanding synaptic transmission. The coefficient of variation of somatic ‘mini’ EPSPs is large enough to suggest that there may be a large difference between EPSPs evoked at different anatomical contacts (Robinson 1976; Hanse and Gustafsson 2001; Franks et al. 2003). It is therefore important to distinguish distance-based attenuation from potential variation in the synaptic parameters at an individual anatomical contact (Koch et al. 1983; Koch et al. 1990). The result in my final chapter that dendritic trees appear to passively optimise and equalise somatic current flow falls in line with the idea of ‘synaptic democracy’ (Jaffe and Carnevale 1999; Häusser 2001; Timofeeva et al. 2008) and is further evidence that somatic EPSPs from different

presynaptic neurons, or at least those that come from a similar source, may generally be treated as equivalent at the level of the assumptions in the first two chapters. Whilst the complexity of individual neurons, with active dendritic processes and complex patterns of inhibition, means that such an assumption is far too crude to work for individual cells, it represents a step towards extracting the spatial features of neuronal transmission most salient at the mesoscopic level of thousands to tens of thousands of neurons (Pinsky and Rinzel 1994; Herz et al. 2006). This can be seen in the context of other attempts to better describe specific physiological features of neuronal function in a way that is both mathematically tractable and capable of generating new insights into the behaviour of brain circuits (Fourcaud-Trocmé et al 2003; Brette and Gerstner 2005; Harrison et al. 2015).

6.2 Extensions

In addition to the extensions mentioned individually in each chapter, the thesis as a whole presents a number of further possibilities. The thesis separately addresses correlations between neurons and within a spike train. As the higher-order correlations within a presynaptic population are an important determinant of neuronal response (Kuhn et al. 2003), it is critical to define the correlation structure correctly. When individual neurons display autocorrelated spike times, the number of correlations between neurons to study is so large that any choice appears arbitrary. One notable example is the phase-locked periodic stimulus used in the numerical study of de la Rocha and Parga (2005) to generate a presynaptic spiking activity that displays both forms of correlation. This technique can, however, only be applied to the entirety of a population (or to a defined and unchanging subsection of that population) and generalisation is difficult. To define a physiological correlation structure containing both aspects is likely to require analysis of spiking data at a scale that is not readily obtainable with current experimental techniques.

Applying Bayesian inference to synaptic datasets reveals that there can be considerable uncertainty in synaptic parameters under normal experimental protocols. As different regions of parameter space can imply qualitatively different responses to different stimulus patterns, there is an opportunity to assign broader probabilities of synaptic behaviour alongside the original parameters. Costa et al. (2013) used the full distributions of their inferred parameters to accurately cluster synaptic connections between different cell classes. The results in chapters 2, 3, and 4 would allow such methods to be extended into clustering synapses functionally, particularly as the quantal inference elucidates the effect of the release site number in tuning sensitivity to correlation.

There is the direct possibility of incorporating a spatial component into the Bayesian analysis; recovering the possible number of anatomical contacts as well as their distance from the soma and any interference effects due to one synapse lying ‘on-path’ between another and the soma (Koch et al. 1983). This would involve resolving the somatically recorded EPSPs into separate components arising from separate contacts and applying a spatial analysis to resolve the likely pattern of anatomical connections. Such a somatically based technique could be easily verified by cellular reconstructions and would provide a simple and more scalable counterpart to current experimental manipulations of individual contacts (Trigo et al. 2012; Park et al. 2012).

Finally, the research described here provides the opportunity to investigate both spatial and temporal synaptic effects at a single neuron level (Poirazi et al. 2003; de Sousa et al. 2015). The negative correlations in vesicle release caused by synaptic depression have the potential to induce a rich and complex array of somatic voltage responses to distal stimulation (Fox 1985; Fox and Chan 1985; Banitt et al. 2005; Frick et al. 2008). The range of responses would be strongly influenced by factors such as active dendrites (Llinás 1988; London and Häusser 2005) and time- (Koch et al. 1983) and location- (Gidon and Segev 2012) dependent inhibition, as well as the intrinsic complexity of a branched dendritic tree. To gain an intuitive and scalable mathematical description of a neuron receiving temporally complex and spatially distributed inputs would require accurately estimating physiological parameters and extracting the salient factors that lead to spiking outputs.

6.3 Concluding Remarks

The human brain is a hugely complex organ, containing hundreds of trillions of cortical synapses, each of which has an effect dependent upon its history and the location of its contacts in the postsynaptic dendritic tree. In this thesis I have presented research revealing novel aspects of synaptic function and derived exact quantitative models describing previously known phenomena. I have developed mathematical tools to infer and describe the stochastic, quantal, and plastic nature of synaptic transmission and accurately approximated the voltage in passive dendrites. Together these results make some progress towards understanding the temporal and spatial factors that underpin the fiendish complexity of synaptic transmission in cortex.

Bibliography

- Abbott L, Farhi E, and S Gutmann. The path integral for dendritic trees. *Biological Cybernetics* 66: 49-60, 1991.
- Abbott L. Synaptic depression and cortical gain control. *Science* 275(5297): 221-224, 1997.
- Abbott L and S Nelson. Synaptic plasticity: Taming the beast. *Nature Neuroscience* 3: 1178-1183, 2000.
- Abbott L and W Regehr. Synaptic computation. *Nature* 431: 796-803, 2004.
- Adrian E and Y Zotterman. The impulses produced by sensory nerve endings: Part II: The response of a single end organ. *Journal of Physiology* 61: 151-171, 1926.
- Aertsen S, Gerstein G, Habib M, and G Palm. Dynamics of neuronal firing correlation: modulation of “effective connectivity”. *Journal of Neurophysiology* 61: 900-917, 1989.
- Alijani A and M Richardson. Rate response of neurons subject to fast or frozen noise: From stochastic and homogeneous to deterministic and heterogeneous populations. *Physical Review E* 84(011919), 2011.
- Antic S, Zhou W, Moore A, Short S, and K Ikonomu. The decade of the dendritic NMDA spike. *Journal of Neuroscience Research* 88(14): 2991-3001, 2010.
- Atwood H and W Morin. Neuromuscular and axoaxonal synapses of crayfish opener muscle. *Journal of Ultrastructural Resolution* 32: 351-369, 1970.
- Averbeck B, Latham P, and A Pouget. Neural correlations, population coding and computation. *Nature Reviews Neuroscience* 7: 358-366, 2006.
- Baker S, Spinks R, Jackson A, and R Lemon. Synchronization in monkey motor cortex during a precision grip task. I. Task-dependent modulation in single-unit synchrony. *Journal of Neurophysiology* 85: 869-885, 2001.
- Akaike H. A new look at the statistical model information. *IEEE Transactions on Automatic Control* 19(6): 716-723, 1974.
- Banitt Y, Martin K, and I Segev. Depressed responses of facilitatory synapses. *Journal of Neurophysiology* 94(1): 865-870, 2005.
- Barbieri F. Irregular persistent activity induced by synaptic excitatory feedback. *Frontiers in Computational Neuroscience* 2(1): 114-122, 2007.
- Bayazitov I, Richardson R, Fricke R, and S Zakharenko. Slow presynaptic and fast postsynaptic components of compound long-term potentiation. *Journal of Neuroscience* 27(43): 11510-11521, 2007.
- Bekkers J. Quantal analysis of synaptic transmission in the central nervous system. *Current Opinion in Neurobiology* 4: 360-365, 1994.
- Bekkers J. Convolution of mini distributions for fitting evoked synaptic amplitude histograms. *Journal of Neuroscience Methods* 130: 105-114, 2003.

- Benda J and A Herz. A universal model of spike frequency adaptation. *Neural Computation* 15: 2523-2564, 2003.
- Benda J, Longtin A, and L Maler. Spike-frequency adaptation separates transient communication signals from background oscillations. *Journal of Neuroscience* 25(9): 2312-2321, 2005.
- Bennett M and T Florin. Statistical analysis of the release of acetylcholine at newly formed synapses in striated muscle. *Journal of Physiology* 238: 93-107, 1974.
- Bennett M and J Kearns. Statistics of transmitter release at nerve terminals. *Progress in Neurobiology* 60(6): 545-606, 2000.
- Berger T, Larkum M, and H Luscher. High I_h channel density in the distal apical dendrite of Layer V pyramidal cells increases bidirectional attenuation of EPSPs. *Journal of Neurophysiology* 85: 855-868, 2001.
- Bird A and M Richardson. Long-term plasticity determines the postsynaptic response to correlated afferents with multivesicular short-term synaptic depression. *Frontiers in Computational Neuroscience* 8(2), 2014.
- Birò A, Holderith N, and Z Nusser. Quantal size is independent of the release probability at hippocampal excitatory synapses. *Journal of Neuroscience* 25: 223-232, 2005.
- Bhumbra G and M Beato. Reliable evaluation of the quantal determinants of synaptic efficacy using Bayesian analysis. *Journal of Neurophysiology* 109(2): 603-620, 2013.
- Boison D. Adenosine kinase, epilepsy, and stroke: Mechanisms and therapies. *Trends in Pharmacological Science* 27: 652-658, 2006.
- Borst A and J Haag. The intrinsic electrophysiological characteristics of fly lobula plate tangential cells: I. Passive membrane properties. *Journal of Computational Neuroscience* 3(4): 313-336, 1996.
- Borst A, Haag J, and D Reiff. Fly motion vision. *Annual Review of Neuroscience* 33: 49-70, 2010.
- Boudreau C and D Ferster. Short-term depression in thalamocortical synapses of cat primary visual cortex. *Journal of Neuroscience* 25(31): 7179-7190, 2005.
- Boyd I and A Martin. The end-plate potential in mammalian muscle. *Journal of Physiology* 132(1): 74-91, 1956.
- Brémaud A, West D, and A Thomson. Binomial parameters differ across neocortical layers and with different classes of connections in adult rat and cat neocortex. *PNAS* 104: 14134-14139, 2007.
- Brenowitz S and W Regehr. Associative short-term synaptic plasticity mediated by endocannabinoids. *Neuron* 45(3): 419-431, 2005.
- Brette R and W Gerstner. Adaptive exponential integrate-and-fire model as an effective description of neuronal activity. *Journal of Neurophysiology* 94(5): 3637-3642, 2005.
- Brunel N and V Hakim. Fast global oscillations in networks of integrate-and-fire neurons with low firing rates. *Neural Computation* 11: 1621-1671, 1999.
- Brunel N and M van Rossum. Lapicque's 1907 paper: From frogs to integrate-and-fire. *Biological Cybernetics* 97(5-6): 337-339, 2007.
- Brunel N and X Wang. What determines the frequency of fast network oscillations with irregular neural discharges? I. Synaptic dynamics and excitation-inhibition balance. *Journal of Neurophysiology* 90: 415-430, 2003.
- Burke R. Composite nature of the monosynaptic excitatory postsynaptic potential. *Journal of Neurophysiology* 30: 1114-1137, 1967.
- Butz E and J Cowan. Transient potentials in dendritic systems of arbitrary geometry. *Biophysical Journal* 14: 661-689, 1974.

- Buzsaki G and A Draguhn. Neuronal oscillations in cortical networks. *Science* 304: 1926-1929, 2004.
- Cain N and E Shea-Brown. Impact of correlated neural activity on decision-making performance. *Neural Computation* 25: 289-327, 2013.
- Cajal R. Textura del sistema nervioso del hombre y de los vertebrados. *Madrid*, 1899.
- Cameron H and R McKay. Adult neurogenesis produces a large pool of new granule cells in the dentate gyrus. *Journal of Comparative Neurology* 435(4): 406-417, 2001.
- Capaday C, Ethier C, Van Vreeswijk C, and W Darling. On the functional organization and operational principles of the motor cortex. *Frontiers in Neural Circuits* 7(66), 2013.
- Cateau H and A Reyes. Relation between single neuron and population spiking statistics and effects on network activity. *Physical Review Letters* 96(058101), 2006.
- Catterall W and A Few. Calcium channel regulation and presynaptic plasticity. *Neuron* 59: 882-901, 2008.
- Chen W and D Buonomano. Developmental shift of short-term synaptic plasticity in cortical organotypic slices. *Neuroscience* 213: 38-46, 2012.
- Clements JD. Variance-mean analysis: a simple and reliable approach for investigating synaptic transmission and modulation. *Journal of Neuroscience Methods* 130(2): 115-125, 2003.
- Cohen M and W Newsome. Context-dependent changes in functional circuitry in visual area MT. *Neuron* 60: 162-173, 2008.
- Cohen M and A Kohn. Measuring and interpreting neuronal correlations. *Nature Neuroscience* 14: 811-819, 2011.
- Costa R, Sjöström P, and M van Rossum. Probabilistic inference of short-term synaptic plasticity in neocortical microcircuits. *Frontiers in Computational Neuroscience* 7(75), 2013.
- Cortes J, Desroches M, and S Rodrigues. Short-term synaptic plasticity in the deterministic Tsodyks-Markram model leads to unpredictable network dynamics. *PNAS* 110(41): 16610-16615, 2013.
- Crandall S, Cruikshank S, and B Connors. A corticothalamic switch: Controlling the thalamus with dynamic synapses. *Neuron* 86: 1-15, 2015.
- Cuntz H, Borst A, and I Segev. Optimisation principles of dendritic structure. *Theoretical Biological and Medical Modelling* 4(21), 2007.
- Cuntz H, Forstner F, Borst A, and M Häusser One rule to grow them all: A general theory of neuronal branching and its practical application. *PLoS Computational Biology* 6(8), 2010.
- de Charms R and M Merzenich. Primary cortical representation of sounds by the coordination of action-potential timing. *Nature* 381: 610-613, 1996.
- de la Rocha J and N Parga. Short-term synaptic depression causes a non-monotonic response to correlated stimuli. *Journal of Neuroscience* 25: 8416-8431, 2005.
- del Castillo J and B Katz. Quantal components of the end-plate potential. *Journal of Physiology* 124(3): 560-573, 1954.
- de Sousa G, Maex R, Adams R, Davey N, and V Steuber. Dendritic morphology predicts pattern recognition performance in multi-compartmental model neurons with and without active conductances. *Journal of Computational Neuroscience* 38(2): 221-234, 2015.
- Desmond N and W Levy. Dendritic caliber and the 3/2 power relationship of dentate granule cells. *Journal of Comparative Neurology* 227: 589-596, 1984.
- DiGregorio D, Rothman J, Nielsen T, and R Silver. Desensitisation properties of AMPA receptors at the cerebellar mossy fiber-granule cell synapse. *Journal of Neuroscience* 27(31): 8344-8357, 2007.
- Dobrunz L, Huang E, and C Stevens. Very short-term plasticity for hippocampal synapses. *PNAS* 94: 14843-14847, 1997.

- Douglas R, Martin, and Whitteridge D. Canonical microcircuit for neocortex. *Neural computation* 1: 480-488, 1989.
- Dudel J and S Kuffler. Mechanism of facilitation at the crayfish neuromuscular junction. *Journal of Physiology* 155: 530-42, 1961.
- Dummer B, Wieland S, and B Lindner. Self-consistent determination of the spike-train power spectrum in a neural network with sparse connectivity. *Frontiers in Computational Neuroscience* 8(104), 2014.
- Eccles J, Katz B, and S Kuffler. Nature of the endplate potential in curarized muscle. *Journal of Neurophysiology* 4(5): 362-387, 1941.
- Eccles J. The physiology of nerve cells. *Baltimore*, 1957.
- Eccles J. The physiology of synapses. *Berlin*, 1964.
- Faisal A, Selen L, and D Wolpert. Noise in the nervous system. *Nature Reviews: Neuroscience* 9: 292-303, 2008.
- Fatt P and B Katz. Spontaneous subthreshold activity at motor nerve endings. *Journal of Physiology* 117(1): 109-128, 1952.
- Feldmeyer D, Lübke J, Silver R, and B Sakmann. Synaptic connections between layer 4 spiny neuronayer 2/3 pyramidal cell pairs in juvenile rat barrel cortex: physiology and anatomy of inter-laminar signalling within a cortical column. *Journal of Physiology* 538(3): 803-822, 2002.
- Fellous J, Rudolph M, Destexhe A and T Sejnowski. Synaptic background noise controls the input/output characteristics of single cells in an in vitro model of in vivo activity. *Neuroscience* 122(3): 811-829, 2003.
- Fino E and R Yuste. Dense inhibitory connectivity in neocortex. *Neuron* 69: 1188-1203, 2011.
- Fioravante D and W Regehr. Short-term forms of presynaptic plasticity. *Current Opinion in Neurobiology* 21: 269-274, 2011.
- Fortune E and G Rose. Short-term synaptic plasticity as a temporal filter. *Trends in Neurosciences* 24(7): 381-385, 2001.
- Foster K and W Regehr. Variance-mean analysis in the presence of a rapid antagonist indicates vesicle depletion underlies depression at the climbing fiber synapse. *Neuron* 43: 119-131, 2004.
- Fourcaud-Trocmé N, Hansel D, van Vreeswijk C and N Brunel. How spike generation mechanisms determine the neuronal response to fluctuating inputs. *Journal of Neuroscience* 23: 11628-11640, 2003.
- Fox S. Location of membrane conductance changes by analysis of the input impedance of neurons. I: Theory. *Journal of Neurophysiology* 54(6): 1578-1593, 1985.
- Fox S and C Chan. Location of membrane conductance changes by analysis of the input impedance of neurons. II: Implementation. *Journal of Neurophysiology* 54(6): 1594-1606, 1985.
- Fox G. A morphometric analysis of synaptic vesicle distributions. *Brain Research* 475: 103-117, 1988.
- Franks K, Stevens C, and T Sejnowski. Independent sources of quantal variability at single glutamatergic synapses. *Journal of Neuroscience* 23(8): 3186-3195, 2003.
- Frick A, Feldmeyer D, and B Sakmann. Postnatal development of synaptic transmission in local networks of L5A pyramidal neurons in rat somatosensory cortex. *Journal of Physiology* 585(1): 103-116, 2007.
- Frick A, Feldmeyer D, Helmstaedter M, and B Sakmann. Monosynaptic connections between pairs of L5A pyramidal neurons in columns of juvenile rat somatosensory cortex. *Cerebral Cortex* 18(2): 397-406, 2008.
- Fuhrmann G, Segev I, Markram H, and Tsodyks M. Coding of temporal information by activity-dependent synapses. *Journal of Neurophysiology* 87(1): 140-148, 2002.

- Fuhrmann G, Markram H, and Tsodyks M. Spike frequency adaptation and neocortical rhythms. *Journal of Neurophysiology* 88(2): 761-770, 2002.
- Fuhrmann G. Multiple mechanisms govern the dynamics of depression at neocortical synapses of young rats. *Journal of Physiology* 557(2): 415-438, 2004.
- Furukawa T, Kuno M, and S Matsuura. Quantal analysis of a decremental response at hair cell-afferent fibre synapses in the goldfish sacculus. *Journal of Physiology* 322: 181-195, 1982.
- Gardiner C. Stochastic methods: A handbook for the natural and social sciences. *Springer*, 2010.
- Gerstein G and B Mandelbrot. Random walk models for the spike activity of a single neuron. *Biophysical Journal* 4: 41-68, 1964.
- Gerstner W. Population dynamics of spiking neurons: Fast transients, asynchronous states, and locking. *Neural Computation*, 12: 43-89, 2000.
- Gidon A and I Segev. Principles governing the operation of synaptic inhibition in dendrites. *Neuro* 75: 330-341, 2012.
- Gobell S. Dendroaxonic synapses in the substantia gelatinosa glomeruli of the spinal trigeminal nucleus of the cat. *Journal of Computational Neurology* 167(2): 165-176, 1976.
- Goda Y and T Südhof. Calcium regulation of neurotransmitter release: Reliably unreliable. *Current Opinions in Cell Biology* 9: 513-518, 1997.
- Goldman M. Enhancement of information transmission efficiency by synaptic failures. *Neural Computation* 16: 1137-1162, 2004.
- Goldstein S and W Rall. Changes of action potential shape and velocity for changing core conductor geometry. *Biophysical Journal* 14: 731-757, 1974.
- Granit R. Reflex rebound by post-tetanic potentiation. *Journal of Physiology*, 131(1): 32-51, 1956.
- Hallermann S and R Silver. Sustaining rapid vesicular release at active zones: potential roles for vesicle tethering. *Trends in Neuroscience* 36(3): 185-194, 2013.
- Hamzei-Sichani F, Davidson K, Yasumura T, Janssen W, Wearne S, Hof P, Traub R, Gutiérrez R, Ottersen O, and J Rash. Mixed electrical-chemical synapses in adult rat hippocampus are primarily glutamatergic and coupled by connexin-36. *Frontiers in Neuroanatomy*, 6(13), 2012.
- Hanse E and B Gustafsson. Quantal variability at glutamatergic synapses in area CA1 of the rat neonatal hippocampus. *Journal of Physiology* 531(2): 467-480, 2001.
- Hardingham N, Read J, Trevelyan A, Nelson J, Jack J, and NJ annister. Quantal analysis reveals a functional correlation between presynaptic and postsynaptic efficacy in excitatory connections from rat neocortex. *Journal of Neuroscience* 30(4): 1441-1451, 2010.
- Harris J, Jolivet R, and D Attwell. Synaptic energy use and supply. *Neuron* 75: 762-777, 2012.
- Harrison P, Badel L, Wall M, and M Richardson. Experimentally verified parameter sets for modelling heterogeneous neocortical pyramidal-cell populations. *PLoS Computational Biology*, 11(8), 2015.
- Hastings W. Monte Carlo sampling methods using Markov chains and their applications. *Biometrika* 57: 97-109, 1970.
- Hausen K, Wolburg-Buchholz W, and W Ribi. The synaptic organization of visual interneurons in the lobula complex of flies: A light and electron microscopical study using silver-intensified cobalt-impregnations. *Cell Tissue Research* 208: 371-387, 1980.
- Häusser M. Synaptic function: Dendritic democracy. *Current Biology*, 11: 10-12, 2001.
- Hay E, Hill S, Schürmann F, Markram H, and I Segev. Models of neocortical layer 5b pyramidal cells capturing a wide range of dendritic and perisomatic active properties. *PLoS Computational Biology* 7(7), 2011.
- Hebb D. The organization of behavior: A neuropsychological theory. *Wiley*, 1949.

- Heine M, Groc L, Frischknecht R, Béïque J, Lounis B, Rumbaugh G, Huganir R, Cognet L, and D Choquet. Surface mobility of postsynaptic AMPARs tunes synaptic transmission. *Science* 320(5873): 201-205, 2008.
- Hennig M. Theoretical models of synaptic short term plasticity. *Frontiers in Computational Neuroscience* 7(45), 2013.
- Herz A, Gollisch T, Machens C, and D Jaeger. Modeling single-neuron dynamics and computations: A balance of detail and abstraction. *Science* 314(5796): 80-85, 2006.
- Hill S, Wang Y, Riachi I, Schürmann F, and H Markram. Statistical connectivity provides a sufficient foundation for specific functional connectivity in neocortical neural microcircuits. *PNAS* 109(42): 2885-2894, 2012.
- Hinch E. Perturbation Methods. *Cambridge*, 1991.
- Hines M and N Carnevale. The NEURON simulation environment. *Neural Computation* 9(6): 1179-1209, 1997.
- Hodgkin A, Huxley A, and B Katz. Measurement of the current-voltage relations in the membrane of *loligo*. *Journal of Physiology* 116: 424-448, 1952.
- Holmes W and W Rall. Electrotonic length estimates in neurons with dendritic tapering or somatic shunt. *Journal of Neurophysiology* 68: 1421-1437, 1992.
- Hosoi N, Sakaba T, and E Neher. Quantitative analysis of calcium-dependent vesicle recruitment and its functional role at the Calyx of Held synapse. *Journal of Neuroscience* 27(52): 14286-14298, 2007.
- Hu Y, Qu L, and T Schikorski. Mean synaptic vesicle size varies among individual excitatory hippocampal synapses. *Synapse* 62: 953-957, 2008.
- Jacob V, Petreanu L, Wright N, Svoboda K, and K Fox. Regular spiking and intrinsic bursting pyramidal cells show orthogonal forms of experience-dependent plasticity in Layer V of barrel cortex. *Neuron* 73: 391-404, 2012.
- Jaffe D and N Carnevale. Passive normalization of synaptic integration influenced by dendritic architecture. *Journal of Neurophysiology* 82: 3268-3285, 1999.
- Jolivet R, T Lewis, and W Gerstner. Generalized integrate-and-fire models of neuronal activity approximate spike trains of a detailed model to a high degree of accuracy. *Journal of Neurophysiology* 92: 959-976, 2004.
- Jones M and G Westbrook. The impact of receptor desensitization on fast synaptic transmission. *Trends in Neuroscience*, 19(3): 96-101, 1996.
- Kandel E. The molecular biology of memory storage: A dialog between genes and synapses. *Bioscience Reports* 21: 565-611, 2001.
- Karmeier K, Tabor R, Egelhaaf M, and H Krapp. Early visual experience and the receptive-field organization of optic flow processing interneurons in the fly motion pathway. *Visual Neuroscience* 18(1): 1-8, 2001.
- Katz B. The release of neural transmitter substances. *Liverpool*, 1969.
- Katona I and T Freund. Multiple functions of endocannabinoid signalling in the brain. *Annual Review of Neuroscience* 35: 529-558, 2012.
- Kerr M, Wall M, and M Richardson. Adenosine a 1-receptor activation mediates the developmental shift at Layer-5 pyramidal-cell synapses and is a determinant of mature synaptic strength. *Journal of Physiology* 591(13): 3371-3380, 2013.
- Kilpatrick Z. Short term synaptic depression improves information transfer in perceptual multistability. *Frontiers in Computational Neuroscience* 7(85), 2013.

- Kirsch L, Liscovitch N, and G Chechik. Localizing genes to cerebellar layers by classifying ISH images. *PLoS Computational Biology* 8(12), 2012.
- Kiskin N, Krishtal O, and A Tsyndrenko Excitatory amino acid receptors in hippocampal neurons: Kainate fails to desensitize them. *Neuroscience Letters* 63: 225-230, 1986.
- Kittelmann M, Liewald J, Hegemann J, Schultheis C, Brauner M, Costa W, Wabnig S, Eimer S, and A Gottschalk. *In vivo* synaptic recovery following optogenetic hyperstimulation. *PNAS* E: 3007-3016, 2013.
- Koch C, Poggio T, and V Torre. Nonlinear interactions in a dendritic tree: Localization, timing, and role in information processing. *PNAS* 80(9): 2799-2802, 1983.
- Koch C and T Poggio. A simple algorithm for solving the cable equation in dendritic trees of arbitrary geometry. *Journal of Neuroscience Methods* 12: 303-315, 1985.
- Koch C, Douglas R, and U Wehmeier. Visibility of synaptically induced conductance changes: Theory and simulations of anatomically characterized cortical pyramidal cells. *Journal of Neuroscience* 10(6): 1728-1744, 1990.
- Korn H, Triller A, Mallet A, and D Faber. Fluctuating responses at a central synapse: n of binomial fit predicts number of stained presynaptic boutons. *Science* 213(4510): 898-901, 1981.
- Kuhn A, Aertsen A, and S Rotter. Higher-order statistics of input ensembles and the response of simple model neurons. *Neural Computation* 15: 67-101, 2003.
- Kuhn A. Neuronal integration of synaptic input in the fluctuation-driven regime. *Journal of Neuroscience* 24: 2345-2356, 2004.
- Kullback S and RA Leibler. On information and sufficiency. *Annals of Mathematical Statistics* 22(1): 79-86, 1951.
- Kuno M. Quantal components of excitatory synaptic potentials in spinal motoneurons. *Journal of Physiology* 175: 81-99, 1964.
- Kuno M. Quantum aspects of central and ganglionic synaptic transmission in vertebrates. *Physiology Review* 51(4): 647-678, 1971.
- Kuno M and J Weakly. Quantal components of the inhibitory synaptic potential in spinal motoneurons of the cat. *Journal of Physiology* 224(2): 287-303, 1972.
- Landisman C and B Connors. Long-term modulation of electrical synapses in the mammalian thalamus. *Science* 310(5755): 1809-1813, 2005.
- Lapicque L. Recherches quantitatives sur l'excitation électrique des nerfs traitée comme une polarisation. *Journal of Physiology and General Pathology* 9: 620-635, 1907.
- Lefort S, Tómm C, Sarria J, and C Petersen. The excitatory neuronal network of the C2 barrel column in mouse primary somatosensory cortex. *Neuron* 61(2): 301-316, 2009.
- Levy W and R Baxter. Energy-efficient neuronal computation via quantal synaptic failures. *Journal of Neuroscience*, 22: 4746-4755, 2002.
- Lindner B. Superposition of many independent spike trains is generally not a Poisson process. *Physical Review E* 73(2), 2006.
- Lindner B, Gangloff D, Longtin A and J Lewis. Broadband coding with dynamic synapses. *Journal of Neuroscience* 29: 2076-2088, 2009.
- Lindsay K, Rosenberg J, and G Tucker. Analytical and numerical construction of equivalent cables. *Mathematical Biosciences* 184: 137-164, 2003.
- Liley A. The quantal components of the mammalian end-plate potential. *Journal of Physiology* 133(3): 571-587, 1956.
- Llinás R. The intrinsic electrophysiological properties of mammalian neurons: Insights into central nervous system function. *Science* 242: 1654-1664, 1988.

- Loebel A, Silberberg G, Helbig D, Markram H, Tsodyks M, and M Richardson. Multiquantal release underlies the distribution of synaptic efficacies in the neocortex. *Frontiers in Computational Neuroscience* 3(27), 2009.
- Loebel A, Le Be J, Richardson M, Markram H, and A Herz. Matched pre- and post-synaptic changes underlie synaptic plasticity over long time scales. *Journal of Neuroscience* 33: 6257-6266, 2013.
- Loewi O. Über humorale Übertragbarkeit der Herznervenwirkung *Pflügers Archiv für die gesamte Physiologie des Menschen und der Tiere* 204: 629-640, 1924.
- London M, Meunier C, and I Segev. Signal transfer in passive dendrites with nonuniform membrane conductance. *Journal of Neuroscience* 19:8 219-8233, 1999.
- London M and M Häusser. Dendritic computation. *Annual Review of Neuroscience* 28: 503-532, 2005.
- Lübke J and D Feldmeyer. Excitatory signal flow and connectivity in a cortical column: Focus on barrel cortex. *Brain Structure and Function* 212: 3-17, 2007.
- Magee J and E Cook.. Synaptic EPSP amplitude is independent of synapse location in hippocampal pyramidal neurons. *Nature Neuroscience* 3: 895-903, 2000.
- Marder E. Neuromodulation of neuronal circuits: Back to the future. *Neuron* 76: 1-11, 2012.
- Markram H, Lübke J, Frotscher M, Roth A, and B Sakmann. Physiology and anatomy of synaptic connections between thick tufted pyramidal neurones in the developing rat neocortex. *Journal of Physiology* 500(2): 409-440, 1997.
- Markram H, Gerstner W, and P Sjöström. A history of spike-timing-dependent plasticity. *Frontiers in Synaptic Neuroscience* 3(4), 2011.
- McGuinness L, Taylor C, Taylor R, Yau C, Langenhan T, Hart M, Christian H, Tynan P, Donnelly P, and N Emptage. Presynaptic NMDARs in the hippocampus facilitate transmitter release at theta frequency. *Neuron* 68(6): 1109-1127, 2010.
- Megías M, Emri Z, Freund T, and A Gulyás. Total number and distribution of inhibitory and excitatory synapses on hippocampal CA1 pyramidal cells. *Neuroscience* 102: 527-540, 2001.
- Metropolis N, Rosenbluth A, Rosenbluth M, Teller A, and E Teller. Equation of state calculations by fast computing machines. *Journal of Chemical Physics* 21: 1087-1092, 1953.
- Meyer H, Wimmer V, Hemberger M, Bruno R, and C de Kock. Cell type-specific thalamic innervation in a column of rat vibrissa cortex. *Cerebral Cortex* 20: 2287-2303, 2010.
- Middleton J, Yu N, Longtin A, and L Maler. Routing the flow of sensory signals using plastic responses to bursts and isolated spikes: Experiment and theory. *Journal of Neuroscience* 31(7): 2461-2473, 2011.
- Moezzi B, Iannella N, and M McDonnell. Modeling the influence of short term depression in vesicle release and stochastic calcium channel gating on auditory nerve spontaneous firing statistics. *Frontiers in Computational Neuroscience* 8(163), 2014.
- Mongillo G, Barak O, and M Tsodyks. Synaptic theory of working memory. *Science* 319: 1543-1546, 2008.
- Moreno-Bote R and N Parga. Role of synaptic filtering on the firing response of simple model neurons. *Physical Review Letters* 92(2), 2004.
- Mountcastle V, Davies P, and A Berman. Response properties of neurons of cat's somatic sensory cortex to peripheral stimuli. *Journal of Neurophysiology* 20: 374-407, 1957.
- Mitchell J, Sundberg K, and J Reynolds. Spatial attention decorrelates intrinsic activity fluctuations in macaque area V4. *Neuron* 63: 879-888, 2009.
- Nagel K, Hong E, and R Wilson. Synaptic and circuit mechanisms promoting broadband transmission of olfactory stimulus dynamics. *Nature Neuroscience* 18(1): 56-65, 2015.

- Nakamura Y, Harada H, Kamasawa N, Matsui K, Rothman J, Shigemoto R, Silver R, DiGregorio D, and T Takahashi. Nanoscale distribution of presynaptic Ca^{2+} channels and its impact on vesicular release during development. *Neuron* 85: 145-158, 2015.
- Nakanishi S. Metabotropic glutamate receptors: Synaptic transmission, modulation, and plasticity. *Neuron* 13: 1031-1037, 1994.
- Neal R. Slice sampling. *Annals of Statistics* 31(3): 705-767, 2003.
- Neher E. Ion channels for communication between and within cells. *Nobel Lecture in Physiology or Medicine*, 1991.
- Neher E and T Sakaba. Multiple roles of calcium ions in the regulation of neurotransmitter release. *Neuron* 59: 861-872, 2008.
- Oberlaender M, de Kock C, Bruno R, Ramirez A, Meyer H, Dercksen V, Helmstaedter M, and B Sakmann. Cell type-specific three-dimensional structure of thalamocortical circuits in a column of rat vibrissa cortex. *Cerebral Cortex* 22(10): 2375-2391, 2012.
- O’Kusky J and M Colonnier. A laminar analysis of the number of neurons, glia, and synapses in the adult cortex (area 17) of adult macaque monkeys. *The Journal of Comparative Neurology* 210: 278-290, 1982.
- O’Rourke N, Weiler N, Micheva K, and S Smith. Deep molecular diversity of mammalian synapses: Why it matters and how to measure it. *Nature Reviews Neuroscience* 13: 365-379, 2012.
- Ostojic S. Interspike interval distributions of spiking neurons driven by fluctuating inputs. *Journal of Neurophysiology* 106: 361-373, 2011.
- Oswald A and A Reyes. Maturation of intrinsic and synaptic properties of Layer 2/3 pyramidal neurons in mouse auditory cortex. *Journal of Neurophysiology* 99: 2998-3008, 2008.
- Otis T, Zhang S, and L Trussel. Direct measurement of AMPA receptor desensitization induced by glutamatergic synaptic transmission. *Journal of Neuroscience* 16(23): 7496-7504, 1996.
- Park H, Li Y, and R Tsien. Influence of synaptic vesicle position on release probability and exocytotic fusion mode. *Science* 335: 1362-1366, 2012.
- Pereda A. Electrical synapses and their functional interactions with chemical synapses. *Nature Reviews Neuroscience* 15: 250-263, 2014.
- Perin R, Berger T, and H Markram. A synaptic organising principle for cortical neuronal groups. *PNAS* 108: 5419-5424, 2011.
- Peron S and F Gabbiani. Role of spike-frequency adaptation in shaping neuronal response to dynamic stimuli. *Biological Cybernetics* 100: 505-520, 2009.
- Peterson A, Irvine D, and P Heil. A model of synaptic vesicle-pool depletion and replenishment can account for the interspike interval distributions and nonrenewal properties of spontaneous spike trains of auditory-nerve fibers. *Journal of Neuroscience* 34(45): 15097-15109, 2014.
- Pin J and R Duvoisin. The metabotropic glutamate receptors: Structure and functions. *Neuropharmacology*, 34(1): 1-26, 1995.
- Pinsky P and J Rinzel. Intrinsic and network rhythmogenesis in a reduced Traub model for CA3 neurons. *Journal of Computational Neuroscience*, 1: 39-60, 1994.
- Pipa G, Grun S, and C van Vreeswijk. Impact of spike-train auto-structure on probability distribution of joint-spike events. *Neural Computation* 25(5): 1123-1163, 2013.
- Poirazi, P, Brannon T, and B Mel. Pyramidal neuron as two-layered network. *Neuron* 37(6): 989-999, 2003.
- Poznanski R. A generalised tapering equivalent cable model for dendritic neurons. *Bulletins in Mathematical Biology* 53: 457-467, 1991.

- Rall W. Branching dendritic trees and motoneuron membrane resistivity. *Experimental Neurology* 1: 491-527, 1959.
- Rall W, Shepard G, Reese T, and M Brightman. Dendrodendritic synaptic pathway for inhibition in the olfactory bulb. *Experimental Neurology* 14(1): 44-56, 1966.
- Rall W. Time constants and electrotonic length of membrane cylinders and neurons. *Biophysical Journal* 9: 1483-1508, 1969.
- Rall W and J Rinzel. Branch input resistance and steady attenuation for input to one branch of a dendritic neuron model. *Biophysical Journal* 13: 648-687, 1973.
- Ramaswamy S and H Markram. Anatomy and physiology of the thick-tufted Layer 5 pyramidal neuron. *Frontiers in Cellular Neuroscience* 9(233), 2015.
- Ramcharan E, Gnadt J, and S Sherman. Burst and tonic firing in thalamic cells of unanesthetized, behaving monkeys. *Visual Neuroscience* 17: 55-62, 2000.
- Redman S. Quantal analysis of synaptic potentials in neurons of the central nervous system. *Physiological Reviews* 70: 165-198, 1990.
- Regehr W. Interplay between sodium and calcium dynamics in granule cell presynaptic terminals. *Biophysical Journal* 73: 2476-2488, 1997.
- Regehr W. Short-term presynaptic plasticity. *Cold Spring Harbor Perspectives in Biology*, 2012.
- Reich S and R Rosenbaum. The impact of short term synaptic depression and stochastic vesicle dynamics on neuronal variability. *Journal of Computational Neuroscience* 35: 39-53, 2013.
- Reyes A and B Sakmann. Developmental switch in the short-term modification of unitary EPSPs evoked in layer 2/3 and layer 5 pyramidal neurons of rat neocortex. *Journal of Neuroscience* 19: 3827-3835, 1999.
- Reyes A. Synchrony-dependent propagation of firing rate in iteratively constructed networks in vitro. *Nature Neuroscience* 6: 593-599, 2003.
- Ribault C, Sekimoto K, and A Triller. From the stochasticity of molecular processes to the variability of synaptic transmission. *Nature Reviews Neuroscience* 12: 375-387, 2011.
- Richardson M and G Silberberg. Measurement and analysis of postsynaptic potentials using a novel voltage-deconvolution method. *Journal of Neurophysiology* 99(2): 1020-1031, 2008.
- Richardson M and R Swarbrick. Firing-rate response of a neuron receiving excitatory and inhibitory synaptic shot noise. *Physical Review Letters* 105: 178102, 2010.
- Roberts G, Gelman A, and W Gilks. Weak convergence and optimal scaling of random walk Metropolis algorithms. *Annals of Applied Probability* 7(1): 110-120, 1997.
- Robinson J. Estimation of parameters for a model of transmitter release at synapses. *Biometrics* 32: 61-68, 1976.
- Rosenbaum R, Rubin J and B Doiron. Short term synaptic depression imposes a frequency dependent filter on synaptic information transfer. *PLoS Computational Biology* 8(6), 2012.
- Roth A and M Häusser. Compartmental models of rat cerebellar Purkinje cells based on simultaneous somatic and dendritic patch-clamp recordings. *Journal of Physiology* 535(2): 445-472, 2001.
- Rothman J, Cathala L, Steuber V, and R Silver. Synaptic depression enables neuronal gain control. *Nature* 457: 1015-1018, 2009.
- Rubio-Garrido P, Pèrez-de-Manzo F, Porrero C, Galazo M, and F Clascà. Thalamic input to distal apical dendrites in neocortical layer 1 is massive and highly convergent. *Cerebral Cortex* 19: 2380-2395, 2009.
- Rumsey C and L Abbott. Synaptic democracy in active dendrites. *Journal of Neurophysiology* 96: 2307-2318, 2006.

- Sakmann B. Elements in synaptic transmission revealed by currents through single ion channels. *Nobel Lecture in Physiology or Medicine*, 1991.
- Salinas E and T Sejnowski. Impact of correlated synaptic input on output firing rate and variability in simple neuronal models. *Journal of Neuroscience* 20: 6193-6209, 2000.
- Savtchenko L, Sylantsev S, and D Rusakov. Central synapses release a resource-efficient amount of glutamate. *Nature Neuroscience* 16: 10-12, 2012.
- Schierwagen A. A non-uniform equivalent cable model of membrane voltage changes in a passive dendritic tree. *Journal of Theoretical Biology* 141: 159-179, 1989.
- Schikorski T and C Stevens. Morphological correlates of functionally defined synaptic vesicle correlations. *Nature Neuroscience* 4(4): 391-395, 2001.
- Schiller J, Major G, Koester H, and Y Schiller. NMDA spikes in basal dendrites of cortical pyramidal neurons. *Nature* 404: 285-289, 2000.
- Schmidt-Hieber C, Jonas P, and J Bischofberger. Subthreshold dendritic signal processing and coincidence detection in dentate gyrus granule cells. *Journal of Neuroscience* 27(31): 8430-8441, 2007.
- Schneidman E, Berry M, Segev R, and W Bialek. Weak pairwise correlations imply strongly correlated network states in a neural population. *Nature* 440: 1007-1012, 2006.
- Schwalger T, Fisch K, Benda J, and B Lindner. How noisy adaptation of neurons shapes interspike interval histograms and correlations. *PLoS Computational Biology* 6(12), 2010.
- Schwalger T and B Lindner. Patterns of interval correlations in neural oscillators with adaptation. *Frontiers in Computational Neuroscience* 7(164), 2013.
- Scott E, Raabe T, and L Luo. Structure of the vertical and horizontal system neurons of the lobula plate in *drosophila*. *Journal of Comparative Neurology* 454: 470-481, 2002.
- Scott P, Cowan A, and C Stricker. Quantifying impacts of short-term plasticity on neuronal information transfer. *Physical Review E* 85, 2012.
- Segev I, Rinzel J, and G Shepherd. The theoretical foundations of dendritic function: Selected papers of Wilfrid Rall with commentaries. *Cambridge*, 1995.
- Seriès P, Latham P, and A Pouget. Tuning curve sharpening for orientation selectivity: Coding efficiency and the impact of correlations. *Nature Neuroscience* 7: 1129-1135, 2004.
- Sherman S. Tonic and burst firing: dual modes of thalamocortical relay. *Trends in Neurosciences* 24(2): 122-126, 2001.
- Sherrington C. The integrative action of the nervous system. *Yale*, 1906.
- Sherrington C. Reflex inhibition as a factor in the co-ordination of movements and postures. *Quarterly Journal of Experimental Physiology* 6(3): 251-310, 1913.
- Shinomoto S, Kim H, Shimokawa T, Matsuno N, Funahashi S, Shima K, Fujita I, et al. Relating neuronal firing patterns to functional differentiation of cerebral cortex. *PLoS Computational Biology* 5(7), 2009.
- Silberberg G, Gupta A, and H Markram. Stereotypy in neocortical microcircuits. *Trends in Neuroscience* 25: 227-230, 2002.
- Silberberg G H Markram. Disynaptic inhibition between neocortical pyramidal cells mediated by Martinotti cells. *Neuron* 53: 735-746, 2007.
- Silver R, Momiyama A, and S Cull-Candy. Locus of frequency- dependent depression identified with multiple-probability fluctuation analysis at rat climbing fibre-Purkinje cell synapses. *Journal of Physiology* 510: 881-902, 1998.
- Silver R. Estimation of nonuniform quantal parameters with multiple-probability fluctuation analysis: theory, application and limitations. *Journal of Neuroscience Methods*, 130(2): 127-14, 2003.

- Song S, Sjöström PJ, Reigl M, Nelson S, and D Chklovskii. Highly nonrandom features of synaptic connectivity in local cortical circuits. *PLoS Biology* 3(3): e68, 2005.
- Spruston N. Pyramidal neurons: dendritic structure and synaptic integration. *Nature Reviews: Neuroscience*, 9: 206-221, 2008.
- Stein R. A theoretical analysis of neuronal variability. *Biophysical Journal* 5(2): 173-194, 1965.
- Steinmetz P, Manwani A, Koch C, London M, and I Segev. Subthreshold voltage noise due to channel fluctuations in active neuronal membranes. *Journal of Computational Neuroscience* 9(2): 133-48, 2000.
- Stuart G and M Häusser. Initiation and spread of sodium action potentials in cerebellar Purkinje cells. *Neuron* 13(3): 703-712, 1994.
- Stuart G and B Sakmann. Active propagation of somatic action potentials into neocortical pyramidal cell dendrites. *Nature* 367: 69-72, 1994.
- Südhof T. The synaptic vesicle cycle. *Annual Review of Neuroscience* 27: 509-547, 2004.
- Taschenberger H, Leão R, Rowland K, Spirou G, and H von Gersdorff. Optimizing synaptic architecture and efficiency for high-frequency transmission. *Neuron* 36: 1127-1143, 2002.
- Testa-Silva G, Verhoog M, Linaro D, de Kock C, Baayen J, Meredith R, de Zeeuw C, Giugliano M, and H Mansvelder. High bandwidth synaptic communication and frequency tracking in human neocortex. *PLoS Computational Biology* 12(11), 2014.
- Thomson A, Deuchars J, and D West. Large, deep layer pyramid-pyramid single axon EPSPs in slices of rat motor cortex display paired pulse and frequency-dependent depression, mediated presynaptically and self-facilitation, mediated postsynaptically. *Journal of Neurophysiology* 70(6): 2354-2369, 1993.
- Thomson A. Activity-dependent properties of synaptic transmission at two classes of connections made by rat neocortical pyramidal axons in vitro. *Journal of Physiology* 502: 131-147, 1997.
- Thomson A and A Bannister. Release-independent depression at pyramidal inputs onto specific cell targets: Dual recordings in slices of rat cortex. *Journal of Physiology* 519: 57-70, 1999.
- Timofeeva Y, Cox S, Coombes S, and K Josic. Democratization in a passive dendritic tree: An analytical investigation. *Journal of Computational Neuroscience* 25: 228-244, 2008.
- Trigo F, Sakaba T, Ogden D, and A Marty. Readily releasable pool of synaptic vesicles measured at single synaptic contacts. *PNAS* 109: 18138-18143, 2012.
- Tsodyks M and H Markram. The neural code between neocortical pyramidal neurons depends on neurotransmitter release probability. *PNAS* 94(2): 719-723, 1997.
- Tsodyks M, Pawelzik K, and H Markram. Neural networks with dynamic synapses. *Neural Computation* 10(4): 821-835, 1998.
- Turner D and M West. Bayesian analysis of mixtures applied to post-synaptic potential fluctuations. *Journal of Neuroscience Methods* 47: 1-21, 1993.
- Turrigiano G and S Nelson. Homeostatic plasticity in the developing nervous system. *Nature Reviews Neuroscience* 5(2): 97-107, 2004.
- Varela J, Sen K, Gibson J, Fost J, Abbott L, and S Nelson. A quantitative description of short-term plasticity at excitatory synapses in layer 2/3 of rat primary visual cortex. *Journal of Neuroscience* 17(20): 7926-7940, 1997.
- Vere-Jones D. Simple stochastic models for the release of quanta of transmitter from a nerve terminal. *Australian and New Zealand Journal of Statistics* 8: 53-63, 1966.
- Verveen A, Derksen H, and K Schick. Voltage fluctuations of neural membrane. *Nature* 216(5115): 588-589, 1967.

- Vetter P, Roth A, and M Häusser. Propagation of action potentials in dendrites depends on dendritic morphology. *Journal of Neurophysiology* 85(2): 926-937, 2001.
- von der Malsburg C. The correlation theory of brain function. *Göttingen Internal Report*, 1981.
- Waldeyer W. Über einige neuere Forschungen im Gebiete der Anatomie des Centralnervensystems *Deutsche Medizinische Wochenschrift* 17: 1231-1356, 1891.
- Wang L and L Kaczmarek. High-frequency firing helps replenish the readily releasable pool of synaptic vesicles. *Nature* 394: 384-388, 1998.
- Wang X. Calcium coding and adaptive temporal computation in cortical pyramidal neurons. *Journal of Neurophysiology* 79: 1549-1566, 1998.
- Wang Y, Gupta A, Toledo-Rodriguez M, Wu C, and H Markram. Anatomical, physiological, molecular and circuit properties of nest basket cells in the developing somatosensory cortex. *Cerebral Cortex* 12: 395-410, 2001.
- White J, Rubinstein J, and A Kay. Noise in neurons. *Trends in Neurosciences* 23(3): 131-37, 2000.
- Whitehead R and J Rosenberg. On trees as equivalent cables. *Proceedings in Biological Science* 252: 103-108, 1993.
- Wilbur W and J Rinzel. A theoretical basis for large coefficient of variation and bimodality in neuronal interspike interval distributions. *Journal of Theoretical Biology* 105: 345-368, 1983.
- Williams S and G Stuart. Dependence of EPSP efficacy on synapse location in neocortical pyramidal neurons. *Science* 295: 1907-1910, 2002.
- Wong A, Graham B, Billups B, and I Forsythe. Distinguishing between presynaptic and postsynaptic mechanisms of short-term depression during action potential trains. *Journal of Neuroscience* 23(12): 4868-4877, 2003.
- Woosley T and H van der Loos. The structural organisation of Layer IV in the somatosensory region of mouse cerebral cortex: the description of a cortical field composed of discrete cytoarchitectonic units. *Brain Research* 17(2): 205-238, 1970.
- Zador A, Agmon-Snir H and I Segev. The morphoelectrotonic transform: a graphical approach to dendritic function. *Journal of Neuroscience* 15: 1669-1682, 1995.
- Zador A. Impact of synaptic unreliability on the information transmitted by spiking neurons. *Journal of Neurophysiology* 79: 1219-1229, 1998.
- Zhong N, Beaumont V, and R Zucker. Roles for mitochondrial and reverse mode $\text{Na}^+/\text{Ca}^{2+}$ exchange and the plasmalemma Ca^{2+} ATPase in post-tetanic potentiation at crayfish neuromuscular junctions. *Journal of Neuroscience* 21(24): 9598-9607, 2001.
- Zucker R and W Regehr. Short-term synaptic plasticity. *Annual Review of Physiology* 64: 355-405, 2002.